In vitro models to evaluate ingestible devices

O'farrell, Connor; Stamatopoulos, Konstantinos; Simmons, Mark; Batchelor, Hannah

DOI:
10.1016/j.addr.2021.113924

Document Version
Peer reviewed version

Citation for published version (Harvard):
O'farrell, C, Stamatopoulos, K, Simmons, M & Batchelor, H 2021, 'In vitro models to evaluate ingestible devices: present status and current trends', *Advanced Drug Delivery Reviews*, vol. 178, 113924. https://doi.org/10.1016/j.addr.2021.113924

In vitro models to evaluate ingestible devices: present status and current trends

Connor O'Farrell[1], Konstantinos Stamatopoulos[1,2], Mark Simmons[1], Hannah Batchelor[3*]

*Corresponding author Hannah.batchelor@strath.ac.uk

1. School of Chemical Engineering, University of Birmingham, Edgbaston, Birmingham B15 2TT, UK
2. Biopharmaceutics, Pharmaceutical Development, PDS, MST, RD Platform Technology & Science, GSK, David Jack Centre, Park Road, Ware, Hertfordshire, SG12 0DP, UK
3. Strathclyde Institute of Pharmacy and Biomedical Sciences, 161 Cathedral Street, Glasgow G4 0RE

Abstract

Orally ingestible medical devices offer significant opportunity in the diagnosis and treatment of gastrointestinal conditions. Their development necessitates the use of models that simulate the gastrointestinal environment on both a macro and micro scale. An evolution in scientific technology has enabled a wide range of in vitro, ex vivo and in vivo models to be developed that replicate the gastrointestinal tract. This review describes the landscape of the existing range of in vitro tools that are available to characterize ingestible devices. Models are presented with details on their benefits and limitations with regards to the evaluation of ingestible devices and examples of their use in the evaluation of such devices is presented where available. The multitude of models available provides a suite of tools that can be used in the evaluation of ingestible devices that should be selected on the functionality of the device and the mechanism of its function.

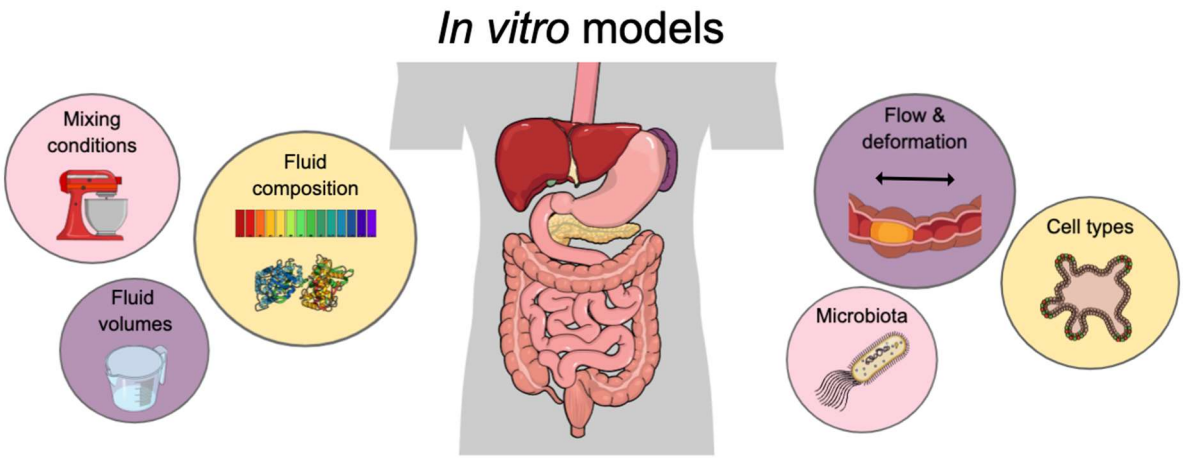

Keywords: In vitro model; stomach; small intestine; colon; macroenvironment microenvironment; organoid; organ-on-a-chip

List of Abbreviations

AC	Ascending colon
AGDS	Artificial Gastric Digestive System
ARCOL	Artificial Colon
ASD	Artificial Stomach Duodenal model
BCFFM	Batch Culture Faecal Fermentation Model
BGR	Bionic Gastrointestinal Reactor
BioGIT	Biorelevant Gastrointestinal Transfer model
CF	Cystic fibrosis
DC	Descending colon
DGM	Dynamic Gastric Model
DGSM	Dynamic Gastric Simulating Model
DIDGI	Dynamic Gastro-intestinal Digester
DIVHS	Dynamic in vitro human stomach system
DIVRS	Dynamic in vitro rat stomach system
EBFM	Enzyme Based Fermentation Model
ER	Extended release
ESIN	Engineered Stomach and Small Intestine model
FaSSCoF	Fasted State Simulated Colonic Fluid
FaSSGF	Fasted State Simulated Gastric Fluid
FaSSIF	Fasted State Simulated Intestinal Fluid
FDA	Food and Drug Administration
FeSSCoF	Fed State Simulated Colonic Fluid
FeSSGF	Fed State Simulated Gastric Fluid
FeSSIF	Fed State Simulated Intestinal Fluid
GDS	Gastric Digestion Simulator
GI	Gastrointestinal
GIT	Gastrointestinal tract
GSM	Gastric Simulation Model
HCl	Hydrochloric acid
HESC	Human embryonic stem cells
HGS	Human Gastric Simulator
hIPSC	Human induced pluripotent stem cell
HMI	Host Microbiota Interaction
IBD	Irritable bowel disease
ICV	Ileocecal valve
IMGS	In vitro Mechanical Gastric System
IR	Immediate release
IV	Intravenous
MIDA	Model of an Infant Digestive Apparatus
MMC	Migratory Motor Complex
MRI	Magnetic Resonance Imaging
M-SHIME	Mucosal Simulator of the Human Intestinal Microbial Ecosystem
O/W	Oil in water
PEG	Polyethylene glycol
PEVA	Polyethylene vinyl acetate
PLGA	Poly(lactic-co-glycolic acid)
RD-IV-HSM	Rope driven in vitro human stomach
Rpm	revolutions per minutes
SBFS	Single Batch Fermentation System

SCFA	Small chain fatty acid
SGF	Simulated Gastric Fluid
SHIME	Simulator of the Human Intestinal Microbial Ecosystem
SI	Small Intestine
SIF	Simulated Intestinal Fluid
SIM	Small Intestinal Model
SIMGI	Simulator of the GI tract
TC	Transverse colon
TIM	Intestinal Transit Model
TIMagc	TIM advanced gastric compartment
TSI	The Smallest Intestine
UC	Ulcerative Colitis
USP	Unites States Pharmacopeia

1 Introduction

Orally ingestible medical devices can be used for site-directed drug delivery in the gastrointestinal (GI) tract, real-time imaging, microsampling and monitoring of intestinal biomarkers. Appropriate methods that predict performance in the human GI tract are required to evaluate these devices prior to their introduction into clinical testing in humans. However, recreating the intestine is complex due to its dynamic nature and the different component parts, specifically the composition of intestinal fluids and the fluctuation in volume and how these change by time and location, particularly after ingestion of food as well as the motility pattern that is irregular and discontinuous. The macro function of the GI tract is as a mixing system to transit nutrients to the appropriate site for absorption. On a micro scale the epithelium works as an absorptive system. An ideal model should incorporate macro and micro parameters whilst also mimicking the transit and regional differences. The regional differences can be significant; these can be considered with respect to the architecture of the organ of interest; the cellular epithelial layer, composition of the luminal fluid within that organ as well as the flow and motility. In addition, these aspects can differ in response to ingestion of food or in response to disease which further complicates the model systems.
The ideal system would incorporate key features of both the macro and microenvironment; these features are detailed in Table 1.

	Features
Macroenvironment [1, 2]	Biorelevant luminal media: composition; volumes and distribution
	Representative motility patterns (hydrodynamic conditions)
	Representative transit times between GI regions
	Representative pressures from within the GI tract
	Dynamic response in luminal media to the ingestion of food/digestion products and intestinal secretions
	Feedback mechanisms (e.g., caloric content in small intestine controlling gastric emptying)
Microenvironment [3]	Human derived cells that represent all layers of the mucosa where this system is stable for sufficiently long to undertake the experiment
	An epithelial substratum with a 3D structure that replicates the in vivo environment
	A fluidic system that provides adequate oxygenation and nutrients to the cell medium, as well as relevant physiological shear stress
	A flexible substrate to provide cycle deformation to the epithelium in a physiologically relevant manner
	A biochemical environment that replicates the crosstalk between epithelium/immune system and the microbiota to maintain homeostasis
	A system that differentiates lymphatic uptake from overall absorption

Table 1. Summary of the macro and micro environmental conditions that should be replicated in a biorelevant system.

A comprehensive understanding of the human gastro-intestinal tract is required as the basis for the development of suitable models. There have been several relevant reviews on GI conditions that the reader is referred to for completeness [4-7], further details on human GI anatomy and physiology are presented in our other paper within this edition [8]. Key factors for in vitro models are fluid volume and composition and these details are reviewed here, similarly, this review highlights current progress with microscale models, with evaluation of models that involve relevant cell types, luminal flow and microbiota. This review is focused on typical models that reflect a healthy adult population, it is recognized that there is also a need for models that replicate all patient populations, including those with GI disease; depending on the nature of the GI changes it is possible to adapt

these models to better replicate a range of GI conditions. This review brings together existing in vitro methods used to replicate the conditions within the healthy adult GI tract to provide a rationale for selection of an appropriate model to use in the evaluation of ingestible devices.

1.1 Ingestible Devices

Ingestible device is a term that can encompass a range of formulated and engineered products. These may include complex pharmaceutical products where their performance is controlled by aspects of their design, for example a coating that will only dissolve in certain conditions. Alternatively, this may include swallowable devices that incorporate sensors and transmitters, for example cameras that can record images of the internal GI tract. The oral delivery of biologics has increased interest in ingestible devices as there is a need to minimize exposure to the harsh GI conditions and deliver the agent to the site of absorption as efficiently as possible [9]. There have been some recent reviews on ingestible devices and ingestible sensors that may be of interest to the reader [10, 11].

1.2 Value of in vitro models for ingestible devices

In vitro models may be used to ensure that the ingestible devices can withstand the conditions within the GI tract, where replication of the fluid volume, composition and motility are important parameters. Due to the diverse range of ingestible systems, additional parameters may need to be included depending on the nature of the system under test. For example, it is essential that for devices that respond to the microbiome, fluid composition and biorelevance must be replicated. Several models are designed as a simplified version of the intestine, where their purpose is to increase mechanistic understanding of a particular aspect of GI function. Thus, a suite of testing models may be required to thoroughly assess the performance of a single ingestible device depending on the research question(s) to be answered. For example, traditionally drug dissolution has been assessed separately to drug permeation; yet there are advanced systems that integrate dissolution and absorption may offer benefits for evaluation of ingestible devices.
There have been several recent reviews [5, 12-17] that have described in vitro gastro-intestinal models mainly in terms of their value for oral drug products or digestion and these are listed in Supplementary Table 1 to provide additional details for the reader. The current review provides the broadest landscape of in vitro models that are presented with reference to their functionality in the evaluation of ingested devices.

1.3 Macromodels of the GI tract

Macroscale models of the GI tract may be useful for simulating the conditions that an ingestible device may have to endure to protect a therapeutic payload. These may be the physicochemical characteristics of GI media in physiologically relevant geometries and volumes or GI motility to produce relevant intraluminal flows and shear forces. Recapitulation of geometry, motility and flow may be useful for ingestible devices that image the GI tract [18-21] or measure intraluminal pressure [22-24]. Macroscale models may be useful for the development of devices that monitor intraluminal physicochemical properties and the products of complex physiological processes such as digestion and fermentation [23-25]. Macroscale models available for simulation of such processes in the stomach, small intestine and colon, from basic compendial apparatus used in the pharmaceutical industry, to more advanced in vitro models for pharmaceutical and food-based research are presented. Dynamic models are defined as those where there can be a change in any relevant component that reflects the GI luminal environment; this may include a change in volume or composition of the media or a change in the motility pattern applied as a function of time to reflect the dynamically changing GI luminal environment. Multicomponent models are those that include more than one region of the GI tract, for example both the stomach and small intestine.

1.3.1 Compendial apparatus that simulate GI conditions

Variations of pharmacopoeial models of the stomach, small intestine and colon are presented in sections 2.5, 3.6 and 4.5 respectively, although, all systems maintain the same underlying principles and as such are outlined in this section. There are four USP apparatus that are used to simulate the gastro- intestinal environment in drug product development: (i) USP I apparatus (basket); (ii) USP II apparatus (paddle); (iii) USP III apparatus (reciprocating cylinder) and (iv) USP IV apparatus (flow through cell). These are summarised in Table 2. Overall, the key benefits of pharmacopoeial models are that they are widely available and reproducible, validated pieces of equipment that are simple, easy to install, use and maintain. USP models may be suitable for the development of ingestible devices that test for media composition; however, the lack of physiologically representative geometry and hydrodynamics make them an unsuitable choice for the development of devices that incorporate sensors for mechanical performance such as motility, pressure and gas volumes, for example, luminal flow rates, Reynolds numbers [26], GI lumen volumes [27] and relevant shear forces. Considering the stomach or upper intestine, volumes of 250 mL and 500 mL should be used for simulating the fasted and fed state respectively [27-30]. In the lower intestine, 200 mL is generally considered appropriate [27, 31].

Feature	**USP1**	**USP2**	**USP3**	**USP4**
Geometry	Cylindrical vessel, hemispherical base	Cylindrical vessel, hemispherical base	Cylindrical vessels, flat meshed base	Cylindrical cell with coned bottom
Volume	0.1, 1, 2, 4 L	0.1, 1, 2, 4 L	300 mL	Standard cell diameters of 12 and 22.6 mm for volume of 8 or 19 mL.
Mixing system	Rotating basket containing dosage form / device	Impeller	Reciprocating cylindrical vessels	Peristaltic pump delivering sinusoidal flow of 240 - 960 $mL*h^{-1}$ at 120 ± 10 pulses min^{-1}.
Transparent	Y	Y	Y	Y
Temperature control	Y	Y	Y	Y
Absorption	N	N	N	N
Microbiota	N	N	N	N
Dynamic pH	Requires media dilution or vessel change	Requires media dilution or vessel change	Requires multiple media in different vessels	Requires operator to change pump source
Peristalsis	N	N	N	N
Relevant pressures	N	N	N	N
Human-derived cells	N	N	N	N

Table 2. Summary of compendial USP in vitro *dissolution apparatus and associated parameters that can replicate the GI tract. Y= yes; N = no*

1.3.2 Modified compendial apparatus to improve simulation of GI conditions

There have been adaptations to this standard apparatus to better replicate the GI environment.

2.2.2.1 Transfer models

To better simulate passage of a dosage form through the GI tract, a dissolution transfer model may be used to subject a dosage form to progressive region-specific environmental changes. A dissolution transfer model using USP apparatus was first described in 1999 [32]. In brief, a peristaltic pump was used to transfer dissolved drug within simulated gastric fluids into a USP dissolution vessel containing fasted state simulated intestinal fluid (FaSSIF) or fed state simulated intestinal fluid (FeSSIF) as the acceptor phase. The apparatus allowed both the transfer rates (0.5-9 $mL*min^{-1}$) and the agitation rate (50, 75 and 150 rpm) within the intestinal vessel to be adjusted [32].

A multicompartment dissolution system has been developed by modifying a conventional six-vessel USP dissolution system to include a "gastric" compartment, an "intestinal" compartment, and an "absorption" compartment [33]. The gastric compartment contained 250 mL dissolution medium (0.1 N HCl, pH 1.2) that is transferred to the intestinal vessel at a rate of 4.5 $mL*min^{-1}$; this rate was reduced to reflect slower gastric emptying in elderly patients with a rate of 3.1 $mL*min^{-1}$ [33]. In addition to fluid flow from the stomach to the intestine undissolved solids were also moved by washing with simulated intestinal media. The gastric vessel was stirred at 100 rpm with a paddle [33]. The “intestinal” compartment is linked to an absorption vessel to simulate the absorption by removing the dissolved drug where the flow rate between these vessels is adjusted based on the permeability of the compound under test [33]. The volume in the intestinal compartment is maintained at 510 mL by use of a reservoir; the media is FaSSIF at pH 6.5 [33]. The system is stirred at 100 rpm by a paddle apparatus [33].

The Biorelevant Gastrointestinal Transfer (BioGIT) model is a transfer model based on USP dissolution apparatus where fluid from the gastric compartment is transferred to the duodenal compartment. It has been shown to be useful for evaluating formulation performance particularly, after administration of conventional or enabling products of highly permeable drugs [34]. The gastric compartment consists of 250 mL FaSSGF (within a mini vessel of 500 mL) with stirring at 75 rpm [34].

2.2.2.1 Supplementary buffer systems

The use of bicarbonate buffer was introduced in 2003 by McNamara et al [35] and improvements on how to use this with standard dissolution apparatus were presented by Fadda et al (2009) [36] and further improved upon by Merchant et al (2014) [37].

The USP1 and USP2 were most commonly used for dissolution of orally ingestible dosage forms, however it was not possible to use the physiologically relevant buffer system. Therefore, Garbacz et al (2013) [38] investigated the pH shift caused by CO_2 loss in different bicarbonate buffer systems and reported that evaporated CO_2 can be partly substituted by sparging with gas mixtures, such as 5 % (v/v) CO_2 and N_2 [38]. Subsequently, the Physio-Stat was introduced, an automated device for monitoring and regulating the pH of bicarbonate buffers, developed using the USP2 dissolution apparatus system. The Physio-Stat is composed of a pH electrode, a gas diffuser, a digital microcontroller and a proportional valve system, driven by a bespoke software based on an AVR-GCC open-source platform.

Later, Garbacz et al (2014) [39] developed the Physio-Grad device, a robust system which enables a biorelevant simulation of intestinal pH gradients without changing the ionic strength of the solution. The Physio-grad system has been used by Zakowiecki et al (2020) [40]. Both the Physio-Stat and Physio-Grad can be used in non-pharmacopeial systems and may be applicable to various models of the small intestine and colon.

1.4 Microscale in vitro models for the development of milli-scale ingestible devices

Orally ingestible microdevices for gut engineering have recently been reviewed [10]. A range of orally ingestible micro or nanodevices have been developed which require interaction with the microenvironment for functionalization and could therefore benefit from the implementation of physiologically accurate in vitro models of the GI microenvironment.

Some features of the macroenvironment mentioned above may also be suitable for the development of ingestible microdevices which may function using aspects of both macro and microenvironmental GI conditions. For example, active ingestible micro or nanodevices can undergo chemical actuation under specific GI macroenvironmental conditions, such as pH, to trigger self-propulsion [41-47] and the delivery of a therapeutic payload to the epithelial microenvironment [41, 42, 45-47]. Due to the lack of such complex *in vitro* models, self-propulsion devices have been tested mostly in murine animal models to date [41-44, 48].

Ingestible microdevices can be passive, such as those containing drug reservoirs for administration of therapeutics, with the aim of achieving enhanced drug stability through protection against harsh GI conditions and improving targeting and uptake [49-59]. These devices must overcome difficulties faced by common dosage forms at the microenvironmental level, such as low drug permeability and retention at the epithelial surface, enzymatic degradation and shear forces due to peristalsis [56]. As such, *in vitro* epithelial models of the GI tract could be useful to test for device binding, mucoadhesion/penetration, and delivery of small molecules and cytotoxicity studies. The muco-adhesion mechanism of these passive devices can be determined by the choice of targeting ligand, and therefore cells expressing different phenotypes could be targeted for drug delivery using these devices. Typically, Caco-2 monolayer models in static Transwell plates have been used for the development of passive drug delivery devices in the past [49, 50, 52, 53, 56-59]. However, improved *in vitro* models would use primary cells from the specific region of interest, recapitulate the human mucosal environment, mimic peristalsis and luminal flow and produce an array of relevant drug-metabolising enzymes.

Several ingestible microdevices serve as sampling and biomolecular detection tools. Chen et al (2020) [60] developed an orally ingestible microdevice for site-specific microsampling of microbiota and protein biomarkers in the GI tract. Mimee et al (2018) [61] devised the ingestible microbio-electronic device (IMBED) to detect GI bleeding. These microsampling and molecular detection devices may benefit from advanced GI in vitro models that can express certain disease-relevant biomarkers. Therefore, this review will explore the disease states modelled by microscale GI models that may be suitable for future development of passive orally ingestible microdevices that target submicron-scale biomarkers and microbiota and/or interact with the epithelial mucosa.

1.4.1 In vitro models of the GI microenvironment

In vitro models of the GI microenvironment are valuable for the development of ingestible microdevices that interact with the epithelium in vivo. For example to deliver therapeutics. For example, ingestible nanostraw microdevices that adhere to epithelial tissue to deliver a tunable drug loading [58]. The epithelium differs along the GI tract, a vital driving factor in regional-specific functionality in terms of digestion and absorption [62]. The gastric epithelium has a simple columnar geometry, specialized for the secretion of hydrochloric acid and digestive enzymes. The mucosa of the small intestine adopts a villi-crypt microarchitecture to complement its absorptive function through a drastic increase in surface area; villi are finger-like projections whilst crypts are deep grooves introverted into the submucosa. The colonic mucosa is similar to that of the small intestine in that it is specialized for absorption and also lined with crypts, however there is a distinct absence of villi [63]. Another distinguishing feature between the small and large intestinal epithelia is the presence of highly specialized secretory Paneth cells in the small intestine, and the elevated abundance of mucous-secreting goblet cells in the colonic epithelium.

Most conventional in vitro models of the GI microenvironment are colorectal adenocarcinoma-derived Caco-2 and HT-29 cell lines cultured on porous, extracellular matrix coated membranes within Transwell insert culture devices. Caco-2 are an immortal human cell line of the colorectal adenocarcinoma; however, these cells are known to differentiate to resemble enterocytes when cultured as a monolayer. These static models are used primarily to study small intestinal barrier function or to model drug permeation and are highly standardised. However, although these cells have the capacity to perform the basic functions of native intestinal epithelial cells, they do not represent the cellular diversity of the intestinal epithelium and present a two-dimensional (2D) culture

format, failing to recapitulate the three-dimensional (3D) villus-crypt microarchitecture of the GI epithelium. Furthermore, other intestinal differentiated functions are absent such as cytochrome P-450-based drug metabolism and the ability to produce a significant mucous layer as these cells secrete the gastric mucin (MUC)5AC, but not MUC2 which is typical of the intestinal tract [64]. Additionally, these models cannot support the coculture of commensal microbiome with the epithelial cells as the bacteria rapidly overpopulate the system and contaminate the human cell cultures within one day. Therefore, static models do not accurately reflect human intestinal physiology. Static 2D models have been widely documented and are not included in this review.

To resemble the epithelium, an in vitro model should comprise many different cell types and be stable in culture media for long periods of time. Some static models of the small intestine have been developed that use 3D scaffolds to aid Caco-2 cells and organoids (see below) in achieving an in vivo representative 3D arrangement, which aids differentiation and increases physiological relevance.

The use of recognized cell lines provides advantages in experimental work that includes ease of access and the ability to compare the output data to that already presented in the literature. However, it is important to note that there can be limitations of such tests in that they do not reflect the diversity of the typical patient population, for example the sex of a cell line should be reported as this can change the results found [65-67]. Caco-2 cells are derived from a male whilst HT-29 from a female human donor [68].

1.4.2 Organoid models of the GI tract

GI epithelial organoids provide a more sophisticated in vitro model of the GI epithelium. Organoids are recently developed self-organising three-dimensional (3D) cellular cultivations embedded in a laminin-rich extracellular matrix and a medium containing specific supplementary growth factors to mimic the native extracellular environment. Compared with other primary cell cultures, organoids are advantageous in that they possess indefinite proliferative capacity in culture without incurring genetic aberrations or alterations and retaining characteristics representative of the original tissue. Organoids can also be stored cryogenically and subsequently thawed like traditional cultures. These models boast a wealth of drug metabolising enzymes, making them attractive for pharmacologic investigations and drug development with high potential for use in the development of ingestible devices. Organoids constitute a valued system to study epithelial mucosal biology and both normal and abnormal GI physiology. Additionally, organoids can replicate infection and disease since they develop according to the genome of the donor, genetic manipulation or bacterial/viral infection. For example, organoids can be modelled to develop cancers, allergic reactions or inflammatory diseases that result in the release of specific biomarkers that may be detectable by ingestible devices. Organoids modelling different regions of the GI tract typically share similar advantages and downfalls which are outlined by this section of the review, whilst sections 2.7, 3.7, and 4.7 highlight the current status of, and key diseases modelled by organoids for the stomach, small intestine and colon respectively. An example image of an organoid is shown in Figure 1, in part B a comparison to traditional monolayers is shown.

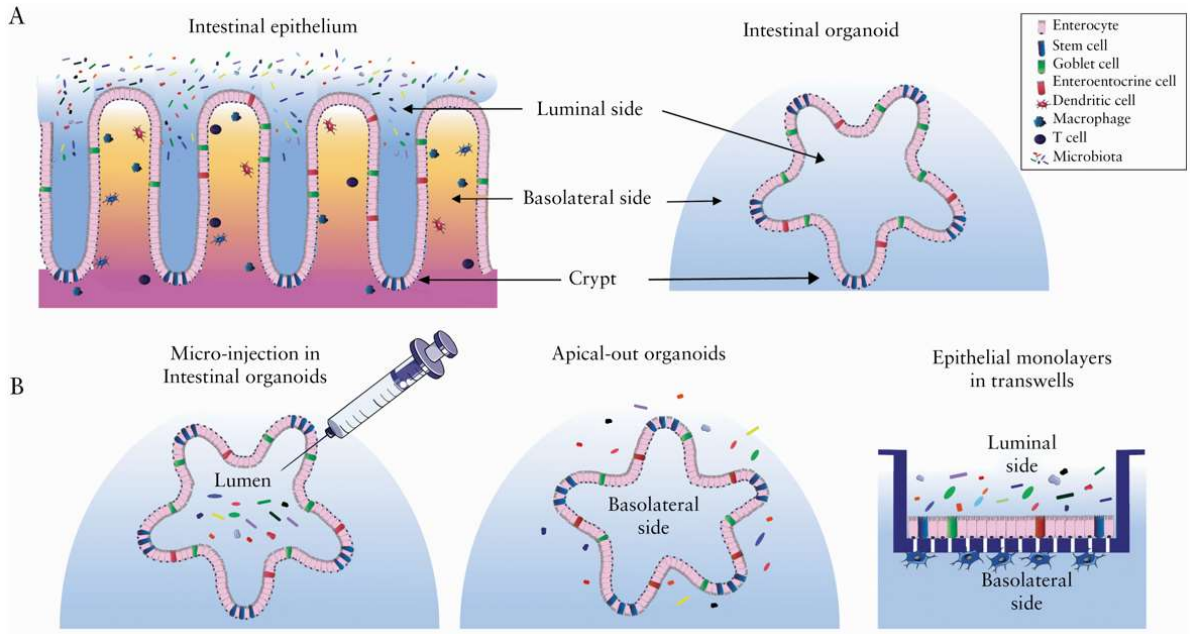

Figure 1. [A] The intestinal epithelium and the organoid model. [B] 3D organoids and organoid-derived models. This image is taken from [69] and was originally published in an Open Access article distributed under the terms of the Creative Commons Attribution License (http://creativecommons.org/licenses/by/4.0/), which permits unrestricted reuse, distribution, and reproduction in any medium.

All key regions of the upper GI tract have been modelled using murine organoids including the tongue [70], taste buds [71, 72], salivary glands [73] and oesophagus [74] [75]. Epithelial organoids derived from primary adult cells of the stomach, small intestine and colon are termed gastroids, enteroids (duodenum, jejunum and ileum) and colonoids respectively. Epithelial organoids form spheroid structures that recapitulate the characteristics of native tissue in a spheroid structure, enclosing a hollow lumen; for example, enteroids develop a folded epithelium with distinct crypts and villi. Similarly, epithelial organoids can be developed via in vitro differentiation of human embryonic stem cells (hESCs), both methods result in organoids comprising all intestinal epithelial cell types found in vivo, in similar proportions and arrangements. However, organoids lack certain elements of the complete organ such as mesenchymal tissue, immune and neural cells.

Induced intestinal organoids are mini-GI models derived from human induced pluripotent stem cells (hIPSCs) [76]. The differentiation protocol of intestinal organoids also promotes generation of mesenchyme. Therefore, induced intestinal organoids are considered more representative of in vivo intestinal conditions, however a longer period is required to generate them, and they remain devoid of immune cells which are necessary to address common intestinal diseases, such as irritable bowel disease (IBD).

Furthermore, several studies have demonstrated the functional orthotopic transplantation of murine [77] and human [78-82] GI organoid-derived monolayer epithelial tissue into mice, where they were observed to develop into mature tissues with morphological semblance of the original tissue [83]. This approach to manipulating organoids and animal models for use as advanced preclinical models may be valuable for the development of ingestible devices and is reviewed in more detail here [8].

Since human GI organoids develop goblet cells, they can produce a mucous layer offering an advantage as it is not currently possible to study intestinal mucous physiology within the living human colon and ex vivo tissue explants permit study over very short timescales (< 1 day). However, the mucus in organoids is trapped within the central lumen of their spheroid structure, making for difficult physiological investigation [64, 84]. The inaccessible lumen also prevents recreation of luminal fluid flow and peristalsis-like deformations and makes luminal drug and microdevice exposure challenging. Additionally, it is not possible to co-culture spheroidal organoids with other cell and tissue types, such

as endothelial cells and immune cells which are important for modelling inflammation and absorption pharmacokinetics.

To overcome this problem, organoids have been fragmented and cultured as a 2D monolayer. This permits apical access which would enable testing of performance testing of microdevices that target the GI mucosa. Additionally, basolateral access is also available, permitting the co-culture of other cell types, commensal microbiota and pathogens. An in-depth comparison of 3D cell culture models and their planar counterparts has been written by Gupta et al (2016) [85].

1.4.3 Organ chip models of the GI tract

Organ-on-a-Chip systems are recently developed microphysiological systems that leverage the manufacturing technology behind computer microchips to create a microfluidic device in which GI-derived epithelial cell culture can take place. Similar to organoids, the advantages and downfalls of these models are typically applicable to all modelled GI regions, therefore these are outlined here, whilst progress in the fields of the stomach, small intestine and colon is presented in Sections 2.7, 3.8 and 4.8 respectively. Other recent reviews of GI organ-on-a-chip models are available [86, 87].

Generally, these models function around two microchannels; one lined with epithelial cells, representing the intestinal lumen (apical) and the other representing a blood vessel (basal). The mimic lumina are typically separated by a flexible, semi-permeable membrane that simulates the barrier between the intestinal lumen and intestinal vasculature, permitting the exchange of soluble molecules between channels. Media is pumped through each channel to replicate the dynamic in vivo environment. Some microfluidic chip models include neighboring channels lined by a confluent layer of microvascular endothelial cells, commensal microbes, immune cells and pathogenic bacteria. Some models also permit the application of cyclic mechanical forces to exert deformation patterns matching in vivo contractile activity. The chip housing permits the integration of elements such as sensors, electrodes or valves. Furthermore, the housing is typically optically transparent to facilitate analysis through light, fluorescence and confocal microscopy. Media samples can be withdrawn to allow assay for drug concentration, dissolved O_2, metabolites, pH and signaling molecules. Human gut-on-a-chip models are typically fabricated from flexible, clear PDMS, allowing for real-time optical imaging of cells, with the additional benefit of low cost. However, this surface also absorbs small hydrophobic molecules which could be problematic for the introduction of microdevices. A diagram of the duodenum-intestine-chip in Figure 2 illustrates the typical setup of an organ on a chip device.

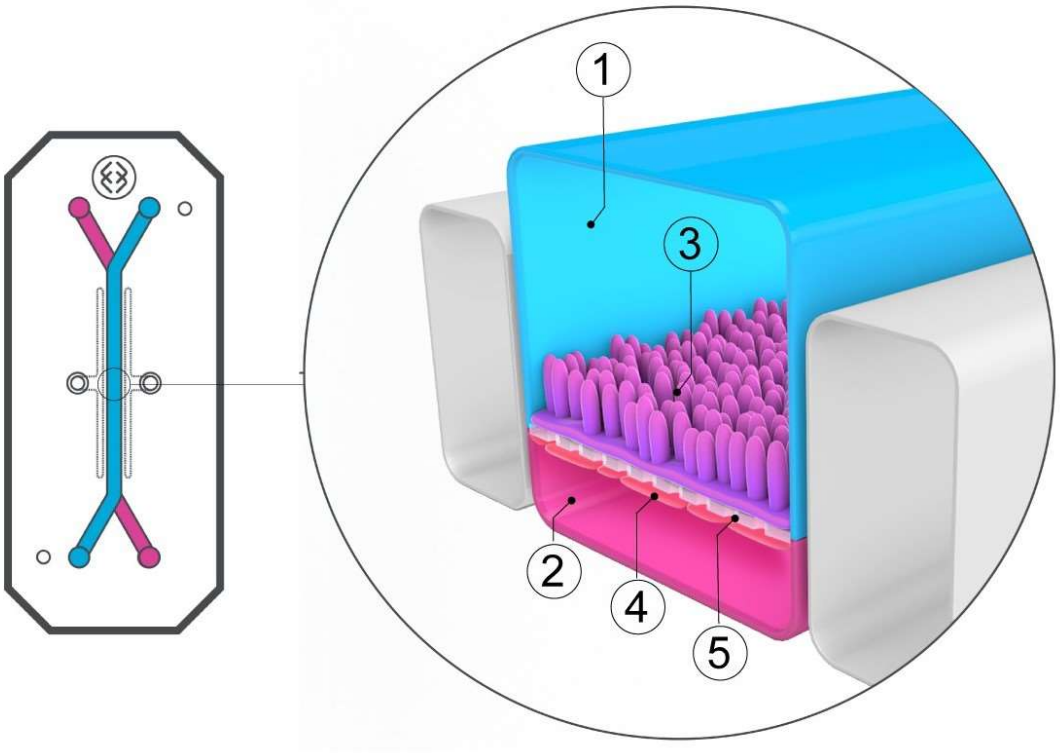

Figure 2. Schematic representation of a Duodenum Intestine-Chip, including its physical macro appearance from the top (left) and vertical section (right) showing: the epithelial (1; blue) and vascular (2; pink) cell culture microchannels populated by intestinal epithelial cells (3) and endothelial cells (4), respectively, and separated by a flexible, porous, ECM-coated PDMS membrane (5). Image taken from [88]

Most in vitro studies have simply placed passive microdevices on the apical face of a Caco-2 monolayer or simply rocked well plates back and forth to distribute microdevices [52, 53, 57, 59]. However, the ability to sustain flow and peristalsis in the apical chamber of organ chip models may present a more physiologically relevant model of the in vivo scenario. Most gut-on-a-chip models use Caco-2 cells where apical flow and mechanical deformation has been shown to promote morphogenesis of the characteristic villus-crypt microarchitecture of the human intestinal epithelium leading to differentiation into absorptive, goblet, enteroendocrine and Paneth cells [89]. Since goblet cells form, the cells also produce MUC-2, which has been shown to vary according to luminal flow rate [90, 91]. Additionally, Caco-2-seeded organ chip models have been shown to support microbiota in co-culture [90]. However, most other previously described drawbacks of using adenocarcinoma-derived cells persist. More recently, cells from fragmented epithelial organoids have been cultured inside microfluidic chips to harness advantages from both technologies. When cultured inside organ chip technology, many benefits are realized over the use of organoids alone. Gut Chips enable the co-culture of a complex microbiome in direct contact with intestinal epithelial mucosa, whilst experiencing luminal flow and peristaltic motion. Of paramount importance, is that this approach allows for both apical and basal access to the organoid, which isn't possible when an organoid exists in its typical spheroid structure. The ability to access continuously flowing apical and basal channels may provide an opportunity for the introduction of microdevices. Organ-on-a-Chip technology therefore holds great potential for the development of ingestible microdevices, as previously suggested in a review by Mandsberg et al (2020) [10]. Particularly the use of organoid-based microfluidic chip models in the development of patient-specific microdevices. This may also benefit from the implementation of high-throughput chip systems [92]. However, correct representation of the GI wall remains an issue due to lack of supportive tissue structures and diverse cell types.

The possibility exists for more complex systems to be developed by combining different organs on chips. Choe et al (2017) [93] created a first-pass metabolism gut-liver microfluidic device. Furthermore, body chip systems are connecting multiple organ chip systems to explore inter-organ connectivity [94].

2 Replicating the gastric environment

2.1 Overview of gastric function and anatomy

The human adult stomach is formed from distinct anatomical regions, the fundus and proximal corpus regions function as a flexible reservoir for food intake with the distal corpus and antral regions control mixing and emptying [95]. The exit from the stomach, the pylorus, is easily recognised as a ring of muscle that marks the transit from the stomach and duodenum (the pyloric sphincter is part of the anatomy of the stomach rather than the duodenum). The pyloric sphincter controls the exit from the stomach and has been measured to be 12.8 ± 7 mm in a healthy adult [96, 97].

One of the functions of the stomach is to grind food into smaller particles and mix them with gastric fluid (pepsinogen autoactivated in the presence of luminal acid) so that they can be passed through the pyloric sphincter. It does this by physically generating hydrodynamic flows and cyclic compressive forces and chemically by the breakdown of protein into peptides due to the presence of enzymes.

The adult human stomach has an approximate length of 20 cm and diameter of 15 cm [98]. The overall capacity of the stomach has been reported to be 1.5 L [99].

The stomach mucosa is folded into ridged structures called rugae. Gastric absorption is limited by the relatively low epithelial surface area of approximately 0.1 m^2 [98]. The structure of the stomach epithelium is dominated by surface mucosal cells rather than absorptive cells. Functionally, the gastric mucosa is divided into acid and pepsinogen-secreting mucosa in the corpus and fundus and non-acid secreting regions [100].

Surface mucosal cells secrete a thick mucous layer. The adherent mucus layer has been reported to have a mean thickness of 180 µm, with a range of 50-450 µm [101-103], which upon hydration forms two distinct layers on the gastric epithelium.

2.2 Gastric fluid volume

The human adult stomach volume varies depending on the fed/fasted conditions. Between meals, gastric secretion in the average adult is relatively low, producing an average of 4 $mEq*h^{-1}$ (25 mL of pure gastric juice) [100]. In normal subjects, the integrated secretory response to a steak meal is about 90 to 100 mEq over 3.5 hours, equivalent to approximately 650 to 700 mL of gastric juice [104].

Measurement of gastric residual volume has been reported for patients at risk of broncho-aspiration, most likely those in critical care. These patients are usually fasted or fed via enteral feeding and as such the data is not always relevant for healthy adults. There are reviews on this topic with gastric residual volumes typically being 0.3-2.8 $mL*kg^{-1}$ (e.g. [105-107]).

Gastric volumes are of interest in drug product performance as many drugs have poor solubility thus low gastric or intestinal volumes can hinder absorption and subsequent exposure. For example, the absorption of cefteram-pivoxil was significantly reduced when administered with 30 mL of water compared with its absorption when administered with 150 mL of water in a study in healthy adults [108]. Several studies have measured gastric volumes in the fasted state using magnetic resonance imaging (MRI) and the data are shown in Table 3.

			Volume (mL)		
Reference	**Health status of participants**	**Number of volunteers**	**Min**	**Max**	**Mean (standard deviation)**
[109]	Healthy	12	13	72	45 (18)
[110]	Healthy	12	103	149	122
[111]	Healthy	8 8			153 (41) 129 (46)
[112]	Healthy	12			35 (7)
[113]	Healthy	12	4	65	31 (20)
[114]	Healthy	6			26 (14)
[115]	Healthy	6 6 6 6			23 (36) 24 (19) 17 (12) 26 (24)
[116]	Healthy	8 8 120			15 (8) 33 (23) 25 (18)
[117]	Oral intake of one Norvir tablet (100 mg ritonavir)	5			37 (12)
[117]	Oral intake of one Norvir tablet (100 mg ritonavir) preceded by once daily dose of esomeprazole for 3 days	5			20 (15)

Table 3. Adult gastric fluid volumes reported in adult subjects as determined by magnetic resonance imaging (MRI) under fasted condition

In the fed state the gastric volume increases with values of 579.6 ± 38.1 mL reported 15 minutes post ingestion of the FDA breakfast [113] yet this is a mix of food and fluids. Measurement of the gastric volume in the fed state is subject to variability in terms of the meal used to induce the fed state thus comparison across studies is complex.

2.3 Gastric media composition

Characterisation of gastric fluids to better understand drug absorption was first reported in 1997 where gastric pH; bile acid and protein concentration were measured [118]; surface tension was measured in a similar study [119]. Later studies to characterise in vivo gastric fluid added buffer capacity and pepsin activity to the aspects to be characterised [120]. Further studies included assessment of lipase activity, viscosity and surface tension. A summary of the data on the properties of fasted gastric fluid is presented in Table 4.

Reference	No of participants	pH	Osmolality ($mOsm*kg^{-1}$)	Buffer capacity ($mmol*(L*pH)^{-1}$)	Surface tension ($mN*m^{-1}$)	Protein content ($g*L^{-1}$)	Bile salt conc ($mmol*L^{-1}$)	Pepsin Concentration ($mg*mL^{-1}$)
[121]	19	2.5 (± 1.4)	220 (± 58)	14.3 (± 9.5)	34.8 (± 5.2)	4.9 (± 1.0)	0.33 (± 0.31)	
[118]	24	2.9 (± 1.97)	191 (± 36)			1.8 (± 0.7)	0.2 (± 0.5)	
[120]	20	Range: 1.23–7.36	140	Median 18	45.7		<0.5	0.22
[119]	8	Range: 0.8-4.7			Range: 33-43			
[122]		2.50 Range: 1.1-7.47		4.23 (± 3.6)				
[123]	8	Median (range) 1.4 (1.2–2.7)	144.0 (± 44.0)	27.6 (± 15.7)	43.22 (± 0.74)	0.71 (± 0.35)	Median (range) 0.054 (0-0.620)	
[124]	9	2.8 (± 1.1)	221 (± 15)		33.6 (± 5.9)		0.82 (± 0.57)	

Table 4. Data on parameters characterised from human gastric fluid to generate simulated gastric fluid to evaluate drug product performance. Data shown are mean (± standard deviation) unless otherwise stated.

The composition of gastric fluid changes upon ingestion of food. Characterisation of the fluid has typically been conducted in the fasted state, following a glass of water or following administration of standardised meals to generate data to enable production of a representative simulated fluid. However, it should be noted that the nature of the food ingested will dictate much of the contents in the fed state and this is inherently variable both inter and intra-individually. Characterisation of the gastric contents provides information upon which simulated media can be developed. A major difference in the fasted and fed gastric media is the pH which is lower in the fasted state with typical values shown in Table 4 whilst the range in the fed state is around 3.5 at 60 minutes after a meal [113].

Detailed characterisation of gastric media composition in the fed state is complicated by the nature of the food ingested as well as the timing of the sampling to mimic digestion. Studies that have characterised the composition of gastric fed media are listed in Table 5.

Reference	Fed conditions	Parameters measured	Time points
[125]	Standard high-calorie, high-fat meal	pH, buffer capacity, lipid content, bile acid content, and viscosity Osmolality, lipid content and bile acid content in the aqueous phase of the gastric contents	45, 105, 165 and 225 minutes post ingestion
[122]	A liquid meal. Two cans of Pulmocare (total volume of 474 mL, containing 29.6 g of proteins, 44.2 g of fat, 25 g of carbohydrates, and a total amount of 710 calories)	pH, buffer capacity	0, 15, 30, 45, 60, 90, 120, 150, 180, 240, 300, 360, 420 minutes post ingestion
[126]	500 mL Ensure plus®	pH, buffer capacity, osmolality, total protein content	30, 60, 120 minutes post ingestion
[120]	500 mL Ensure Plus® (Abbott Laboratories B.V., Zwolle, the Netherlands). One portion 200 mL (Ensure plus) has an energy content of 300 kcal of which lipids, carbohydrates and proteins constitute 29%, 54%, and 17%, respectively.	pH, buffer capacity, pepsin activity, protein content, osmolality, surface tension	30, 60, 90, 120, 150, 180, 210 minutes post ingestion

Table 5. Studies that have characterised the composition of gastric fed media

A recent UNGAP review on GI variability associated with drug absorption is available as a further resource for the reader [7]. In addition there is a detailed review on the variation in GI lipases, pH and bile acid levels associated with food intake, age and disease [127].

2.3.1 Simulated gastric media

USP simulated (fasted) gastric fluid has been used since the 1960s; this contains 3.2 g pepsin; 2.0 g sodium chloride and 7.0 mL HCl per litre to provide a pH of 1.2. Limitations in USP SGF were recognised in the 1990s and alternative simulated gastric fluids were proposed to better mimic the in vivo conditions. Fasted state simulated gastric fluid (FaSSGF) was first reported in 2005 and was developed based on a comprehensive literature search [128] to identify and replicate the most relevant aspects of gastric fluid. Further work was conducted to compare drug solubility values in FaSSGF with aspirated fasted gastric fluid from both dogs and humans where a good correlation was noted [129]. Details on the composition and manufacture of FaSSGF can be found here [130]. The pH of FaSSGF is 1.6 to reflect the mean data from clinical studies [128].

Simulation of fed gastric fluid is more complex due to the variability in food components. In drug research homogenised FDA breakfast has been used as well as milk [131] and Ensure® plus [29]. Fed state simulated gastric fluid (FeSSGF) was introduced in 2007 [132]; this comprised three alternative fluids to represent the early; middle and late stages of the fed state with a pH range from 3-6.4. An alternative to FeSSGF is available commercially, FEDGAS™ (Biorelevant.com). FEDGAS™ contains 62.5 g of fat and carbohydrate per 900 mL to match that in the partially digested high fat FDA breakfast. The suppliers of FEDGAS™ (Biorelevant.com) stated that the fat content is too low in FeSSGF and the stability of FESSGF can complicate analysis.

Simulated gastric media used in food research to mimic digestion was subject to immense variability. A recent EU initiative (INFOGEST) sought to harmonise in vitro digestion methods [133]. The simulated gastric fluid within this protocol contains electrolytes, pepsin and gastric lipase and bile [134].

In summary there seems to be agreement on the media to use to replicate the fasted state yet there are multiple media that can be used to simulate the fed state; it is important to recognise the differences in these media and to select the most appropriate for the system under evaluation, or to select a model that allows dynamic changes in the media to better reflect the in vivo data on the composition of gastric media in the fed state. There may also be a need to include a solid component within the model rather than a liquid to better mimic the fed state.

2.4 Gastric motility

The stomach has three muscle layers: an inner circular layer; a middle longitudinal layer, and an outer but incomplete oblique layer. These muscle layers provide motility to the stomach. The motor function differs by region, the fundus relaxes as fluids and solids enter the oesophagus, and further as food enters the funds, a process known as adaptive relaxation [100]. This response allows the liquid to pool in the fundic pouch while the solid components of the meal remain in the mainstream of flow toward the pylorus. The corpus and antrum work together to provide a coordinated propulsion of the luminal contents towards the pylorus. The pylorus itself, remains open in anticipation of the wave of peristalsis where it acts as a sieve. However, the pylorus closes as the peristaltic wave hits the site to act as a barrier causing contraflow and mixing where the chyme is digested by enzymes prior to transfer to the small intestine.

The Magenstrasse is the term used for a phenomenon observed in vivo where gastric contents, rather than antral emptying, passes from the fundus along a ribbon-like pathway (the Magenstrasse) through the centre of the antrum and (via the pylorus) directly into the small intestine [135]. It is important that the motility is replicated in models, this may also include replication of the Magenstrasse to replicate gastric emptying of solids and liquids.

In the fasted state gastric motility is controlled by the interdigestive Migratory Motor Complex – the MMC. The MMC is a peristaltic contraction starting from the gastric midcorpus region and subsequently migrates along the gastric wall, increasing in propagation velocity and amplitude to the pyloric sphincter. The MMC can either stop at the upper part of the small intestine or travel all the way to the colon. The MMC is a four-phase, continuous cyclical pattern, each phase differing in contraction frequency and amplitude. Gastric motility is characterized by tonic contraction in the proximal areas and peristaltic muscular contractions in the distal region. The result of these muscular

contractions is to churn the ingested contents towards the pyloric sphincter and generate hydrodynamic conditions, that serve to mix gastric contents and reduce the size of ingested materials. There are four phases of the MMC in the stomach with a total cycle length of 85-120 minutes [16]; this is summarised in Table 6 taken from [16].

Phase	Characteristics	Percentage of cycle length or actual time
I	Resting/quiescent period, little to electrical activity, spike potentials occasionally	40 – 60%
II	Irregular contraction, low amplitude (up to 40 mmHg or 5.3 kPa), irregular spike potential	20 – 30%
III	Regular movement, regular rhythm, at spike potential, contractions are strong (up to 80 mmHg or 10.7 kPa)	3 – 6% (4 – 6 min)
IV	Transition period, regular declining (some researchers include this phase in Phase III)	< 12% (15 min)

Table 6. Description of the four phases of the MMC in the stomach, information based on [16]

The contents of the stomach are subject to fluid motion that exerts disruptive forces on the surfaces of ingested solid objects, resulting in shear stresses from forces acting parallel to the surfaces and normal stresses from forces acting perpendicular (or normal) to the surfaces. Replication of these shear and normal stresses in model systems and the rate at which they are applied is complex.
For further details on GI transit time the reader is referred to [8, 136].

2.4.1 Gastric emptying

The exact mechanism of how gastric contents are emptied is complex as this can depend upon the volume, buffer capacity, viscosity and caloric content of materials ingested. Liquids will ordinarily empty faster than solids, and smaller objects faster than larger [137]. Further details on gastric emptying can be found in [8] where there is a full discussion on gastric emptying rates and how this relates to ingestible devices.

2.5 In vitro models of the stomach

A brief outline of in vitro models that incorporate a gastric environment is presented in the order in which they were published, the relative attributes are also compared in Table 7.
The evaluation of the in vitro models was based on criteria associated with the features of the macroenvironment that were presented in Table 1. The evaluation of the biorelevance of the luminal media was based upon factors associated with the luminal composition used within the system. These were scored using the levels of simulation of luminal composition that have previously been reported [138, 139]. These levels are: level 0 is pH only; level 1 is pH plus buffer capacity; level 2 includes bile components, dietary lipids, lipid digestion products and osmolality (this includes FaSSGF) and level 3 also includes dietary proteins, enzymes (not digestion products) and viscosity effects. The ability to adjust the composition of this media via dynamic secretions during the test was also included as a marker of biorelevance; this was scored 1 if dynamic secretions were possible and 2 if these secretions were automated and responsive by the system under test according to an internal feedback mechanism. The volume used within the system was considered to be biorelevant where the volume was less than 150 mL in the fasted state and in the region of 500 mL where the system was replicating the fed state; biorelevant conditions scored 1 where as non-biorelevant scored 0. An overall score for 'biorelevance of luminal media' is given as the sum of the scores for the 3 previous criteria.
The representative anatomy provides details of the shape and dimensions of the compartment used to mimic the stomach; where these were broadly similar to the dimensions of the stomach they scored 1 and where the dimensions were accurately mimicked they scored 2. The presence of a pyloric sphincter within the model provided a score of 1 for the biorelevance and a score of 2 if the dimensions matched those found in vivo. The overall score for the biorelevance of the anatomy was the sum of the scores for the representative anatomy and the pyloric sphincter.

The level of biorelevant motility score comprised the components of the agitation mechanism and pattern of agitation. Where the mixing mechanism applied was consistent with mixing in the stomach, via compression of the walls of the mixing vessel a score of 1 was applied. The pattern of agitation scored 1 for discontinuous mixing and 2 where the profile of discontinuous mixing matched that reported in vivo. Where the pressures matched those in vivo a score of 1 was awarded to the model. The overall score for the biorelevance of motility was the sum of the scores for mixing mechanism, pattern of agitation and pressures. The gastric emptying or transit time was recorded and this scored 1 where it was aligned with in vivo data and zero where it was not.

2.5.1 Standardised digestion models

There are many in vitro models that have been developed to replicate digestion, particularly within the gastric environment. There have been recent efforts to standardize methods [13]. The pH-stat lipolysis model is a frequently used digestion model which comprises a single or two-step thermostatic chamber. The gastric digestion phase is simulated gastric fluid with gastric enzymes (pepsin and gastric lipase) [140]. The mixing is undertaken via an overhead paddle which does not replicate physiological mixing as evidenced from the information provided in section 2.4.

2.5.2 SHIME

The simulator of the human intestinal microbial ecosystem (SHIME) was developed by Molly et al (1993) [141], the reactor simulating the stomach was added in 1996 De Boever et al (1996). The stomach model can simulate food uptake and digestions and mimics the composition within the stomach in a dynamic way. The vessel is not designed to mimic the stomach anatomy and the mixing is generated via a magnetic stirrer. The volume of the stomach section is 0.2 L and the pH from 2.0-2.5 with a transit time of 2 hours [142]. The gastric compartment is fed three times daily to replicate three meals in human eating patterns and the media used is a mix of complex carbohydrate and protein sources with addition of mucins, minerals and vitamins [141]. The pH within the gastric compartment or the gastric emptying rate can be controlled to follow a predefined profile [143].

The gastric environment, specifically the time taken for the pH to increase following ingestion of formulated antacid tablets has been evaluated within the SHIME apparatus [144]. SHIME has been commercialized by ProDigest where access to the equipment is managed by their team.

2.5.3 TIM-1 Gastric compartment

The TIM-1 system is a multicompartmental, dynamic, computer-controlled system that simulates the human GI tract. The focus of the apparatus is the dynamic control of the intestinal media within each compartment. Each compartment is made from a flexible silicone membrane secured within a waterfilled outer jacket maintained at body temperature. The transit is then regulated by opening or closing the peristaltic valves that connect the compartments [145]. The gastric conditions of infants and adults with fast and slow GI transit have been modelled [145].

The TIM-1 apparatus has been used to evaluate the survival of probiotics in a capsule within capsule (Duocap®) ingested device [146]. The ability to directly observe the disintegration of the capsules within the gastric compartment was noted as a useful feature of the TIM-1 apparatus in this particular study [146].

TIM-1 has also been reported to have been used to optimize the composition of an enteric coating as well as the thickness that should be applied to a probiotic ingested tablet [147]. This study also permitted an alteration in the GI conditions to replicate an elderly as well as a healthy adult population to ensure that the results observed are relevant to the appropriate patient population [147]. TIM has been commercialized by The TIM Company where access to the equipment is managed by their team, although the apparatus is available for purchase and exists in some large pharmaceutical companies.

2.5.4 Artificial stomach duodenal model (ASD)

This apparatus is a transfer model where the gastric and intestinal compartments are adjacent to one another and fluid is transferred from one vessel to the next using a peristaltic pump. The main use of this is to explore the risks associated with physical chemistry processed, for example precipitation, upon transfer from the stomach to the small intestine [148]. The original paper that described this

model replicated both fasted and fed conditions within a dog and as such the fluids volumes and composition were designed to mimic a dog rather than a human.
This apparatus has also been used to mimic dosing conditions; specifically the coadministration of capsules co-formulated with Captisol (10% drug load) with Sprite as a co-administration vehicle [149].

2.5.5 Dissolution Stress Test device

This apparatus is designed to expose a dosage form to a sequence of movements, pressure waves and phases of rest to mimic in vivo conditions [150]. It is based on a USP dissolution apparatus where in place of a paddle or basket there is a novel mixing unit housed at the surface of the vessel. This unit is designed to hold the dosage form and apply stresses to the surface whilst exposing the unit to fluid for periods of time and having periods of time where the dosage form is not submerged within the dissolution fluid to mimic in vivo motion. The apparatus combined aspects of both gastric and intestinal physiology in a single unit; the pressure matches gastric emptying yet the fluid is simulated intestinal fluid [150].
Specifically the motility was designed to match gastric emptying which included three pressure waves (6 seconds duration, duty cycle of 50% and a fortitude of 300 mbar) [151]. In addition, the rate of tablet transport observed in humans was replicated during gastric emptying with velocities that ranged from 15-60 $cm*s^{-1}$. This apparatus was used to consider the rate of release for erodible modified release where the stresses on the surface of a tablet can control the rate of erosion [150, 151]. The pre-conditioning of the tablet using in vitro methods can be important when assessing the performance in the large intestine where the drug load is designed to be released.

2.5.6 Human gastric simulator (HGS) Riddet Institute, New Zealand

The motility in the HGS is provided by a system of rollers to create peristaltic contractions on 4 planes around a latex stomach [152]. The latex stomach chamber does not reflect the anatomical shape of the human stomach but provides a flexible chamber such that the motion applied mimics that within the in vivo stomach [152]. The stomach chamber has a diameter of 10.2 cm and a length of 28 cm [153]; however the bottom end of the cylinder is tapered to reduce the exit diameter to 2.5 cm. A thin polyester mesh with a pore size of 1.5 mm is used during experiments to mimic the size of particles that can pass through the pyloric sphincter [153]. The maximum force recorded was 3.39 ±0.95 N which was considered to be representative of in vivo forces [153]. The fluid used in this system was SGF containing pepsin and the flow into the stomach model of this fluid was controlled as well as the exit flow. The motility applied to the stomach model was set at a frequency of 3 contractions per minute to match in vivo data. This model has predominantly been used to understand the digestion of functional foods and the bioaccessibility of nutrients.

2.5.7 FloVitro dissolution system

The FloVitro system includes a gastric and small intestinal chamber and an additional third compartment connected to the small intestinal component that is intended to function as an absorptive compartment [154]. This apparatus was mainly focused on small intestinal absorption yet the gastric compartment is included to evaluate the effects of transfer. The system was used to compare the performance of hard gelatin capsules [154].

2.5.8 Chen et al (2011) In vitro digestion model

A hemispherical vessel, similar in shape to a USP1/2 dissolution vessel was used as the basis of a model for gastric mixing. In this system a spherical probe was used to create mixing where the probe was moved in a vertical plane, rather than rotating as within the USP dissolution apparatus [155]. The rationale for this apparatus was that probe movement relative to the wall of the vessel creates a similar flow pattern to that of the contraction waves of the stomach wall [155]. In this model the simulated gastric juice contained: pepsin (1 $g*dm^{-3}$); mucin (1.5 $g*dm^{-3}$), and NaCl (8.775 $g*dm^{-3}$), and pH 1.3 to 1.5, adjusted using HCl. This model demonstrated that factors that influence gastric digestion (such as digestion time, pepsin concentration, food to gastric juice ratio, shearing action and hydrodynamic flow) could be monitored as useful indices for the characterization and quantification of digestion processes [155]. This model has been proposed for use in studies that measure the kinetic process of gastric digestion under well controlled conditions.

2.5.9 Dynamic gastric model

The Dynamic Gastric Model (DGM) was developed to address the need for an in vitro model which could simulate both the biochemical and mechanical aspects of gastric digestion in a realistic time-dependent manner [156]. The systems has a feedback pH sensor to provide real time adjustments to reflect gastric acid flow rate; enzymes secretions in response to pH and food bolus; temperature controls; a dynamic pyloric sphincter that allows exit of material; Dynamic mixing to reflect gastric contractions that can be adjusted based on meal viscosity and particle sizes [156]. The physical forces within the DGM differ with the fundus/main body being subjected to rhythmic squeezing (0.05 Hz) and the antral part higher shear forces. The DGM has been shown to have value in pharmaceutical research predominantly to understand the performance of dosage forms (eg [157-159]) rather than ingestible devices. Studies have been conducted to better understand the survival of probiotics in the stomach [160] and to compare the performance of capsule shell materials [159].

2.5.10 Dynamic in vitro rat stomach system (DIVRS)

The rat is a commonly used preclinical species to evaluate digestion; thus an in vitro system based on the rat stomach is of value. This model mimics the shearing and pulsing motion within the rat stomach using a silicone flexible structure that is based on the anatomy of a rat stomach [161]. The internal fluid composition was managed using inlet and outlet tubes and the motion via a mechanical system of angled plates that acted on the exterior of the silicone stomach [161]. The frequency of the applied contraction force was 1.6-2 times per minute based on prior literature [162]. The amplitude and rate of contractions could be changed within this system [161]. This model was adapted to include a rolling extrusion motility pattern which improved the correlation between this in vitro model and in vivo data [163]. A further advance to this model was the use of a 3D printer to generate the silicon stomach structure which improved the uniformity of the wall thickness and hence the reproducibility in the motion applied [164]. This model would be suitable to assess the transit of devices through a rat stomach due to the considerable efforts made to replicate the anatomy and motility.

2.5.11 Dynamic Gastro-intestinal Digester (DIDGI)

The DIDGI® system consists of two consecutive compartments simulating the stomach and the small intestine. This model was built in order to monitor the deconstruction and the kinetics of hydrolysis of the food occurring during a simulated digestion. A PTFE membrane with 2 mm holes is placed before the transfer pump between the gastric and the intestinal compartment to mimic the sieving effect of the pylorus in human [165]. This model can accurately control the composition of the luminal media by controlling secretions in response to pH sensors. The flow rate into and out of the gastric compartment is also closely controlled and can be varied to mimic a range of patterns. This model has been used primarily for digestion studies and has been correlated to studies conducted in pigs [166].

2.5.12 SIMulator of the GastroIntestinal tract SIMGI

The SIMGI comprises of five compartments (units), simulating the stomach, small intestine and the ascending, transverse and descending colon regions [167]. The stomach compartment is formed of a flexible silicon tube that is housed within plastic where water flow provides peristaltic motion to the flexible wall [167]. The major focus of this apparatus is the colon sections rather than the stomach. The media used within the stomach contained gastric electrolytes and enzymes and the pH is controlled. The system can operate in a fed state where the pH following the meal can follow a predetermined protocol. Most of the work conducted on this model has been related to digestion with a focus on screening and development of pre- and probiotics. SIMGI has been commercialised by the Institute of Food Science Research in Spain and they offer services where products can be evaluated using this system for a fee.

2.5.13 Rope-driven in vitro human stomach (RD-IV-HSM)

This model incorporates a flexible silicone gastric body that is modelled on an actual human specimen [168]. As well as mimicking the dimensions of an adult stomach the surface characteristics of the internal lumen are recreated to include the rugae observed in vivo [168]. Despite matching the anatomy of a human stomach this model did not accurately mimic the pyloric sphincter. Multiple input tubes are incorporated into the model to simulate the role of gastric secretory glands. Motility is

generated via a rope that is wrapped around the body of the stomach where the frequency of contractions matches that found in vivo [168]. The maximum antral force achieved within the system was 3.37 ±0.59 N which matches human values and is sufficient for grinding of food [168]. The anatomy and motility are the strengths of this model that mimics human digestion and it has been shown that this model replicates the lag phase on solid emptying yet it may not reproduce the gastric sieve effect [168]. The accurate replication of the anatomy, morphology and motility would make this a useful model to evaluate the gastric retention of ingested devices and their stability (if retained) in biorelevant gastric media.

2.5.14 Engineered Stomach and small INtestine (ESIN) model

The ESIN model is a multi-compartmental system that is composed of six successive compartments: a meal reservoir; a salivary ampoule; the stomach and the three parts of the small intestine [169]. The stomach compartment is housed in a cylindrical compartment where pressures are applied from each end; the pressure applied is adjusted based on an integrated pressure sensor within the gastric compartment [169]. This model offers advantages to other multicompartmental models as it provides a tool to assess the swallowing function and "ingestion" of food. The gastric emptying follows a two-phase profile where only particles smaller than 2 mm can exit the gastric compartment replicating in vivo data [169]. The impact of differential gastric emptying of solids and liquids can be evaluated in this apparatus, particularly in terms of how this may affect the performance of oral medicines (eg paracetamol and sustained release theophylline) where an in vitro in vivo correlation was demonstrated [169].

2.5.15 Dynamic Gastric Simulating Model (DGSM)

The DGSM is formed from a cylindrical vessel with a truncated cone at the lower end, the total capacity is 300 mL [170]. Motion is applied in the vertical plane at a frequency to match in vivo data. The exit is restricted to particles smaller than 2 mm in size to match the pyloric sphincter closed size reported for adults. Inlet and outlet tubing controls the media within the vessel and the gastric emptying rate for the apparatus [170]. The DGSM incorporates compressive forces to disintegrate food, mimics continuous gastric emptying, and simulates gastric secretions that generate pH profiles similar to those of the human stomach. This model was used to evaluate the efficacy of supplementary enzymes in assisting food digestion and is a useful tool to study enzyme activity under dynamic physiologically relevant conditions [170].

2.5.16 In vitro mechanical gastric system (IMGS)

This system is formed from a 3D printed flexible stomach compartment that incorporates realistic morphology and dimensions (900 mL volume capacity) [171]. The system includes a J-shaped stomach, a mechanical system with realistic peristaltic frequency and force magnitude, and a reproduction of the gastric pH curve. Motility was controlled using 8 pistons arranged around the gastric compartment to replicate forces taking into consideration the relevant force by region of the stomach. The model was used to evaluate the impact of a more realistic gastric peristalsis on the intestinal lipolysis of protein-stabilized O/W emulsions, This model showed good correlation to in vivo force data, particularly peristalsis [171]. There is no transit within this model as it is a closed system.

2.5.17 Biorelevant Gastrointestinal Transfer (BioGIT) model

This model is a transfer model based on USP dissolution apparatus where fluid from the gastric compartment is transferred to the duodenal compartment. It has been shown to be useful for evaluating formulation performance particularly, after administration of conventional or enabling products of highly permeable drugs [34]. This model can accurately replicate the composition of intestinal fluid and the rate of transfer can be controlled yet there is no attempt to mimic the motility within the stomach in this apparatus.

2.5.18 TIM Advanced gastric compartment (TIMagc)

The TIMagc has been demonstrated to simulate gastric anatomy, motility and physiology. The apparatus comprises 3 parts: the gastric body, proximal antrum, and distal antrum [172]. The size of the TIMagc is three times smaller than the adult human where the maximum gastric volume is 300 mL [172]. TIMagc can replicate a range of mixing protocols including one that mimics the simulated fasted

state migrating motor complex phases 1 and 2. The amount of content that is pushed through the pyloric valve can be determined by setting the difference between the amount of contraction and relaxation of the distal and proximal antrum parts, respectively.
Mix 1 is a pattern of mixing to replicate phase 1 of the MMC that includes oscillation between the proximal and distal antrum with 12 second pauses between cycles where the frequency of contraction profiles repeats every 21 seconds. The maximum flow rate experienced was 0.081 $m*s^{-1}$ during mix 1.
Mix 2 is a pattern of mixing to replicate phase 2 of the MMC that includes an independent proximal antrum compression and expansion, a concurrent proximal antrum compression and distal antrum expansion, followed by the reverse operation, and then a 9 second pause. The frequency of contraction profiles repeats every 20 seconds. The maximum flow rates experienced was 0.19 $m*s^{-1}$ during mix 2.
The highest shear rates within the TIMagc were at the vessel walls; the shear rates were found to vary between 0.001 and 360 s^{-1}. The fluid hydrodynamics produced within TIMagc during Mixes 1 and 2 were predominantly within the range of Reynolds numbers observed in vivo [173].
The gastric component used in the TIM was based on a bionic gastric reactor (BGR). Measurements within the TIMagc have been compared to in vivo data using the SmartPill technology as a means of validating the biorelevant conditions produced in the TIMagc system [172]. This is a clear example of an ingestible device (SmartPill) being used within an in vitro model and as such this model could be used to evaluate other similar devices.

2.5.19 V-form glass vessel

This model was introduced as a semi-dynamic model that can replicated changes in pH; gastric emptying and dynamic addition of digestive enzymes and gastric fluid [174]. It can handle both liquid and semi-solid materials and has a maximum capacity of 70 mL [174]. The fluids used within this model are based on a digestion protocol as reported [175]; where the simulated fluids are matched based on the electrolyte concentrations; yet enzymes were also included to better replicate gastric fluid. The gastric emptying is designed to mimic physiological emptying where the exit is limited to material of less than 2mm diameter to match reports of the size of materials that exit the pyloric sphincter in vivo [99]. Experimental data in this model on the extent to which food structures impact on nutrient delivery was compared to results from a previous human study on the same foods where the gastric behaviour in the model was similar to that in vivo [174].

2.5.20 Model of an Infant Digestive Apparatus (MIDA)

A model designed to reproduce the physiology of the GI tract of a six-month-old infant, MIDA has been described. This model consists of four consecutive compartments to replicate the oesophagus, the stomach, the pyloric sphincter and the intestine [176]. The construction used two concentric tubes for each section to enable motion to replicate peristalsis. The gastric compartment had an inner diameter of 35 mm and a length of 185 mm [176]. This is a flow through system where the composition of fluid can change over time according to the input materials. This model has been used to evaluate the starch digestibility of baby foods. The model employed electrolyte solutions mixed with enzymes to simulate digestive fluids. A total gastric volume of 280 mL was used [176]. No details on the motility or mixing applied were found in the literature.

2.5.21 Gastric Digestion Simulator (GDS)

The gastric digestion simulator has transparent observation windows that enable researchers to see how the mixing affects solid particles and observe physical changes [177]. This model was developed to analyze the effects of physical digestion including the break-down of solid food particles and the mixing of gastric contents. The vessel is made of flexible material and its volume (capacity) is 550 mL and peristaltic forces are applied via mechanical action of rollers. The exit incorporates a sieve set to restrict exit of particles greater than 2 mm in diameter. The input and output flow can be controlled to enable replication of gastric media and gastric emptying [177]. Specifically this model has been used to observe the disintegration and/or swelling of food particles under biorelevant motion.

2.5.22 Mechanical antrum model

This device as developed to evaluate the gastroretentive potential of dosage forms by simulating antral contraction waves in a realistic manner [178]. The gastric compartment consists of an elastic silicone tube with a diameter of 3.5 cm that is surrounded by an inflatable ring-shaped balloon. The balloon is inflated which results in a local occlusion inside the silicone tube. Motion of this balloon along the cylindrical tube via a stepping motor mimics the propagation of an antral contraction wave [178]. This model was used to evaluate the gastro-retentive potential of a range of objects that differed in size, shape and material, the results showed different times for each object showing some discrimination of the model yet there was no link to in vivo data [178]. This model may be of particular interest to evaluate gastric retention of larger ingestible devices.

2.5.23 GastroDuo

GastroDuo is a biorelevant dissolution test device combines a fed stomach model and a dynamic open flow-through dissolution system [179]. This apparatus was designed to simulate particular aspects of the postprandial stomach, including dynamic pH changes, gastric peristalsis, and the kinetics of gastric emptying, with a specific focus on how gastric emptying can impact upon the performance of oral solid dosage forms, specifically to replicate the Magenstasse (stomach road). This apparatus includes a gastric cell where the dosage form is placed between two blades that are located inside this cell. The blades are moved with defined velocities to simulate realistic movements of a formulation present in the human stomach [179]. In addition, pressure events can be replicated using a balloon placed between the blades that can be inflated to mimic the occurrence of pressure events in the stomach as they are observed in the fasted and fed state. The cell is fed by a flow of gastric media and the flow rate can be adjusted to mimic a range of gastric emptying rates. Data obtained from fed state in vivo studies on two oral immediate release drug products was explained by the results obtained from the GastroDuo apparatus particularly highlighting how the interplay of drug properties, formulation properties and GI physiology, can contribute to the variability of drug plasma concentrations. Further work with this apparatus has explained in vivo data on fast disintegrating and dissolving aspirin tablets compared to conventional tablets where the rapid emptying of dispersed aspiring in the fed state could be replicated in vitro [180]. Further work exploring the link between this apparatus and in vivo data compared the performance of one film-coated tablet and three different capsule immediate release formulations of caffeine; although the in vitro apparatus discriminated between the performance of these dosage forms the in vivo data was not in line with this in vitro data [181].

2.5.24 Artificial Gastric Digestive System (AGDS)

The artificial gastric digestive system (AGDS) is a 3D printed silicone stomach model that replicates the detailed anatomy and morphology of an adult stomach, including the size, the shape and the folds of the inside stomach wall (rugae) [182]. It uses a system of externally applied rollers to generate forces to mix the contents of the gastric model. The fluid used within this model has included gastric fluid with digestive enzymes; fluid can be added and removed during the experimental process to provide a dynamic environment. The pressures generated within this model (27 mmHg) were reported to be similar to those in vivo (25 mmHg) [182]. A major limitation of this apparatus is that there is no exit to the duodenum. This model has been used to evaluate the digestion of α-lactalbumin (which is sensitive to pepsin and pH changes), the results showed that the hydrolysis and morphology of protein, peptide and amino acids accumulation obtained by AGDS were different from static digestion and semi-dynamic digestion models [182]. This finding suggests that pH and gastric motility have an effect on protein hydrolysis. The data found with AGDS was similar to in vivo data which aids in validating this model [182].

2.5.25 Gastric Simulation Model (GSM)

The gastric simulation model is formed from an anatomically representative latex chamber where the motility is applied from a series of external syringes that surround the stomach chamber where the distribution, amplitude and frequency of contractions are similar to human gastric conditions [183]. The model has a maximum capacity of 600 mL and the pyloric sphincter has an opening

diameter of 1.0 cm and it sieves material only allowing those smaller than 1-2 mm to pass [183]. Motility patterns can be applied to mimic peristaltic motion where the amplitude, frequency and trends of mechanical forces can be adjusted. The highest pressure recorded was 70 mmHg at the terminal antrum position [183]. A pump controlled the input flow into the stomach model [183]. The model uses simulated gastric fluid that is delivered into the model via 8 tubes to allow uniform distribution to better mimic secretion of gastric juice. This model has been used to evaluate digestion [183] where a range of simulated media can be incorporated. Existing work evaluated the breakdown kinetics and size distribution of sausage particles as a function of contraction force applied, however this was not correlated to in vivo data [183].

2.5.26 Near Real Dynamic In Vitro Human Stomach (DIVHS)

This model is an advance on the RD-IV-HSM described previously (2.5.13). The dynamic in vitro human stomach (DIVHS) has been designed to match the anatomy of the human adult stomach; it is 3D printed in a soft-elastic silicone and has a similar stomach morphology, dimensions and wrinkled inner structure to in vivo [184]. It has a maximum internal volume of 400 mL as the stretch of the material would not allow expansion to match the reported capacity of the human stomach at 1.5 L [184]. The motility is mimicked using a combination of rollers that are applied externally; the mechanical stress generated within the DIVHS corelated to a reasonable level to that in a human stomach ranging from 5134 to 67 292 $N*m^2$ [184]. Fluids are added and removed from the DIVHS using peristaltic pumps to reflect dynamic changes in composition within the system. The junction to the duodenum does not house a pyloric sphincter yet the geometry limits transfer only to particles <1-2 mm in diameter [184]. This model has been used to evaluate the gastric emptying of meals as it replicated the mixing and grinding of foods as well as enzymatic breakdown due to the nature of the fluids used within the system. The performance of the model was evaluated by comparing the gastric emptying, pH and particle size of beef stew with in vivo data. The gastric emptying was similar to that from the reported in vivo gastric emptying curve [185].

2.5.27 Bionic Gastrointestinal Reactor (BGR)

The BGR is similar to the TIMagc in terms of the stomach component bulk structure however the BGR also incorporates the morphology of the stomach with folds in the gastric body [186]. The BGR was manufactured using elastic and contractile silica gel and the simulated stomach component consists of three parts, namely, fundus, gastric body, and antrum [186]. These gastric component parts can be contracted and dilated independently because they are placed in transparent glass vessels filled with water. GI wall peristaltic contractions and gastric diastole were simulated by adjusting the water pressure that circulated in the space between a glass jacket and a flexible membrane. A contraction strength of 22 mmHg was generated by BGR with the basic motility pattern and 120-220 mmHg when simulating the housekeeper wave [186]. There is no data on the use of this model that can link to in vivo data although great efforts have been made to replicate the forces and crushing strength within the BGR.

2.5.28 Human Gastric Simulator (HGS) Food Engineering Laboratory (University of California Davis)

The Human Gastric Simulator (HGS) simulates ACWs through a mechanical system of rollers. The stomach compartment is formed of a bag that is sealed at one end. The bag has a length of 70 cm and the diameter varied from 3-24 cm [187]. Two tracks of rollers initiate a contraction at the beginning of the distal region of the stomach liner and carry the contraction through the simulated pylorus at a rate of 3 contractions per minute. The forces within the HDS system have been correlated to in vivo data demonstrating that the forces applied replicate the forces involved in mixing in vivo [187]. The maximum force recorded was 5.9 ±0.3 N [187]. Detailed experiments have probed the hydrodynamics within this apparatus to determine fluid flow based on the gastric region [187].

2.5.29 3D printed in vitro dynamic digestion model (ARK®)

A 3D printed stomach model was used to determine the gastric retention of material based on particle size [188]. This is a very new paper and it was not possible to access the full text version to extract further details on this model at the time of writing this review.

Model name and reference	Single or multi-compartment	Biorelevant composition	Dynamic gastric secretions	Volume (mL)	Biorelevant luminal media score	Representative anatomy	Pyloric sphincter exit	Biorelevance of representative anatomy	Mixing mechanism	Pattern of agitation	Pressures	Biorelevance of motility score	Gastric emptying/transit	Biorelevant transit time score
Simulator of the human intestinal microbial ecosystem (SHIME) [142]	Multi	Fed a representative liquid meal. Level 3	Yes	200	5	A duran flask	A narrow tube	1	Magnetic stirrer	Continuous stirring at 150 rpm	Not stated	0	2 hours residence time within the stomach	1
TNO TIM1 original gastric compartment [145]	Multi	Level 3	Internal feedback controls sectiotions	300	5	Cylindrical tube	A narrow tube	1	The flexible walls are compressed and relaxed by changing the water pressure, which enables mixing	Can be adjusted	Not stated	2	Peristaltic valves control flow	1
Gu et al (2005) model to include absorption [33]	Multi	0.1N HCl Level 0	Yes	250	1	USP dissolution vessel	A narrow tube	1	Vessel stirred	Continuous stirring at 100 rpm	Not stated	0	Mapped to in vivo data	1
Artificial stomach-duodenum (ASD) [148]	Multi	0.01N HCl Level 0	No	70	1	A cylindrical beaker	Not stated	0	Magnetic stirring	Continuous stirring	Not stated	0	Mapped to in vivo data	1

Dissolution Stress Test device [150]	Single	HCl (pH 1.0) Level 0	No	1150	0	A chamber above a USP dissolution vessel	N/A	0	Dissolution media stirred at 200 rpm. The dosage form spent 50% of time submerged in the media	Pulsatile inflation and deflation of balloons inside the chamber. Continuous stirring of dissolution media	Representative forces reported	3	N/A	0
Human gastric simulator (HGS) Riddet Institute, New Zealand [152], [153].	Single	SGF with pepsin Level 3	No	70	4	Soft latex conical shaped vessel	0.32 cm diameter plastic tube	3	Contractions by mechanical driving device providing vertical and rotational motion	3 times per minute	Maximum antral contraction forces of up to 3.39 ± 0.95 N	4	3.0 $mL*min^{-1}$	1
FloVitro [154]	Multi	SGF Level 0	No	40-60	1	Cylindrical vessel	A narrow tube	1	Stirred at 300 rpm with a paddle	Continuous stirring	Not stated	0	Not stated	0
Chen et al (2011) In vitro digestion model [155]	Single	SGF with pepsin Level 3	No	100	4	Hemispherical vessel	N/A	0	Vertical motion of a probe	Continuous motion	Not stated	0	Not stated	0
Dynamic Gastric Model	Single	SGF with lipids Level 2	Internal feedback	20 in rested state	5	Conical shaped flexible vessel	Not stated	1	Rhythmic squeezing of the	Contractions at three	Representative forces reported	4	Not stated	0

(DGM) [156, 189]			controls secretions						vessel for the upper part ad peristaltic motion toward the pyloric sphincter	times per minute				
Dynamic in vitro rat stomach system (DIVRS) [161].	Multi	0.25 M HCl Level 0	No	3 (to match the volume in the rat)	1	Silicone mold of an actual rat stomach	3.5mm internal diameter tube	3	External compression	Three compressions per minute (cpm), and the amplitude of the angle plate was set at 2.6 mm	Compressive forces are larger than the contractive forces produced during in vivo experiments	4	Gastric emptying controlled by motility and pressure	1
Dynamic Gastro-intestinal Digester (DIDGI) [165]	Multi	SGF Level 2	Yes	30 (fasted volume) plus 150 ingested	4	Cylindrical beaker	A Teflon membrane with 2 mm holes to mimic the sieving effect of the pylorus	2	Magnetic stirring	Continuous stirring	Not stated	0	Transit time (t1/2) = 70 minutes	1
SIMulator of the GastroIntestinal tract SIMGI [167].	Multi	SGF Level 2	Yes	Not stated	3	Flexible cylinder	Tubing port	1	Externally applied water pressure to create peristalti	Not stated	Not stated	2	Programmable transit	1

									c waves and magnetic stirrer					
Rope-driven in vitro human stomach (RD-IV-HSM) [168]	Single	Artificial gastric juice Level 1	20 silicone tubes are connected to the gastric corpus in a random fashion to simulate the roles of gastric secretory glands	25	3	Silicone mold of an actual human stomach	6mm exit pipe	3	Ropes wrapped around the antrum produce contractions in the stomach model	Contractions at 3 times per minute. The amplitude of the contractions on the model was set at 1 cm	Maximum antral contraction forces of 3.37 ± 0.59 N	4	6.25 $mL*min^{-1}$	1
Engineered Stomach and small INtestine (ESIN) model [169].	Multi	SGF that can include food Level 3	Yes	50	6	Cylindrical shape	Allows the passage of small size particles (< 2mm) and liquids	2	Agitation is performed by shaft stirrers equipped with adjustable rotors	Contractions at 3 times per minute	Not stated	1	Mapped to in vivo data	1
Dynamic Gastric Simulating Model	Single	Level 3	Yes	300	4	Cylinder with a truncated cone	a 2 mm gap is left at bottom	2	Vertical planar movement of a probe	Contractions at 3 times per minute	Not stated	1	Mapped to in vivo data	1

(DGSM) [170].									attached to a texture analyzer					
In vitro mechanical gastric system (IMGS) [171].	Single	Level 3	pH respon sive	360	4	J-shape flexible structure	N/A	2	External compres sion	Contracti ons at 3 times per minute	Mechanist ic forces ranged from 0.20-1.89 N	3	Mapped to in vivo data	1
Biorelevant Gastrointe stinal Transfer (BioGIT) model [34]	Multi	Level 2 FaSSGF	yes	250	3	USP dissolution vessel	Not stated	0	USP Paddle rotation	Continuo us stirring at 75 rpm	Not stated	0	half-life of gastric emptying was set at 15 min	1
TIMagc [173] [172].	Multi	Level 3	Yes	300	4	3 parts to replicate J shape	Not stated	1	External compres sion	Motilitly mapped to in vivo data	Represent ative forces reported	4	Mapped to in vivo data	1
V form glass [174]	Single	Level 3	Yes via a syringe pump	70	5	A V-form vessel	No	0	Mini gyro rocker	Continuo us motion at 35 rpm	Not stated	0	Mapped to in vivo data	1
Model of an Infant Digestive Apparatus (MIDA) [176]	Multi	Level 3	Yes	280	4	Flexible cylindrical tube	3 way valve (deimens ions not stated)	0	External compres sion	Frequenc y and amplitud e not mentione d	Not mentione d	1	Time not stated.	0
Gastric Digestion Simulator (GDS) [177].	Single	Level 2	Yes	100	4	Conical shaped with dimension s similar to the human antrum	A sieve with 2mm pore size	1	Gastric peristalsi s is simulate d by compres sing deforma ble rubber	Contracti on waves at a speed of 2.5mm/s and frequenc y of 1.5 per minute	Estimated compressi on forces range from 0.65-1.9N	4	Contents emptied every 15 minutes	0

									walls using pairs of rollers					
Mechanical antrum model [178].	Single	0.5% m/m Tween 80 in water Level 0	No	150	1	A cylindrical tube	N/A	0	An occluding ring along a flexible cylinder mimicking antral contraction	Propagation velocity of waves was 3mm/s. Frequency was 1 per minute	Not stated	3	N/A	0
GastroDuo [179]	Single	SGF Level 1	Yes	Flow through system	3	No	N/A	0	Blades to simulate realistic movements present in the human stomach	Programmed to replicate in vivo data	Not stated	2	Mapped to in vivo data	1
Artificial gastric digestive system (AGDS) [182]	Single	SGF with enzymes Level 3	Yes	400	4	3D printed silicone stomach model	2 mm diameter silicone tube	4	External compression	Designed to replicate in vivo data	Representative forces reported	4	Mapped to in vivo data	1
Gastric Simulation Model (GSM) [183]	Single	SGF with enzymes Level 3	Yes at 8 positions within the stomach model	150	6	Reproduced gastric geometry	1 cm pyloric sphincter that can sieve particles <2mm	3	External compression	Contractions 3 times per minute	Representative forces reported	4	Mapped to in vivo data	1

Near real dynamic in vitro human stomach (DIVHS) [184].	Multi	SGF Level 1	Yes	400	2	A flexible silicon shape based on a human stomach	Sieve to restrict flow to particles <2 mm	4	External compression	Designed to replicate in vivo data	Representative forces reported	4	Mapped to in vivo data	1
Bionic gastrointestinal reactor (BGR) [186]	Multi	Not stated	Not stated	Not stated	0	3 parts to replicate J shape	Not stated	1	External compression	Designed to replicate in vivo data	Representative forces reported	4	Not stated	0
Human gastric simulator (HGS) Food Engineering Laboratory (University of California Davis) [187].	Single	Not stated	No	Not stated	0	Approximated j shape	Sealed unit	1	External compression	Contractions 3 times per minute	Maximal contraction force in the antrum was 5.9 ± 0.3 N	4	N/A sealed unit	0

Table 7. Summary of dynamic in vitro *gastric models (presented in order in which they were published*

Table 7 highlights the diversity of gastric models available. The majority have focused on the fluid composition yet many also mimic the anatomy and motility. Most models are derived from pharmaceutical or food research and therefore they mimic disintegration and dissolution to measure the bioaccessibility of nutrients or drugs; therefore adaptations may be required to evaluate monolithic devices due to their size.

2.6 Gastric organoid models

Human gastric organoid models have been reported derived from both primary human gastric tissue [80, 190-197] or hIPSCs [198]. Many studies have also used murine primary gastric organoids [192, 196, 199, 200] including co-culture with autologous immune cells [200] and immortalized stomach mesenchymal cells [201], in addition to murine pluripotent stem-cell-derived gastroids [202, 203]. Mainly, these models have been used to investigate H. Pylori infection [190-192, 194, 195, 197, 198], cancer [80, 193, 196, 199, 200] and pharmaceuticals [201]. H2D human fundic organoid layers have been used to study H. Pylori infection [197].

Gastric organoid models have mainly been developed to better understand disease progression although there is scope for such models to be used in toxicity assessment and pharmacokinetic analysis [204].

2.7 Gastric Organ-on-a-chip models

Lee et al [205] has reported a human stomach-on-a-chip system by embedding a single hIPSC-derived antral gastric organoid in Matrigel inside a chamber. A pair of borosilicate micropipettes, ~50 µm in tip diameter, were inserted into opposite sides of the organoid and connected to a peristaltic pump to recreate luminal flow through the organoid. Flow was periodic in order to mimic that induced by rhythmic stomach contractions. This study demonstrated the proof-of-concept for long term delivery and observation of luminal agents, which could include ingestible micro or nanodevices in the future. Moreover, the use of gastric organoids enables such testing to take place in patient-derived stem cells from the perspective of ingestible devices in personalised medicine. However, this is the only stomach-on-a-chip model to date (known by the authors). This replication of the "microphysiology" of the stomach can be used to simulate dissolution rates, for example, from oral solid dosage forms, to observe the effect on precipitation or other relevant factors.

3 Replicating the small intestinal environment

3.1 Overview of small intestine function and anatomy

The human adult small intestine (SI) is approximately 7 meters in length, starting at the duodenum and ending at the ileocecal valve. It is divided into three sections: the duodenum, jejunum, and ileum. The majority of the duodenum is located in the retroperitoneum, whereas the jejunum and ileum are intraperitoneal structures [4]. The duodenum is the proximal section of the small intestine and is reported to be 25 cm long in adults [4]. The main pancreatic duct and the common bile duct join and empty into the midportion of the duodenum. The pancreas secretes about 500 mL of fluid each day in a healthy adult which contains the highest amount of bicarbonates in all GI secretions. This bicarbonate rich secretion is responsible for the post-gastric rise in luminal pH within the small intestine, further details on pancreatic secretions can be found here [206]. Bile is secreted into the SI to aid in the solubilisation of ingested nutrients or drugs. Bile micelles form at bile salt concentrations in excess of 25mmol*L^{-1} [206]. For further details on bile formation and secretion the reader is directed to this review [207]. The ligament of Treitz is a fixed point that marks the junction between the duodenum and jejunum. The jejunum and ileum follow on from the duodenum with reported lengths of 2 and 3 metres respectively [4]. There is no clear anatomic landmark that marks the transition from the end of the jejunum to the beginning of the ileum. Further details on regional differences between the duodenum, jejunum and ileum were highlighted in a recent review [103]. The ileocecal valve (ICV) is a distinct feature of the small intestine that prevents the faecal contents in

the colon from entering the small intestine and controls the flow of contents from the small intestine into the colon. The valve is triggered by distention in the small intestine where if the ileum becomes distended, the valve will relax and allow the passage of contents from the small intestine into the colon.

The function of the small intestine is the absorption of nutrients, maintaining water and electrolyte balance, providing an immunologic barrier, and endocrine secretion. The lumen of the small intestine is designed to aid nutrient absorption where the structures maximise surface area with a total absorptive surface area of up to 250 to 400 m^2 [4]. However, it should be noted that there is some debate in the literature on the actual overall surface area with lower values of 32 m^2 reported [208]. The complexity in reporting the overall surface area comes from the transverse folds of mucosa and submucosa that increase the surface area of the small intestine; these structures are more prominent in the proximal intestine and diminish along the length of the small intestine. Villi are finger-like projections of the mucosa that further increase the surface area; they are longest in the duodenum and shortest in the distal ileum. Microvilli line the apical border of the enterocyte and further increase the surface area. As reported for the in vitro models of the stomach only few models replicated the morphology of the stomach to accurately reproduce the true surface area; this aspect is potentially more important for the small intestine, particularly when considering the overall surface area for absorption.

The villus is coated with a single layer of enterocytes and goblet cells that secret mucin are found between the enterocytes; the density of goblet cells increases along the length of the small intestine. The epithelium of the small intestine is replaced every 3 to 6 days.

3.2 Small intestinal fluid volume

The fluid volume in the small intestine can control the dissolution of a drug, particularly for poorly soluble drugs. It is important that in vitro models replicate the small intestinal volume present to mimic in vivo conditions. A summary of studies that report small intestinal volume is provided in Table 8.

			Volume (mL)		
Reference	**Health status of participants**	**Number of volunteers**	**Min**	**Max**	**Mean (standard deviation)**
[109]	Healthy	12	45	3192	105
[112]	Healthy	12	5	158	43
[115]	Healthy	6 6 6 6			45 (35) 52 (43) 51 (32) 54 (37)
[117]	Oral intake of one Norvir tablet (100 mg ritonavir)	5			12.5

Table 8. Intestinal fluid volumes reported in adult subjects as determined by magnetic resonance imaging (MRI) under fasted conditions.

The volume of fluid in the small intestine has been reported to decrease upon ingestion of a meal with a reduction from 105 mL to 54 mL 60 minutes after a meal [109] and 86 mL to 34 mL 90 minutes after ingestion of breakfast [209]. This reduction in free water is a result of the liquification of the meal mixing with water to produce a viscous slurry within the intestine which is not observed as free water using MRI.

Another factor to be considered is the fact that the water present in the small intestine is not homogenously distributed but located in pockets along the small intestine. These pockets are hard to replicate within in vitro models of the intestine, particularly as many are small. The number of pockets present has been reported to be 16 following ingestion of a glass of water [112] with fewer in the fasted state and following a meal [109].

3.3 Small intestine media composition

Characterisation of small intestinal media has been undertaken to determine relevant parameters in order to generate simulated media representative of the fasted state. A summary of the studies is presented in Supplementary Table 2. Detailed characterisation of small intestinal media composition in the fed state is complicated by the nature of the food ingested as well as the timing of the sampling to mimic digestion. Studies that have characterised the composition of small intestinal fed media are described in supplementary Table 3.

3.3.1 Simulated intestinal media

USP simulated intestinal fluid has been used for many years with reports of its use dating back to the early 1960s [210]. The original recipe was a buffered system with a pH of 7.5 although this was reduced to pH 6.8 to better reflect in vivo conditions [211]. There is a detailed review of small intestinal pH values reported in the literature [212]. The buffer strength of USP simulated intestinal fluid is listed as 0.05M strength buffer which provides an osmolality of 114 $mOsm*kg^{-1}$ and a buffer capacity of 18 $mmol*(L*pH)^{-1}$ [213]. There is a simulated intestinal fluid with pancreatin and without it is termed SIF-blank.

Despite phosphate buffer being the most common choice for simulated intestinal fluid it is a bicarbonate buffer that is present in vivo. However, the use of a bicarbonate buffer in vitro requires a permanent carbon dioxide source to maintain the pH which adds complexity and cost [214]. The impact of counter ions may need to be considered for certain drugs, for example, dipyridamole and ketoconazole have been shown to precipitate as phosphate salts in neutral or basic solutions [215].

Fasted state simulated intestinal fluid (FaSSIF) was developed based on characterisation of human small intestinal aspirates [216]. Since the development of the first Fasted State Simulated Intestinal Media (FaSSIF V1) in 1998 [217]; there have been at least two further versions reported: FaSSIF V2 [218] and FaSSIF V3 [219]. These updated fluids better reflect the complexity within intestinal fluids by incorporation of bile salts, phospholipids and fatty acids that form colloidal structures (mixed micelles) that can solubilise lipophilic drugs. The composition of each of these fluids is presented in Table 9.

Component	FaSSIF V1	FaSSIF V2	FaSSIF V3
Cholesterol (mM)	–	–	0.2
Lecithin (mM)	0.75	0.2	0.035
Lysolecithin (mM)	–	–	0.315
Sodium glycocholate (mM)	–	–	1.4
Sodium oleate (mM)	–	–	0.315
Sodium taurocholate (mM)	3	3	1.4
Hydrochloric acid			
Maleic acid (mM)	–	19.12	10.26
Potassium dihydrogen phosphate (mM)	28.65	–	–
Sodium chloride (mM)	105.85	68.62	93.3

Sodium hydroxide (mM)	10.5	34.8	16.56
pH	6.5	6.5	6.7

Table 9. Composition and physicochemical characteristics of three versions of FaSSIF

In the first two versions of FaSSIF, sodium taurocholate was used as a representative bile salt present due to ease of availability and cost. The second version was introduced to improve the stability of the fluid and better reflect the composition within the intestine [218]. In FaSSIFV2 the osmolality is somewhat lower to reflect in vivo data and the buffer system was switched from phosphate to maleate [218, 220]. The updates in FaSSIFV3 accounts more accurately for the amount and type of micelle forming components, as these have a significant influence on the solubility of highly lipophilic drugs. The recipe reported was better able to match the solubility of drugs in aspirated human intestinal fluid. FaSSIFV3 also has a lower surface tension compared to previous versions which is considered to better aid in the wetting of poorly soluble drugs [219]. Recent work has compared all three variants and suggests that the FaSSIFV1 giving the best correlations to human aspirated intestinal fluid [221]. It is thus important to understand how biorelevant media affect the solubility and to understand, particularly for poorly soluble drugs, how well the simulated media reflects the micellar solubilisation to obtain the best prediction. There is a great deal of literature evidence that demonstrates that lipophilic drug solubility is increased in biorelevant fluids that contain bile salt micelle components compared to in buffers alone, an overview is provided by Bou-Chacra et al (2017) [222].

Fed state simulated intestinal fluid (FeSSIF) was introduced in 1998 by Galia et al [216]. The major differences between FaSSIF and FeSSIF are the buffer system which is a phosphate buffer in FaSSIF versus an acetate buffer in FeSSIF, the pH, and the higher concentration of taurocholate and lecithin in FeSSIF. Due to the changing nature of the fed state three snapshot media were created to better replicate the timeframe post ingestion. An update, FeSSIFV2 was introduced subsequently as a composite of the three "snapshot" media where the second generation FeSSIF contained two digestion products: glyceryl monooleate and sodium oleate compared to the original FeSSIF [218].

The composition of the FeSSIF media is shown in Table 10.

For poorly soluble drugs the increased bile and lecithin present in FeSSIF compared to FaSSIF can lead to faster dissolution and higher solubility [220], and is the reason why many insoluble, lipophilic drugs show improved absorption in the fed state.

Composition	FeSSIF	FeSSIF Early	FeSSIF Middle	FeSSIF Late	FeSSIF-V2
Bile salt (taurocholate) (mM)	15.00	10.00	7.50	4.50	10.00
Phospholipid (lecithin) (mM)	3.75	3.00	2.00	0.50	2.00
Acetic acid (mM)	144.00	–	–	–	–
Sodium chloride (mM)	173.00	145.20	122.80	51.00	125.50
Maleic acid (mM)	–	28.60	44 50	8.09	55.02
Sodium hydroxide (mM)	101.00	52.50	65.30	72.00	81.65
Glyceryl monooleate (mM)	–	6.50	5,00	1.00	5.00
Sodium oleate (mM)	–	40.00	30.00	0.80	0.80
pH	5	6.5	5.8	5.4	5.8
Osmolality (mOsmol*kg^{-1})	635.00	400.00	390.00	240.00	390.00 ± 10
Buffer capacity (mEq*(pH*L)$^{-1}$)	76.00	25.00	25.00	15.00	25.00

Table 10. Composition and physicochemical characteristics of FeSSIF media published in the literature [218]

Simulated intestinal media used in food research to mimic digestion was subject to immense variability where typically the pH was 7 and the media contained a broad range of enzymes and surfactants [223]. The ionic content is reported to reflect in vivo conditions [223] as shown in Table 11.

Constituent	SIF (pH 7) (mmol*L^{-1})
K+	7.6
Na+	123.4
Cl−	55.5
H2PO4 −	0.8
HCO3 −, CO3 2−	85
Mg2+	0.33
NH4 +	–
Ca2+	0.6

Table 11. The ionic composition of simulated intestinal fluid used in digestion research [223].

The enzyme content can be added in one of two ways. Either use a pancreatic extract (pancreatin) that contains all the relevant enzymes but in a fixed ratio (the amount to add must be based on a specific enzyme activity and should be added in sufficient quantity to provide 100 U*mL^{-1} of intestinal phase content [223]. The alternative is to use individual enzymes (protease, amylase and lipases); in this case there are recommended enzyme activities to be met per mL of fluid. Endogenous surfactants of bile acids and phospholipids are also added to the simulated intestinal fluid. Further details on standardised protocols for simulated intestinal fluid are available from the InfoGest network [224]. The incorporation of microbial media into this simulated intestinal fluid has been described to enable in vitro growth of bacteria native to the GI tract in an environment that is reflective of the small-intestinal environment [225]. The replication of the media is important as it is recognised that microbiota can affect drug bioavailability due to metabolism within the small intestine [226]. There have been recent reviews on this topic [227, 228].

3.4 Small Intestinal motility

The motility within the intestinal lumen affects the mixing of the luminal contents and can affect the rate of disintegration and dissolution of ingested oral solid dosage forms. The motility can also affect the transit rate of materials through the intestine. Details of small intestinal motility was first reported by Kellow et al in 1986 based on data from 16 healthy volunteers via manometry [229]. The frequency of maximal contractile activity decreased along the length of the small intestine with values of 11.7 ± 0.1 in the duodenum and 8.5 ± 0.2 per minute in the terminal ileum [229]. The MMC propagated fastest in the jejunum with speeds of 4.3 ± 0.6 cm*min^{-1} and slower speeds in the distal ileum of 0.6 ± 0.2 cm*min^{-1} [229]. The duration of the phase III MMC was also reported with times of 8.7 ±0.1 minutes in the duodenum and 13.8 ± 1.3 minutes in the terminal ileum [229].

A recent systematic review on motility patterns in the terminal ileum has been conducted and shows differences in motility patterns in the fasted and fed states [230]. In healthy individuals in the fasted state the mean duration of phase III of the MMC ranged from 6.5-18.8 minutes; the mean propagation velocity (for the phase III MMC) was 0.3-3.1 cm*min^{-1} and the frequency of contractions was 8.0-11.9 per minute [230]. After ingestion of food, most researchers found replacement of the interdigestive motility patterns, such as the MMC, with intense contractions that appeared irregular and failed to meet the definition criteria of any known motility patterns [230]. The mean motility index was significantly higher following food ingestion, and this increase was sustained for only 30 min before returning to fasting levels.

3.5 Small intestinal transit time

Measurement of small intestinal transit time can be difficult as invasive methods are required to note the entry and exit times. This has previously been measured using medical imaging techniques including scintigraphy or MRI or by visualizing the motion of a solid unit via magnetic markers or by medical devices such as telemetric capsules [7].

A detailed review and meta-analysis on small intestinal transit time of single and multiple unit dosage forms reported a mean small intestinal transit time of 3.49 hours [136]. The caloric content had no

significant effect on the small intestinal transit which is of relevance to ingestible devices as this result is likely to translate to some larger units [136].
The impact of small intestinal transit time on drug absorption is complex to measure however there are suggestions that rapid transit will reduce the overall absorption of drugs, particularly in those where disease may affect transit time [231].

3.6 In vitro models of the small intestine

A brief outline of in vitro models that incorporate a small intestinal environment is presented in the order in which they were published, the relative attributes are also compared in Table 12.
The evaluation of the in vitro models was based on criteria associated with the features of the macroenvironment that were presented in Table 1. The evaluation of the biorelevance of the luminal media as based upon factors associated with the luminal composition used within the system. These were scored using the levels of simulation of luminal composition that have previously been reported [138, 139]. These levels are: level 0 is pH only; level 1 is pH plus buffer capacity; level 2 includes bile components, dietary lipids, lipid digestion products and osmolality (this includes FaSSIF) and level 3 also includes dietary proteins, enzymes (not digestion products) and viscosity effects. The ability to adjust the composition of this media via dynamic secretions during the test was also included as a marker of biorelevance; this was scored 1 if dynamic secretions were possible and 2 if these secretions were automated and responsive by the system under test according to an internal feedback mechanism. The volume used within the system was reported and this was considered to be biorelevant where the volume was less than 100 mL in the fasted or fed state; biorelevant conditions scored 1 where as non-biorelevant scored 0. The column on the biorelevant luminal media is the sum of the biorelevance scores for the previous three columns.
The representative anatomy provides details of the shape and dimensions of the compartment used to mimic the small intestine; where these were broadly similar to the dimensions of the small intestine they were scored 1 and where they accurately mimicked the dimensions they scored 2.
The level of biorelevant motility score comprised the components of the agitation mechanism and pattern of agitation. Where the mixing mechanism applied was consistent with mixing in the SI, via compression of the walls of the mixing vessel a score of 1 was applied. The pattern of agitation scored 1 for discontinuous mixing and 2 where the profile of discontinuous mixing matched that reported in vivo. Where the pressures matched those in vivo a score of 1 was provided to the model. The overall scores for the biorelevance of motility was the sum of the scores for mixing mechanism, pattern of agitation and pressures. Where the transit time was recorded this was scored 1 where it was aligned to in vivo data and zero where it was not.
Several models of the intestine also include a gastric compartment thus there is overlap here with the previous section. However, it will be the intestinal conditions that are detailed here and summarized in Table 12.

3.6.1 SHIME

The simulator of the human intestinal microbial ecosystem (SHIME) includes five compartments simulating the upper (stomach, small intestine) and the lower (ascending, transverse and descending colon) digestive tract. The small intestinal compartment is a glass vessel that sits within the series and is connected via peristaltic pumps. Three times a day a defined medium is added to the small intestine vessel that includes pancreatin and bile liquid [143]. The small intestinal vessel has a volume of 300 mL and a pH from 5.0-6.0 with a retention time of 6 hours [142]. The main focus of this model has been the colon, however there is potential to evaluate small intestinal digestion as described in [232]. Work has demonstrated survival of *B. cereus* spores within the SHIME apparatus, in addition bacterial growth and endotoxin production can be explored in the SI environment.

3.6.2 TIM-1

The TIM-1 system is a dynamic, computer-controlled system that simulates the human GI tract where the small intestine is subdivided into the duodenum, jejunum and ileum [145]. The volume

and pH in each compartment are monitored to allow feedback control. Simulated fluids are maintained by the addition of pancreatin and bile salts via computer-controlled pumps. The pH is maintained at 6.5 for the duodenum; 6.8 for the jejunum and 7.2 for the ileum [145]. The geometry of the apparatus somewhat mimics the small intestine as it is a cylindrical tube although the length and surface area are very different to the in vivo environment. Variation of the water pressure external to the flexible cylindrical tubing enables mixing of the contents (chyme) by alternate compression and relaxation of the flexible walls to simulate peristalsis [233]. The rate of transit can be varied depending on the physiological state being simulated [233]. Advances on the TIM-1 system including the TinyTIM are described in section 3.6.12.
The SI parameter of TIM-1 can be used to measure both survival or probiotics and the behavior of oral drugs. Several publications have correlated in vivo data with in vitro data from this apparatus including a exploring drug product performance under reduced gastric acid secretion conditions [234].

3.6.3 pH-stat lipolysis model

The pH-stat lipolysis model is a frequently used digestion model which comprises a single thermostatted chamber that is mixed within a digestion medium resembling fasted or fed state intestinal fluid, prepared with an appropriate pH, buffer capacity, as well as concentrations of bile salts and phospholipids simulating the effects of bile secretion in the duodenum [235]. The intestinal phase consists of a well-mixed vessel into which the gastric phase resides and components to adapt the composition of the fluid to better reflect the small intestine are added [175]. A pH-titrator is included in the experimental design to maintain a constant pH throughout the experiment, often set at pH 7.4 [235]. The media can be centrifuged to separate an aqueous, lipidic and sediment phase where drug in either the aqueous or lipid phase id available for absorption. The major limitation of this method in terms of replicating the small intestine is that it does not remove digestive products during the digestion process, which may cause inhibition of enzymes. Results from this apparatus have been compared to in vivo studies in rats and the output has been used to aid in the selection of suitable lipid components for enhanced oral bioavailability of BCS class 2 compounds [235].

3.6.4 Artificial stomach duodenal model (ASD)

This apparatus consists of a gastric and a duodenal chamber. The duodenum has a volume of 30 mL of ASD and simulated duodenal fluid was 0.05 M sodium phosphate buffer (pH 6) [148]. During the simulation, the duodenal fluids was infused at 0.5 $mL*min^{-1}$ where the volume is maintained at 30 mL via emptying rate matching the infusion rate [148]. This apparatus was designed to mimic canine rather than human physiology and the results from the apparatus were compared to in vivo data on carbamazepine formulations on both the fasted and fed state [148]. A particular strength of this apparatus lies in its ability to detect precipitation of drugs when passing from the gastric to the SI environment.

3.6.5 Dissolution Stress Test device

This apparatus was described previously in section 2.5.5. The apparatus combines aspects of both gastric and intestinal physiology in a single unit; the pressure matched gastric emptying yet the fluid is simulated intestinal fluid (pH 6.8 buffer) [150]. The main advantage of this apparatus is that it includes time spend submerged in fluid and not submerged which was designed to mimic in vivo data. In addition, the tablet was subjected to physical stresses to mimic transit within the SI. The output from the in vitro data was compared to in vivo data for both IR and ER drug products and the results may help explain irregular absorption profiles due to peristaltic stress events [150]. This apparatus has been commercialised by Physiolution where access to the equipment is managed by their team.

3.6.6 Benchtop Small Intestinal Model (SIM)

The small intestinal model (SIM) consisted of an inner porous flexible membrane and an outer flexible tube that is impermeable to water. This model uses membrane tubing to represent the small intestine with a diameter of 30 mm and a length of 500 mm [236]. A flexible tube was selected to enable deformation in a physiologically representative manner. Segmentation based motility is

reproduced using concentric constriction of the flexible tube with the use of inflatable cuffs. The fluid within the tube was at pH 6.4 and biopolymer solutions at a range of viscosities were evaluated [236]. The apparatus was used to study the effects of viscosity on starch breakdown by glucose as a model reaction relevant to digestion. The internal semi-permeable membrane allowed sampling of glucose from within and external to the "lumen". The data generated was not correlated to in vivo data [236].

3.6.7 FloVitro dissolution system

The FloVitro system includes a gastric and small intestinal chamber and an additional third compartment connected to the small intestinal component that is intended to function as an absorptive compartment [154]. The small intestinal vessel has a volume that can range from 60-400 mL and is agitated with a paddle at speeds of 300 rpm [154]. Simulated intestinal fluid flows through the vessel at a rate of 1-8 $mL*min^{-1}$. The flow rates for this apparatus were based in in vivo data where both fasted and fed state were simulated for furosemide tablets and danazol capsules, however there was no further verification of the model with alternative in vivo data sets [154].

3.6.8 Dynamic Gastro-intestinal Digester (DIDGI)

The DIDGI® system consists of two consecutive compartments simulating the stomach (see section 2.5.11) and the small intestine. The intestinal compartment the fluid was maintained at pH 6.5 a 1% solution of porcine bile and a 10% solution of porcine pancreatin were added at a constant flow rate of 0.5 $mL*min^{-1}$ and 0.25 $mL*min^{-1}$, respectively [165]. The overall intestinal transit time was 200 minutes. This model was validated against piglet digestion of a liquid infant formula where a good correlation between the two systems was found [165].

3.6.9 Dynamic gastric model: duodenal static model

Following ejection from the dynamic gastric model (see section 2.5.9), samples can be subjected to further digestion using a static duodenal model. Within the static duodenum model the sample is adjusted to pH 6.8 to reduce further activity of gastric enzymes and to simulate the change of pH in the duodenum [156]. These duodenal samples are then mixed on an orbital shaker at 170 rpm for 3-4 hours where samples are taken at defined intervals to establish a duodenal release profile [156]. This apparatus has been used to evaluate the delivery of potential prebiotics to the distal GI tract [237].

3.6.10 SIMulator of the GastroIntestinal tract SIMGI

The SIMGI comprises of five compartments (units), one of which is the small intestine, one the stomach (see section 2.5.12). The intestinal
unit is a double-jacketed glass reactor vessel that is continuously stirred at 150 rpm by means of a magnetic stirrer. The fluid within the vessel includes gastric content which is mixed with pancreatic juice and bile maintained at pH 6.8 [167]. The intestinal transit time is 2 hours. The major focus of this apparatus is the colon and no studies could be found that reported on the SI functionality or in vivo correlation for this apparatus

3.6.11 Biorelevant Gastrointestinal Transfer (BioGIT) model

The Biorelevant Gastrointestinal Transfer (BioGIT) model is a three compartment system introduced in 2016 [34]. The intestinal compartment is fed from the gastric compartment (see section 2.5.17) and its volume is maintained at 40 mL via the use of a reservoir compartment. The rates of flow are based on in vivo data [34]. The low volume in the duodenum necessitates the use of a mini vessel (100 mL total volume) within the dissolution apparatus. The media within the duodenal compartment is designed to match FaSSIF and this is stirred at 75 rpm [34]. The output data from this model has shown correlations to in vivo data from a range of lipophilic weakly basic drug products [34].

3.6.12 TinyTIM

The TinyTIM apparatus is a dynamic, computer controlled, two-compartmental in vitro system of the stomach and small intestine which is a simplified version of the TIM-1 apparatus [238]. Whilst the TIM-1 apparatus has 3 sections to represent the small intestine the TinyTIM has just one without an ileo-cecal valve [238]. The pH in the fasted state is 6.3 ± 0.2 and in the fed state is 5.8 ± 0.2 [238].

The bioaccessibility of essential amino acids from proteins in TinyTIM was compared to the body weight gain of chickens for the same materials and a good correlation was shown. In addition the glucose response to maltodextrin correlated in Tiny TIM to data from humans [239].

3.6.13 Engineered Stomach and small INtestine (ESIN) model

The Engineered Stomach and small INtestine (ESIN) model is a dynamic computer-controlled system that reproduces the complex physiology of the human stomach (see section 2.5.14) and small intestine, including pH, transit times, chyme mixing, digestive secretions, and passive absorption of digestion products [169]. There are three components to the small intestine: the duodenum, jejunum, and ileum maintained at pH values of 6.4, 6.9 and 7.2. In the fasted state the volumes of the compartments are 80 mL in the duodenum; 150 mL in the jejunum and 150 mL in the ileum. The transit times are 10 minutes for the duodenum; 105 minutes for the jejunum and 150 minutes for the ileum. The geometry of the three intestinal sections does not replicate the in vivo anatomy as glass vessels are used and agitated by overhead mixing [169]. An in vitro in vivo correlation between data from ESIN and two model drugs (paracetamol immediate release form and theophylline sustained release tablet) has been demonstrated [169].

3.6.14 Model of an Infant Digestive Apparatus (MIDA)

A model designed to reproduce the physiology of the GI tract of a six-month-old infant, MIDA has been described [176]. The compartment representing the small intestine consisted of five tubular sections. The inner tube of the intestinal compartment had an inner diameter of 10 mm and a wall thickness of 1 mm. The outer tube had an inner diameter and a wall thickness of 20 and 1 mm, respectively. During the small intestinal digestion, these tubes were continuously squeezed to reproduce the peristaltic and segmentation motions. The total length of the intestinal compartment was 350 cm. The volume within the small intestine section was maintained at 160 mL [176]. The small intestinal compartment ended with two concentric glass tubes (inner diameter of 10 mm) attached to a three-way valve whereby it was possible to collect samples of the small intestinal contents. No details on the motility or mixing applied were found in the literature. MIDA has been able to differentiate between the starch hydrolysis of starch based infant foods yet there is no data that correlates this to in vivo findings [176].

3.6.15 The Smallest Intestine (TSI)

The TSI consists of five parallel reactors, with a working volume of 12 mL each and simulates the passage through the human SI by an adjustment of pH and concentration of bile salts, pancreatic enzymes and dialysis to mimic absorption [240]. The 5 reactors provide 5 replicates rather than 5 segments of the GI tract. The fluid composition within each vessel is developed to mimic in vivo conditions on both the fasted and fed state. The duodenal passage takes 2 hours during which the pH is elevated from 6.5-6.8; the jejunum has a transit time of 4 hours and a pH gradient of 6.8-7.2; the ileal passage maintains the pH at 7.2 for 2 hours [240]. This model has been used to evaluate the survival of three probiotics, this model includes the microbiota in the ileum experiments which is unusual for a model that does not contain a colon section [240]. The small volume and use of 5 simultaneous replicates make this an attractive system to evaluate the survival of probiotics, particularly as a screening tool.

3.6.16 Biocell Reactor

The Biocell reactor combines a semipermeable membrane that enables osmotic nutrient interchange in the intestine with rhythmic peristaltic movement [241]. The bioreactor is composed of two chambers; an apical chamber, with a 5 mm-diameter dialysis tube and a flow through basal chamber, with a wet volume of 5 mL. It is surrounded by two helices that rotate to squeeze the dialysis tube to simulate the peristalsis [241]. The bioreactor flow system has two independent fluidic circuits, one for the apical chamber and another for the basal chamber, which collects the media into a sampler compartment for further analysis. This apparatus is a miniaturised apparatus that replicates the motility within the intestine. There are no reports of validation of this miniaturised model against in vivo data.

3.6.17 Bionic Gastrointestinal Reactor (BGR)

The small intestine component of the BGR was fabricated using silica gel with an intestinal wall and villi and was divided into duodenum, jejunum, and ileum [186]. The geometry of all three parts was the same: the internal diameter was 30 mm and this incorporated villi of 0.2 mm diameter and 3mm length in a cylindrical tube that was 250 mm long [186]. This is the only model that incorporates morphological features of the small intestine where these features increase the surface area of the SI by 112%. No work has been reported on the functionality of the intestinal compartment of this model.

Model name and reference	Single or multi-compartment	Media used	Dynamic intestinal secretions	Volume (mL)	Biorelevant luminal media score	Representative anatomy	Biorelevance of representative anatomy	Mixing mechanism	Pattern of agitation	Pressure	Biorelevance of motility	Intestinal transit	Biorelevant transit time
Simulator of the human intestinal microbial ecosystem (SHIME) [142]	Multi	Level 3 borelevant fluid	Yes, responsive	300	4	A beaker/duran flask	0	Magnetic stirrer at 150 rpm	Continuous constant stirring	Not stated	0	6 hours retention time	1
TNO TIM1 original model [145]	Multi	Level 3 borelevant fluid	Yes, responsive	Duodenum: 55 mL Jejunum: 130 mL Ileum: 130 mL	4	Cylindrical tube. Does not reflect length or surface area	0	External compression of flexible walls	Mimics peristalsis	Not stated	2	Mapped to in vivo data	1
Gu et al (2005) model to include absorption [33]	Multi	Level 2 FaSSIF	Yes	500	3	USP vessel used	0	Vessel stirred at 100 rpm	Overhead stirrer	Not stated	0	90 minutes	0
pH Stat lipolysis [235]	Single	Level 3 borelevant fluid	pH is responsive	35.5	6	A conical beaker	0	Overhead stirrer	Continuous mixing	Not reported	0	N/A	0
Artificial stomach-duodenum (ASD) [148]	Multi	Level 1 simple buffer	Yes	30	3	A cylindrical beaker	0	Magnetic stirring	Continuous stirring	Not stated	0	Duodenal fluid was flowing through at a rate of 0.5 $mL*min^{-1}$	1
Dissolution Stress Test device [150]	Multi	Level 1 simple buffer	No	1150	1	USP Dissolution vessel	0	Dissolution media stirred at 200 rpm. The dosage form spent 50% of time submerged in the media	Discontinuous exposure to fluid	To match in vivo	4	N/A	0

Benchtop Small Intestinal Model (SIM) [236]	Single	Level 1 viscosity only	No	Flow through system (total volume not reported)	1	Flexible tube 30mm diameter and 50 cm long	0	External forces applied to mimic segmentation contractions and peristalsis	Frequency matched to in vivo data	Not reported	3	N/A	0
FloVitro [154]	Multi	Level 2 FaSSIF or FeSSIF	No	60-400	3	No cylindrical vessel	0	Stirred with a paddle	Continuous stirring at 300 rpm	Not stated	0	Not stated	0
DIDGI Dynamic Gastro-intestinal Digester (DIDGI) [165]	Multi	Level 3 borelevant fluid	Yes	Flow through system (total volume not reported)	4	Cylindrical beaker	0	Mixing	Continuous stirring	Not stated	0	Mapped to in vivo data	1
Duodenal static model [156]	Multi	Level 3 borelevant fluid	No	Not stated	3	Cylindrical beaker	0	Orbital shaker	Continuous stirring	Not stated	0	3-4 hours	1
SIMGI [242]	Multi	Level 3 borelevant fluid	Yes	105	4	Cylindrical beaker	1	Mixing	Continuous stirring	Not stated	0	2 hours	0
Biorelevant Gastrointestinal Transfer (BioGIT) model [34]	Multi	Level 2 FaSSIF or FeSSIF	Yes	40		No a USP mini (100 mL) dissolution vessel	0	USP Paddle rotation	Continuous stirring at 75 rpm	Not stated	0	Not stated	0
TNO TinyTIM [243]	Multi	Level 3 borelevant fluid	Yes	Volume not stated	4	Cylindrical tube. Does not reflect length or surface area	0	External compression of flexible walls	Mimics peristalsis	Not stated	2	Mapped to in vivo data	1
Engineered Stomach and small INtestine (ESIN) model [169].	Multi	Level 3 borelevant fluid	Yes	Not stated	4	Hemispherical vessels	0	Overhead stirring	Continuous stirring	Not stated	0	Mapped to in vivo data	1

Model of an Infant Digestive Apparatus (MIDA) [176]	Multi	Level 3 borelevant fluid	Yes	160	4	Flexible cylindrical tube	0	Tubes squeezed to reproduce the peristaltic motion	Continuous motion	Not mentioned	2	Time not stated.	0
The Smallest Intestine (TSI) [240]	Single	Level 3 borelevant fluid	Yes	12	5	Solid beaker	0	Overhead mixer stirs continuously	Continuous stirring at 170 rpm	Not stated	0	Duodenum 2 hours; jejunum 4 hours; ileum 2 hours	1
Biocell [241]	Flow through	Level 0 deionised water	No	5	1	Flexible dialysis tubing	0	Tubes squeezed to reproduce the peristaltic motion	Not stated	Not stated	1	Not stated	
Bionic gastrointestinal reactor (BGR) [186]	Multi	Level 0 deionised water	No	Not stated	0	Flexible cylindrical tube that includes folds and villi in the structure	2	Not stated	Not stated	Not stated	0	Not stated	

Table 12. Summary of in vitro *models of the small intestine*

3.7 Organoid models of the small intestine

Enteroids have been developed from primarily human [244-251] and murine [252-255] primary tissue. Induced human intestinal organoids have also been reported [256-259] and human fetal intestinal organoids [260]. Like their gastric counterparts, intestinal organoids have been used to study cancer [255], but over the past decade enteroids have been increasingly used as disease models for the study of host-pathogen interactions using dissociated spheroid structures, seeded as monolayers. This has been particularly useful for the study of viruses that lack a robust cell system such as rotaviruses and noroviruses. Successful co-culture of human rotaviruses [245, 249, 251, 256], noroviruses [244, 247, 249, 259] and astroviruses [250] that have previously not been possible to grow in transformed cells has been demonstrated. Interestingly, a study of rotavirus infection in induced human intestinal organoids also showed infection of mesenchymal cells [256]. Additionally, studies have covered Salmonella [252, 257], E. Coli [258], avian influenza [253], human adenoviruses [248] and SARS-CoV-2 [261], *L. intracellularis* [254] parasitic infection [246] and a diverse range of enteroviruses were tested by Drummond et al (2017) [260]. Human enteroids and intestinal organoids may therefore be useful as physiologically relevant universal culture models to study ingestible device that may deliver therapeutics that act against enteroviruses.

3.8 Organ-on-a-chip and microfluidic models of the small intestine

Organ-on-a-Chip models of the small intestine have mostly been seeded with colorectal adenocarcinoma-derived Caco-2 and HT-29 cell lines [89, 90, 92, 262-265]. In 2011 Sung et al [266] produced a 3D collagen scaffold that replicated the geometry of intestinal villi with villus depth of around 500 microns and spacing of 25 villi mm^{-2}. Since, similar studies have proliferated monolayers of Caco-2 on 3D villus-like scaffold to promote differentiation [266-271] which can increase physiological relevance through enabling co-culture [269, 271] and influencing host-microbial interaction [271], drug absorption [267] and mucous production [269, 270]. These models were static until Costello et al (2017) [272] developed a bioreactor that contained provided both accurately-sized villus topography and fluid flow based on the baseline MMC of a fasting healthy human. This model also used PEVA as a scaffolding as previous models using PLGA may be eroded by the shear stress exerted by fluid flow over time.

Peristalsis-like motions and luminal / basolateral flow have been recreated to induce morphogenesis of villi [89, 90, 263] and even develop basolateral proliferative crypts to culture vascular endothelial cells, recreating the intestinal tissue-tissue interface [263]. Flow profiles and shear stress distribution in the channel of a Caco-2-seeded microfluidic gut chip device has been simulated by Ramadan et al (2016) [273] according to Navier-Stokes equations, assuming incompressible, Newtonian flow with no wall slip.

In 2018, Kasendra et al [274] reported the first method for creating a Small Intestine-on-a-Chip device containing primary human duodenal epithelial cells from dissociated enteroids, and microvascular endothelial cells. The transcriptome of this device more closely represented the adult human duodenum in vivo than the organoids used to fabricate them, and compared with Caco-2 chip models, especially with respect to expression of genes that relate to cell proliferation, digestive function and response to infection and nutrition [274]. Since this has been studied for expression of drug metabolizing genes [88]. Yin et al (2020) [275] cocultured jejunal organoids in a similar system with human umbilical vein endothelial cells (HUVEC) and studied the relationships between cardiac and luminal flows, mimicked peristalsis and cell differentiation and NaCl absorption. Gazzaniga et al (2021) [276] recently demonstrated that small intestine chips can be created with cells derived from murine duodenal, jejunal and ileal organoids. A summary of some gut-on-a-chip models that represent the small intestine are provided in Table 13.

Separately, Naumovska et al (2020) [277] reported differentiation of iPSCs into 3D gut-like tubules directly inside microfluidic devices, eradicating the need for external organoid culture and subsequent dissociation, ultimately ctting the differentiation procedure to only 14 days. Furthermore, this study employed the OrganoPlate platform, enabling simultaneous use of 40 microfluidic chips. Pim de Haan

et al (2021) [278] presented a compartmentalized in vitro model of the small intestine microenvironment, wherein the feed is first subjected to mimicked mouth, stomach and intestinal digestion before continuing to a flow-through barrier model of the intestinal epithelium using Caco-2 cells.

Considering any microdevices that may interact with the endothelium through the epithelial barrier, membrane thickness may be important. The membrane used for human gut-on-a-chip design is typically relatively thick, commonly over 10 µm in thickness [263, 279], whereas the physiological basement is only around 400 nm thick. This large difference may impede transport kinetics of small molecules delivered by any microdevices, or any devices that practice microinjection that may be tested in these systems.

The value of these intestine on a chip model for ingestible devices lie in their ability to recreate the microenvironment of the intestine; particularly where they include sensor devices so that they can monitor aspects of the GI lumen to evaluate the accuracy of sensors to small changes in either flow or composition under controlled conditions, including host-microbiome reactions [280].

Ref	Cell type	Luminal dimensions	2D/3D	Luminal flow	Molecular transport	Wall shear stress	Mucous layer thickness	Peristalsis	Commensal microbiota	Disease / pathogen	Other cell types
[278]	Caco-2 & HT-29MTX	Mixing channels: W: 300 µm L: 51.5 µm V: 1.48 µL Flow-through Transwell	-	200 $\mu L*h^{-1}$	N	0.006 dyne $*cm^{-2}$	n/a	N	N	N	N
[276]	Murine duodenal, jejunal and ileal enteroids	H: 1000 µm W: 1000 µm MT: 50 µm	2D & 3D	N	N	n/a	n/a	N	Probiotic lactobacillus rhamnosus GG	WT Y. pseudotuberculosis YPIII	Caco-2, HT29-MTX & H-MyoFib
[275]	Healthy jejunal enteroids	n/a		60 $\mu L*h^{-1}$	NaCl	n/a	n/a	10% strain at 15 Hz	N	N	HUVEC (endothelium)
[88]	Healthy adult duodenum intestinal organoids	Channel H: 1 mm W: 1mm MT: 50 µm		30 $\mu L*h^{-1}$	Dextran	n/a	n/a	10% strain at 0.2 Hz	N	N	N
[265]	Human Caco-2 (HTB-37)	H: 0.65 mm W: 15 mm MT: n/a	-	Y	Antipyrine, ketoprofen & digoxin	0.002 dyne cm^{-2}	n/a	N	N	N	N
[277]	hIPSCs	3-lane 400 µm OrganoPlate		N	N	N	n/a	N	N	N	Endothelium
[281]	Caco-2	H: 150 µm W: 1000 µm L: 10 mm long		30 $\mu L*h^{-1}$	N	0.02 dyne $*cm^{-2}$	n/a	10% strain at 0.15 Hz	Y (VSL#3)	Inflammation, pathogenic bacteria (EIEC)	PBMCs (immune cells)

		MT: 20 µm									
[282]	Terminal ileum enteroids (macroscopically unaffected tissue from 15-year-old UC patient biopsy)	n/a	3D PDMS porous membrane	60 µL*h^{-1}	N	n/a	10 µm	10% strain at 0.15 Hz	Bacteroides fragilis		
[283]	Caco-2	H: 200 µm W: 1000 µm L: 14 mm long MT: 50 µm	3D	30 µL*h^{-1}	N	0.02 dyne *cm^{-2}		10% strain at 0.15 Hz	N	Radiation injury	HUVECS(Vascular endothelium)
[274]	Healthy adult duodenum intestinal organoids (from endoscopic biopsy) on a chip.	Channel H: 1 mm W: 1mm MT: 50 µm **Villi** Major and minor axes 232 ± 17 and 122 ± 7 µm ~30 villi cm^{-2}	3D PDMS porous membrane	60 µL*h^{-1}	N	n/a	n/a	60% strain at 0.2 Hz	N	n/a	N
[284]	Caco-2	W: 1 mm L: 10 mm H: 200 µm MT: 20 µm	3D PDMS porous membrane	50 µL*h^{-1}	N	0.02 dyne *cm^{-2}	n/a	10% strain at 0.15 Hz	N	Inflammation	N
[285]	Dissociated iPSC-derived human intestinal organoids (non-specific) and Caco-2	H: 1000 µm W: 1000 µm		30 & 60 µL*h^{-1}	N	n/a	n/a	N	N	Interferon (IFN)-γ and tumor necrosis factor-α	Mesenchyme

[286]	Caco-2	MT: 15 µm		0.04 µL*min^{-1} 2.4 µL*h^{-1}	Caffeine, atenolol and lipophilic prodrugs of SN38	0.02 dyne *cm^{-2}	n/a	N	N	N	N
[272]	Caco-2		3D matrix		Glucose	0.001-0.05 dyne *cm^{-2}	n/a	N	N	N	N
[93]	Caco-2	H: 1.5 mm W: 200 µm	2D	96 µL*h^{-1}	Fluorescein, apigenin	7.89 *x* 10^{-5} dyne *cm^{-2}	n/a	N	N	N	HepG2
[262]	Caco-2	W: 1 mm L: 1.4 cm H: 200 µm MT: 10 µm	3D	30 & 60 µL*h^{-1}	N	0.02 dyne *cm^{-2} at 30 µL*h^{-1}	n/a	10% strain at 0.15 Hz	N	coxsackievirus B1 (CVB1)	N
[264]	Caco-2 on 3D scaffold	W: 120 µm H: 200 µm		100 µL*min^{-1} 6000 µL*h^{-1}	Rhodamine 123	n/a	n/a	N	N	N	N
[263]	Caco-2	n/a	3D	30 & 40 µL*h^{-1}	N	0.02 dyne *cm^{-2}	n/a	10% strain at 0.15 Hz	Y VSL#3	LPS endotoxin (15 µg*mL^{-1}) isolated from *E. coli,* EIEC cells	PBMCs (immune cells)
[287]	Caco-2 (HuMiX)	W: 4 mm L: 200 mm H: 0.5 mm	2D	25 µL*min^{-1} 1500 µL*h^{-1}	N	n/a	n/a		*Lactobacillus rhamnosus, Bacteroides caccae*	N	N
[273]	Caco-2	n/a	2D	1 µL*min^{-1} 60 µL*h^{-1}	FITC-dextran	0.02 dyne *cm^{-2}	n/a	N	N	Inflammatory cytokines and endotoxin LPS affecting barrier permeability	U937 (immune cells)
[288]	Caco-2	Matrix 3D	3D (scaffold)	N	N	N	10 – 20 µm	N	N	N	Caco-2 & HT29 & H-MyoFib
[91]	Caco-2	W: 50 µm L: 2 cm H: 50 µm MT: 10 µm		0.1, 0.5, 2.5 & 10 µL*min^{-1} 6, 30, 150 & 6000 µL*h^{-1}	FITC-dextran	0.0002 dyne *cm^{-2}	n/a	10% strain at 0.15 Hz	Y	*S.* Typhimurium	N

[270]	Caco-2	3D matrix Villi height 400 µm Villi diameter at base 200 µm 25 villi mm^{-2}	2D	N	N	N	n/a but expression of MUC17	N	N	*S.* Typhimurium, E. Coli	N
[271]	Caco-2	500 µm Villi height	3D (scaffold)	N	N	N	n/a	N	Probiotics *Lactobacillus gasseri* and *E. coli* Nissle 1917	*Salmonella typhimurium* a nd *Pseudomon as aeruginosa*	N
[269]	Caco-2 with HT29-MTX and murine intestinal crypts	Villi 500 µm high and 200 µm wide at base	3D (scaffold)	N	N	N	Co-culture with mucous producing HT29-MTX	N	N	*N*	N
[89]	Caco-2	H: 150 µm W: 1000 µm L: 10 mm long MT: 30 µm	3D	30 $\mu L*h^{-1}$	N	0.02 dyne cm^{-2}	n/a	10% strain at 0.15 Hz	N	N	N
[289]	Caco-2	n/a	2D	0.1 $\mu L*min^{-1}$ 6 $\mu L*h^{-1}$	Curcumin	N	n/a	N	N	N	N
[90]	Caco-2	H: 150 µm high W: 1000 µm MT: 30 µm	3D (differentiated)	30 $\mu L*h^{-1}$	N	0.02 dyne cm^{-2}	n/a	10% strain at 0.15 Hz N	Y	N	N
[268]	Caco-2	3D matrix, villi with aspect ratios up to 4:1 25 villi mm^{-2}	3D (scaffold)	Computational simulation	N	N	n/a	N	N	N	N
[267]	Caco-2	3D matrix	3D (scaffold)	N	Antenolol	N	N	N	N	N	N
[266]	Caco-2	3D matrix	3D (scaffold)	N	N	N	n/a	N	N	N	N

[290]	Caco-2	H: 1 mm W: 1.5 mm L: 4 mm	2D (Monolayer)	Y	Cyclophosphamide	N	n/a	N	N	N	N

Table 13. Summary of organ on a chip models of the small intestine. In order of occurrence: Y = yes, N = no, n/a = data not available. H = height, W = width & MT = membrane thickness. WT = wild type. HUVEC = human umbilical vein endothelial cell.

4 Replicating the colonic environment

4.1 Overview of colonic function and anatomy

The colon is anatomically divided into four sections: ascending (AC) (or proximal), transverse (TC), descending (DC) (or distal), and sigmoid, with a total length of up to 1.5 m in adult humans.
The colon can be distinguished from the small intestine by the presence of three longitudinal bands of muscle on the outer surface that leads to the haustrated appearance [291].
The caecum is at the junction of the ileum and colon and is a downward pouch that is about 5-7 cm long. The ascending colon (AC) extends vertically from the caecum and is 15 cm long; at the top there is a sharp bend where it becomes the transverse colon [291]. The transverse colon (TC) is typically 45 cm long and is considered to be the most mobile portion of the large intestine [291]. Another sharp turn defines the start of the descending colon (DC) which is about 25 cm long and joins to the sigmoid colon [291]. The sigmoid colon is 35-40 cm long and joins to the rectum which is 12-15 cm in length [291, 292]. The diameter of the colon varies from the widest part being the caecum with a diameter of 7.5 cm and the sigmoid colon being the narrowest at 2.5 cm [292].
The major function of the colon is maintaining water balance, supporting the microbiome, and the production of faeces. Although the surface of the colon is smoother than that in the small intestine, microvilli are present on transverse furrows of the colon to improve the surface area and aid in the maintenance of osmolarity. Much of the surface of the colon is columnar epithelial cells which explains the smooth surface appearance [291].

4.2 Colonic fluid volume

Table 14 presents colonic fluid volumes determined using magnetic resonance imaging (MRI). Volumes represent anatomical volume rather than fluid volume, unless stated. Development of appropriate models of the colon rely on replication of the capacity of this organ and as such the information in Table 14 can inform the biorelevance of the range of in vitro apparatus available. The data shows that the volume of the colon can change depending upon the conditions and that the fluid within the colon does not fill this organ. Furthermore, the fluid that is present is not present as a continuous body, rather in pockets each of a small volume, primarily located in the AC [293].

				Volume (mL) Mean ± standard deviation or range shown (unless otherwise stated)			
Reference	Subjects	Measurement taken	Prandial state	Ascending Colon (AC)	Transverse Colon (TC)	Descending Colon (DC)	Key finding
[27]	12, healthy		Fasted & fed - Consumed non-disintegrating tablets	Colonic water volumes (13 ± 12 mL), intersubject variability 1 – 44 mL (fasting), 2 – 97 mL (fed). Water pockets were mainly located close to the caecum, AC and DC with total capacity of 2 mL (median).			Food had minimal effect on colonic water volumes but increased the number of colonic pockets from 4 to 6 ($p < 0.005$).
[294]	18, healthy	Water in ascending colon	Ingested capsules containing placebo or 12 mg loperamide (LOP) or 12 mg LOP + 125 mg simethicone (SIM). After 100 min, given a drink containing 5% mannitol in 350 mL water.	6.9 ± 1.2 mL LOP 6.8 ± 1.5 mL and LOP + SIM 4.5 ± 0.9 mL	-	-	LOP & LOP + SIM delayed arrival of fluid to the AC.
[295]	25 IBS-D	Fasting and postprandial volumes of the undisturbed colon	Fasted	205 ± 69 mL	232 ± 100 mL	151 ± 71 mL	10% expansion of AC volume when fed (rice pudding meal).
	75 healthy		Fasted	203 ± 75 mL	198 ± 79 mL	160 ± 86 mL	No significant effect of feeding (rice pudding meal) on AC volume.
[296]	25 healthy	Segmental and whole intestinal chyme content (water volume)	Fasted	177 mL (147 – 208) (including caecum)	192 mL (159-226)	133 mL (110 – 157), rectosigmoid colon 257 mL (213 – 302)	No intrapatient variability on different days ($p>0.05$). Overall volume 760 mL (662 – 858) and 757 mL (649 – 865).
				186 mL (159 – 212)	197 mL (155 – 240)	193 mL (111-168), rectosigmoid colon 235 mL (193-277)	

	7 healthy	Segmental and whole intestinal chyme content (water volume)		-			Impact of defaecation on regional volumes only significant for rectosigmoid colon (329 mL (248-409) before and 183 mL (130-236) after.
[297]	4 healthy	Regional colonic water	No restrictions to feed state.	200 (169.5 – 260) mL	200.5 (113.5-242.5) mL	148 (121.5 – 178.5) mL, rectosigmoid 277 (192 – 345) mL	Total colonic volume 819 (687 – 898.5) mL
[298]	12 healthy	Colonic volume and gas effects of gluten	Fasted then given GF bread	250 ± 119 mL	289 ± 95 mL	209 ± 73 mL	-
			Fasted then given normal bread	256 ± 149 mL	212 ± 73 mL	187 ± 92 mL	-
			Fasted then given normal bread with added gluten	224 ± 128 mL	178 ± 86 mL	172 ± 77 mL	-
[299]	24 patients with functional constipation	Effect of PEG electrolyte formulation on gut volumes	Fasted	314 ± 101 mL	-	-	Total colon volume: 847 ± 280 mL
			120 min after PEG ingestion	597 ± 170 mL	-	-	Total colon volume: 1505 ± 387 mL
	24 patients with IBS-C		Fasted	226 ± 71 mL	-	-	Total colon volume: 662 ± 240 mL
			120 min after PEG ingestion	389 ± 169 mL	-	-	Total colon volume: 1039 ± 418 mL
[300]	11 healthy male 10 healthy female	Effect of IV corticotropin-releasing factor on fructose malabsorption	Baseline fasted	210 ± 77 mL	-	-	-
			45 min after ingestion of fructose	270 ± 109 mL	-	-	-
		Effect of IV saline on fructose malabsorption	Baseline fasted	226 ± 74 mL	-	-	-
			45 min after ingestion of fructose	252 ± 83 mL	-	-	-
[301]	25 healthy male	Opioid-induced bowel dysfunction	Oxycodone Day 1	177 (147 – 208) mL	192 (159 – 226) mL	133 (110 – 157) mL	Increase in AC, TC, DC (significant) decrease in RSC (insignificant)
			Oxycodone Day 5	249 (202-291) mL	230 (190-270) mL	153(132 – 175) mL	

			Placebo Day 1	186 (159-212) mL	197 (155 – 240) mL	139(111 – 168) mL	Increase in AC and RSC (significant), decrease in TC and DC (significant). No significant increase in whole colon volume.
			Placebo Day 2	211 (184 – 238) mL	183 (152 -213) mL	121 (101 – 142) mL	
[302]	10 healthy	Effect of meals, defecation and diet on colonic content	Low-residue diet day 4	479 ± 36 mL (non-gaseous content)			Daily faecal volume 145 ± 15 mL 10.6 ± 1.6 daytime gas evacuations
			High residue diet day 4	616 ± 55 mL (non-gaseous content)			Daily faecal volume 223 ± 19 mL 16.5 ± 2.9 daytime gas evacuations
[293]	12 healthy	Total and segmental free water	Fasted	11 ± 5 pockets of 2 ± 1 mL resting liquid primarily in AC.			High inter-subject variability with number of pockets ranging from 0 – 89 and amount of water ranging from 0 – 49 mL.
			30 mins post-administration of 240 mL water	17 ± 7 pockets of 7 ± 4 mL resting liquid primarily in AC.			
. [303]	11 healthy	Colonic free water distribution	Fasted	2 (0 – 7) mL			-
			Fed macrogol t = 60 min	140 (104 – 347) mL			-
			Fed macrogol t = 120 min	146 (32 – 227) mL			-
	11 constipated		Fasted	11 (1-29) mL			-
			Fed macrogol t = 60 min	228 (91 – 259) mL			-
			Fed macrogol t = 120 min	84 (3 – 195) mL			-
[304]	9 healthy	Effect of psyllium on colonic volumes	Fasted placebo (maltodextrin)	138 (114 – 208) mL	132 (99 – 188) mL	111 (60 – 185) mL	-
			Fasted psyllium 10.5 g / d	213 (152 – 285) mL	215 (119 – 332) mL	142 (117 – 213) mL	-
			Fasted psyllium 21 g / d	251 (191 – 301) mL	228 (163 -362) mL	132 (87 – 225) mL	-
	20 constipated		Fasted placebo (maltodextrin) (n = 9)	270 (174 – 361) mL	362 (221 – 438) mL	221(130 – 278) mL	-
			Fasted psyllium (n = 11)	390 (320 – 412) mL	366 (267 – 547) mL	246 (221 – 336) mL	-

[305]	20 healthy	Effect of oxycodone plus macrogol and PR naloxone and oxycodone on segmental gut water	Oxycodone plus PR naxalone Baseline day 1	220 ± 25 mL	258 ± 42 mL	187 ± 32 mL	RSC increased from 276 ± 60 mL to 273 ± 71 mL. Total from 941 ± 108 mL to 1036 ± 176 mL.
			Oxycodone plus PR naxalone day 5	257 ± 41 mL	295 ± 47 mL	210 ± 51 mL	
			Oxycodone plus Macrogol	216 ± 39 mL	270 ± 59 mL	184 ± 55 mL	RSC from 242 ± 55 mL to 287 ± 52 mL. Total from 812 ± 158 mL to 1123 ± 145 mL.
			Oxycodone plus Macrogol	277 ± 53 mL	328 ± 51 mL	231 ± 44 mL	

Table 14. Details on colonic volume present in adults reported in the literature. Note that some studies report colonic volume and not the volume of fluid present within the colon. RSC= right sigmoid colon

Colonic transit time

It is known that there is wide variability in the transit time within the colon of adults with range of 12-72 hours reported in a normal population [306]. The technique used to measure the transit can affect measurements reported and this is discussed in further detail in the second part of this review paper [8]. There is a meta-analysis on colonic transit times of ingested solid oral dosage forms that may also be useful for the reader [136]; particularly as this highlighted that larger units can move more quickly through the colon compared to multi-units.

4.3 Colonic motility

Colonic motility has a circadian rhythm where motility is typically inhibited at night time [292]. During waking hours the transverse and descending colon show more activity to promote function activities including absorption, mixing, propulsion of contents, as well as formation and storage of faeces [292]. Ingestion of food also influences colonic motility and fatty meals have been shown to have a stronger influence on motility compared to carbohydrate based meals [307]. Further details on colonic motility are presented in the second part of this review paper [8], alternatively detailed information can be found in this paper [292].

4.4 Colonic media composition

Sampling of colonic media is difficult due to the inaccessibility of the colon. Tang et al (2020) [308] have recently reviewed techniques for colonic sampling with a focus towards microbiota. However, some studies have characterized the contents of the AC by taking samples during colonoscopy to establish relevant components required to reproduce a simulated media representative of the AC lumen, shown in

Contents of human ascending colon (AC) post-ultracentrifugation								
Ref.	**Population**	**Sample location**	**Prandial state**	**Colon prep.**	**pH**	**Aqueous fraction (%)**	**Buffer capacity (mmol*(L*pH)$^{-1}$)**	**Sample volume (mL)**
[309]	UC patients in relapse		Fasted	Ingestion of bisacodyl tablets	6.6 (5.5–7.7)	n/a	32.0 ± 18.1 (using HCl solution n=11) 18.3 ± 10.4 (using NaOH solution n=3)	26.8 (13.5)
[309]	UC patients in remission		Fasted		6.5 (6.1–7.3)	n/a	37.7 ± 15.4 (using HCl solution n=11) 16.7 ± 5.8 (using NaOH solution n=3)	21.2 (8.8)
[31] Pilot study	6 x Healthy adults, aged 18-60 years		Fasted	Ingestion of PEG 3350 solution (Klean-Prep) or bisacodyl tablets (Dulcolax®, Boerhinger Ingelheim, Athens, Greece).	n/a	n/a	6.0 ± 3.6 (using NaOH solution) 11.0 ± 7.8 (using HCl solution I)	27.1 (6.1)
[31] Main study	12 x Healthy adults aged 19-28 years		Fasted		7.8 (median)	70.3 (17.0)	21.4 (using HCl solution) 10.3 (using NaOH solution)	22.3 (7.7)
			Fed		6.0 (median)	56.0 (9.0)	37.7 (using HCl solution) 16.4 (using NaOH solution)	29.9 (10.8)

Supernatant of contents of human ascending colon (AC) post-ultracentrifugation									
Ref.	**Population**	**Prandial state**	**Colon prep.**	**Osmolarity post-centrifugation (mOsmol*kg^{-1})**	**Surface tension (mN*m^{-1})**	**Protein content (mg*mL^{-1})**	**Carbohydrate content (mg*mL^{-1})**	**SCFA content (mg*mL^{-1})**	**Bile acids (mg*mL^{-1})**
[309]	UC patients in relapse	Fasted	Ingestion of bisacodyl tablets	199.6 ± 127.4	41.6 ± 3.1	18.9 ± 8.1	5.4 ± 2.7	23.2 ± 14.9	75.83 ± 42.96
[309]	UC patients in remission	Fasted		290.1 ± 165.6	40.6 ± 3.4	19.0 ± 10.8	6.4 ± 4.1	45.3 ± 26.8	115.15 ± 100.20
[31] Pilot study	6 x Healthy adults, aged 18-60 years	Fasted	Ingestion of PEG 3350 solution (Klean-Prep) or bisacodyl tablets (Dulcolax®, Boerhinger Ingelheim, Athens, Greece).	328.83* / 286.67**	n/a	n/a	n/a	n/a	n/a
[31] Main study	12 x Healthy adults aged 19-28 years	Fasted		81.0 (102)	42.7	9.7 (4.6)	8.1 (8.6)	30.9 (15.4)	587.4 (412.8)
		Fed		224.0 (125)	39.2	6.9 (2.3)	14.0 (7.4)	48.1 (21.7)	115.2 (119.3)

Table 15. However, colonic preparation is required for a colonoscopy, which is likely to have resulted in unnatural properties of the luminal fluid. Stamatopoulos et al [8] present a review detailing the characteristics of the caecum and AC in commonly used animal models. No published data is available on the viscosity of human AC contents.

Contents of human ascending colon (AC) post-ultracentrifugation								
Ref.	**Population**	**Sample location**	**Prandial state**	**Colon prep.**	**pH**	**Aqueous fraction (%)**	**Buffer capacity (mmol*(L*pH)$^{-1}$)**	**Sample volume (mL)**
[309]	UC patients in relapse		Fasted	Ingestion of bisacodyl tablets	6.6 (5.5–7.7)	n/a	32.0 ± 18.1 (using HCl solution n=11) 18.3 ± 10.4 (using NaOH solution n=3)	26.8 (13.5)
[309]	UC patients in remission		Fasted		6.5 (6.1–7.3)	n/a	37.7 ± 15.4 (using HCl solution n=11) 16.7 ± 5.8 (using NaOH solution n=3)	21.2 (8.8)
[31] Pilot study	6 x Healthy adults, aged 18-60 years		Fasted	Ingestion of PEG 3350 solution (Klean-Prep) or bisacodyl tablets (Dulcolax®, Boerhinger Ingelheim, Athens, Greece).	n/a	n/a	6.0 ± 3.6 (using NaOH solution) 11.0 ± 7.8 (using HCl solution l)	27.1 (6.1)
[31] Main study	12 x Healthy adults aged 19-28 years		Fasted		7.8 (median)	70.3 (17.0)	21.4 (using HCl solution) 10.3 (using NaOH solution)	22.3 (7.7)
			Fed		6.0 (median)	56.0 (9.0)	37.7 (using HCl solution) 16.4 (using NaOH solution)	29.9 (10.8)

Supernatant of contents of human ascending colon (AC) post-ultracentrifugation									
Ref.	**Population**	**Prandial state**	**Colon prep.**	**Osmolarity post-centrifugation (mOsmol*kg^{-1})**	**Surface tension (mN*m^{-1})**	**Protein content (mg*mL^{-1})**	**Carbohydrate content (mg*mL^{-1})**	**SCFA content (mg*mL^{-1})**	**Bile acids (mg*mL^{-1})**
[309]	UC patients in relapse	Fasted	Ingestion of bisacodyl tablets	199.6 ± 127.4	41.6 ± 3.1	18.9 ± 8.1	5.4 ± 2.7	23.2 ± 14.9	75.83 ± 42.96
[309]	UC patients in remission	Fasted		290.1 ± 165.6	40.6 ± 3.4	19.0 ± 10.8	6.4 ± 4.1	45.3 ± 26.8	115.15 ± 100.20
[31] Pilot study	6 x Healthy adults, aged 18-60 years	Fasted	Ingestion of PEG 3350 solution (Klean-Prep) or bisacodyl tablets	328.83* / 286.67**	n/a	n/a	n/a	n/a	n/a
[31]	12 x Healthy adults aged 19-28 years	Fasted		81.0 (102)	42.7	9.7 (4.6)	8.1 (8.6)	30.9 (15.4)	587.4 (412.8)

Main study		Fed	(Dulcolax®, Boerhinger Ingelheim, Athens, Greece).	224.0 (125)	39.2	6.9 (2.3)	14.0 (7.4)	48.1 (21.7)	115.2 (119.3)

Table 15. Studies where the composition of colonic fluids has been characterised. UC=ulcerative colitis

Diakidou et al. [31] found that the level of triglycerides, diglycerides and cholesterol esters was undetectable in the supernatant of healthy human AC contents after ultracentrifugation. However, palmitic acid, linoleic acid, oleic acid, phosphatidylcholine, and cholesterol were measured at levels (mean (±standard deviation)) of 49.6 (±43.7), 37.4 (±29.6), 32.8 (±36.7), 362 (±210), and 1703 (±1764) µM respectively in the fasted state, and 103.8 (±112.1), 47.8 (±30.0), 73.4 (±81.7), 539 (±393), and 1882 (±1325) µM in the fed state [31]. Fed state colonic contents tend to have decreased protein concentration compared to fasted state [31]. Surface tension is generally higher in the colonic contents (42.7 $mN*m^{-1}$ in the fasted state and 39.2 $mN*m^{-1}$ in the fed state) than in the small intestine [309]. Osmolarity is typically lower (81 $mOsm*kg^{-1}$ in the fasted state and 227 $mOsm*kg^{-1}$ in the fed state) than in the small intestine [309]. This may be because the majority of protein digestion occurs upstream of the colon, resulting in dilution of protein contents when contents arrive from the terminal ileum into the AC. In animals it has been shown that fasting reduces concentration of small chain fatty acids (SCFAs) [310]. No published data is available on the viscosity of human AC contents. Composition of the colonic microbiota is beyond the scope of this review.

4.4.1 Simulated colonic media

The fluid within the colon changes from the watery fluid that exits the small intestine to the drier faeces that exits the colon. Simulated fluid thus may be dependent upon the region of the colon as well as the purpose for which they are used. Colonic drug delivery systems can be designed to release their drug load based on changes in media pH; the presence of microbiome or time; thus, the media used in any in vitro test needs to be relevant for the conditions to be simulated.
There are fewer standardized simulated colonic fluids in comparison the FaSSIF and FeSSIF recipes that are widely used as simulated small intestinal fluids. In addition, research into foods and digestion has also generated a wide number of simulated colonic fluids. Basic simulated fluids use buffers at the most suitable pH of the colon whereas other methods incorporate the use of enzymes. There are several recipes for simulated colonic fluid (SCoF) that replicate the pH, osmolality, buffer capacity and ionic strength of colonic fluid characterized from humans [130]. There are also recognized recipes that replicate fasted state and fed state simulated colonic fluid (FaSSCoF and FeSSCoF) [130]. It should be noted that the composition of the media can affect the release profile for oral drugs, particularly the use of the more physiologically relevant bicarbonate buffer in place of phosphate buffers [311].
Due to the large variety in media that can be used the reader is referred to other papers on this topic: dissolution media for dosage forms triggered by colonic microflora [312, 313]; simulated fluids of the AC [314]; simulated fluid to evaluate probiotics [315]; the reproducibility of using faecal slurries in bioreactors [316].

4.5 Overview of in vitro models of the colon

4.5.1 Modified pharmacopoeial apparatus to mimic the colon

Pharmacopoeial apparatus has been used previously to mimic colonic conditions. The range of methods used is presented in Table 16 which also shows the simulated fluids used within these studies. Modified dissolution apparatus is widely used due to the accessibility and reproducibility of this apparatus globally.

Ref	Dissolution apparatus	Media volume [mL]	Composition of media	Bile salt [Y/N]	Viscosity [Y/N]	Microbiota (Y/N)	Mixing conditions	Prior exposure to GI fluids [Y/N]	Sampling duration [min]	Link to in vivo data
[317]	USP Apparatus II	500 mL	sodium phosphate buffer with NaCl and Na_2SO_4 to alter ionic strengths	N	N	N	75 rpm	N	240	N
[318]	USPII	500 mL	FaSSCoF	N	N	N	50 rpm	N	1440	N
		mL								
[319]	USPIII	250 mL	SCoF	Y	N	N	10 dpm	Y	960	N
[151]	USPII stress test device	1160 mL	Hanks hydrogen carbonate buffer (pH 6.8) with 0.1 % Tween 80	N	N	N	200 rpm +stress cycles	Y	1560	N
[38]	USPII	1000 mL	Hanks buffer, Krebs buffer, $NaHCO_3$ solution	N	N	N	50 rpm & 100 rpm	Y(Dynamic pH changes throughout experiment)	720	N
	USPII +stress-test device	1150 mL	USP pH6.8 buffer with 1% SDS	N	N	N	50 and 100 rpm	N	360	N
[320]	GISS (based on USPII)	1000 mL	simulated colonic fluid	N	N	N	50 rpm	Y	400	N
[321]	USP Apparatus III, reciprocating cylinder, RRT 10, Erweka, Heusenstamm, Germany. AND USP apparatus II, paddle apparatus	200 mL	SCoF	N	N	N	10 dpm, 420 um mesh. USP II undefined	y	240	y
[322]	Paddle apparatus (provider unspecified)	6 mL	FaSSIF,	N	N	N	100 rpm	N(HCl for pH)	120	y
[323]	mini USP apparatus with paddle - paddle adapted for viscosity effects	200 mL	FaSSCof, FeSSCoF v2	y	Y (for fed state)	n	40 rpm (pr 100 rpm)	y	160	y
[324]	USP Apparatus I	1000 mL	FTM	Y	N	Y	100 rpm	N(HCl for pH)	1440	Y

[325]	USP III, USP IV	235 mL	Fasted= FaSSCoF. Fed= FeSSCoF	N	N	N	6 dpm, 4 $mL*min^{-1}$	N	360	Y
[326]	USPIII, USPIV	235 mL	Fasted= FaSSCoF. Fed= FeSSCoF	N	N	N	6 dpm, 4 $mL*min^{-1}$	Y	360 minimum fasted 540 minimum fed	Y
[327]	USPIII & USPIV	235 mL	Fasted= FaSSCoF. Fed= FeSSCoF	Y	N	N	6 dpm, 4 $mL*min^{-1}$	Y	120	Y
[328]	USPI	1000 mL	FTM supplemented with probiotics (BIOMIX-1)	N	N	Y	100 rpm	Y	1080	Y
[329]	USPII	500 mL for acid stage, 900 mL for buffer stages	HCl, pH6 phosphate buffer	N	N	N	100 rpm acid stage, 50 rpm buffer stages	Y(HCl)	210	Y

Table 16. Summary of studies that use pharmacopoeial apparatus to mimic the colonic environment

4.5.2 Fermentation models of the colon

Multi-compartmental fermentation models of the colon typically feature three fermentation reactors, as initially proposed in 1988 by Gibson et al [330]. Fermentation is not possible to study in vivo, therefore in vitro simulated fermentation models are highly valuable. These models make possible the study of metabolite production by complex microbial ecosystems. Sampling from faecal matter does not reflect the *in situ* production of metabolites, and the ecological composition of colonic content varies drastically with progress along the GI tract, therefore faecal sampling is most valid for evaluation of the rectal environment. However, most in vitro models however lack absorption capacity to model uptake of metabolites by the epithelium and therefore reflect true intraluminal concentrations. Most in vitro fermentation models are fed through fecal inoculum whereas the PolyFermS uses a microencapsulation technique. Many in vitro fermentation models are static, however Venema and van den Abbeele [331] highlighted a non-physiologically relevant slow rate of conversion in "static cultures" (as opposed to continuous "dynamic" culture conditions). Furthermore, most models only include microbial populations common to the colonic lumen, neglecting those of the mucosa. Overall, fermentation models of the colon may be suitable for ingestible devices that monitor luminal composition for the presence of particular microbiological populations, metabolites or gas volumes produced.

4.6 Comparison of in vitro models of the colon

A brief outline of in vitro models that incorporate a colon environment is presented in the order in which they were published, the relative attributes are also compared in Table 17.

The evaluation of the in vitro models was based on criteria associated with the features of the macroenvironment that were presented in Table 1. The evaluation of the biorelevance of the luminal media as based upon factors associated with the luminal composition used within the system. These were scored using the levels of simulation of luminal composition that have previously been reported [138, 139]. These levels are: level 0 is pH only; level 1 is pH plus buffer capacity; level 2 includes bile components, dietary lipids, lipid digestion products and osmolality (this includes FaSSCoF and FeSSCoF) and level 3 also includes dietary proteins, enzymes (not digestion products) and viscosity effects. For the colon additional details on the pH control in each section of the colon is provided as well as whether the microbiota is present; these were scored as 1 where the pH was controlled to a value matching those found in vivo and also 1 where the microbiota was present. The volume used within the system was reported and this was considered to be biorelevant where the volume was similar to the capacity of the human adult colon; biorelevant conditions scored 1 where as non-biorelevant scored 0. The column on the biorelevant luminal media is the sum of the biorelevance scores for the previous four columns.

The representative anatomy provides details of the shape and dimensions of the compartment used to mimic the colon; where these were broadly similar to the dimensions of the colon they scored 1 and where they accurately mimicked the dimensions, they scored 2.

The level of biorelevant motility score comprised the components of the agitation mechanism and pattern of agitation. Where the mixing mechanism applied was consistent with mixing in the colon, via compression of the walls of the mixing vessel a score of 1 was applied. The pattern of agitation scored 1 for discontinuous mixing and 2 where the profile of discontinuous mixing matched that reported in vivo. Where the pressures matched those in vivo, a score of 1 was provided to the model. The overall scores for the biorelevance of motility was the sum of the scores for mixing mechanism, pattern of agitation and pressures. Where the transit time was reported this was scored 1 where it was in line with in vivo data and zero where it was not.

Several models of the colon also include a gastric and/or small intestine compartment thus there is overlap here with the previous sections. However, it will be the colon conditions that are detailed here and summarized in Table 17.

4.6.1 Three-stage continuous culture system

The original three stage continuous culture system proposed by Gibson et al (1988) [330] consisted of three fermentation reactors of size 0.3, 0.5 and 0.8 L connected in series. The pH of each vessel was maintained at 6.0, 6.5 and 7.0 sequentially. No sparging took place but the vessels were maintained under an anaerobic nitrogen gas. To inoculate each vessel, 100 mL 20 % (w/v) faecal slurry, buffered with 0.1 mol*L^{-1} sodium phosphate at pH 7.2 was used. A medium and distilled water or mucin were added to the first vessel. In the case of the former, sulfate-reducing activity was comparatively insignificant and methanogenesis was prominent. In the case of mucin addition, mucin was degraded extensively, as indicated by the production of volatile fatty acids. There was no literature that linked data from this model to in vivo data. This model was also reported by Macfarlane et al (1998) who reported that the results obtained with the three-stage continuous culture system compared well with measurements made on intestinal material obtained from sudden death victims [332].

4.6.2 SHIME

The simulator of the Human Intestinal Microbial Ecosystem (SHIME) (ProDigest, Ghent) is composed of five reactors connected in series to reproduce the entire GIT with a focus on fermentation, representing the stomach (see section 2.5.2) and small intestine (see section 3.6.1) followed by the ascending, transverse and descending colon respectively. The system was validated in 1993 based on evaluation of fermentation fluxes and products such as indicator bacterial groups, volatile fatty acids, enzymatic activity and headspace gases, however simulation is limited to luminal microbes only. Reactors are double jacketed glass vessels interconnected through peristaltic pumps; the transit time from beginning to end being 72-76 h [333]. The entire system is anaerobic, and each reactor is a double jacketed glass vessel. The colon simulators are continuously stirred reactors with constant volume, residence and pH control; ascending colon: 500 mL, 20 h, pH 5.6 – 5.9; transverse: 800 mL, 32 h, 6.1-6.4; descending: 600 mL, 24 h, pH 6.6 – 6.9. These reactors are filled with nutritional medium and inoculum prepared from human faecal matter [333] and the ascending colon mimic reactor receives media from the small intestine reactor containing a mixture of artificial stomach and pancreatic juices and the initial feed which includes resistant starches. The SHIME model is an evolution of the Reading Model, introduced by Macfarlane et al (1989) [334], in that the SHIME includes simulation of upper GI conditions. An updated version of this apparatus is presented in section 4.6.12. The SHIME model offers the opportunity to evaluate the stability of APIs under colonic conditions, including the complete gut microbiota, however it was not possible to find data with in vivo correlations from this apparatus.

4.6.2.1 Host-Microbiota Interaction (HMI)

The Host-Microbiota Interaction (HMI) module was introduced into the SHIME apparatus by Marzorati et al [335] in 2014. The HMI is a mini device used to study bacterial adhesion under relevant shear forces and microaerophilic conditions. It is comprised of an upper and a lower compartment, separated by a double layer of polyamide semipermeable membrane and a mucous layer. The upper compartment represents the luminal compartment and is continuously fed a bacterial suspension, whilst the lower compartment contains enterocyte cell lines. The HMI module when coupled to the SHIME is continuously fed a bacterial slurry [335]. The HMI module exposes the enterocyte cell lines to a relevant, complex microbial community and permits the exchange of signals and metabolites between compartments for up to 48 hours. The experimental set up is shown in Figure 1, this provides an example of combining a macro and micro in vitro model to better replicate the complex environment of the GI tract.

The design of the shear forces inside the HMI was based on physiological levels of shear stress found in the intestinal epithelium during peristalsis, ranging from 0.02 – 35 dynes*cm^{-2} but lower values below 5 dynes*cm^{-2} were chosen as this was representative for the beginning of the proximal colon in the absence of microvilli.

Based on an elastohydrodynamic mathematical model, Guo et al (2000) [336] predicted the forces and torques along brush border cells in the absence of villi to range from 0 – 5 dynes*cm^{-2} given

Poiseuille flow. However, the renal luminal environment of a brush border cell differs greatly to that of a colonic epithelial cell, and Poiseuille flow is unlikely.

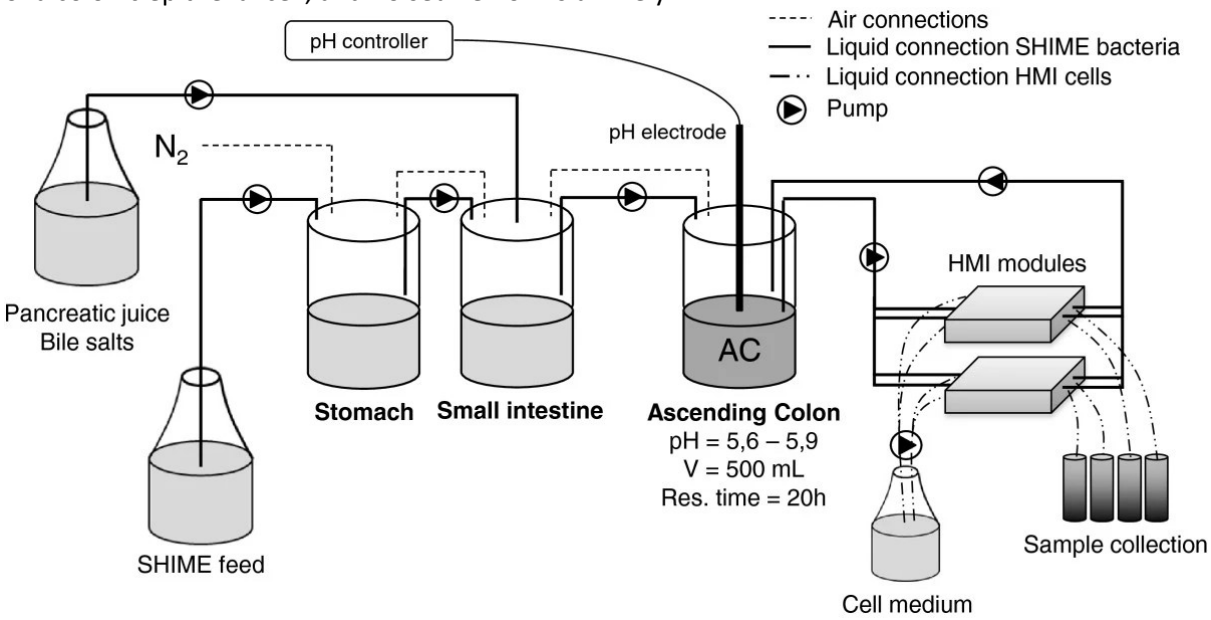

Figure 3. Diagram of the adapted SHIME system (consisting of stomach, small intestine and ascending colon - AC - compartments) used for the long-term study coupled to the HMI module. Image is taken from [335] which was distributed under the terms of the Creative Commons Attribution License (https://creativecommons.org/licenses/by/2.0), which permits unrestricted use, distribution, and reproduction in any medium

4.6.3 Batch culture faecal fermentation model (BCFFM)

100 mL fermentation vessels purged with N_2 and maintained at 37 ºC contained a homogenised, potassium phosphate buffered medium at pH 7.2 of 10 % (w/w) freshly voided faeces from three healthy human subjects [337]. This enzyme-based fermentation models was used to assess film digestion and drug release from coated pellets [337]. To determine drug release from the coated pellets, samples were removed from the fermenters at 0, 2, 4, 6, 8, 12 and 24 h.

4.6.4 3.2.16 Enzyme-based fermentation model (EBFM)

Siew et al [337] proposed an enzyme-based fermentation model for the in vitro assessment of colonic digestion of amylose films and coatings. Such a system would have increased practicality over faecal-based fermentation systems for obvious reasons. Identical vessel and buffered medium was used as in the BCFFM (section 4.6.3), with four different commercially available amylase enzymes separately introduced, in place of the faecal matter. The enzymes were oxygen-stable, so anaerobic conditions were not necessary which is a significant practicality benefit. It was found that the enzyme from bacterium Bacillus licheniformis was most active in digestion of the amylose/ethyl cellulose coating. Dissolution results were comparable to those obtained using a control faecal-based fermentation model.

4.6.5 Three-stage tubular model

The three-stage tubular model was developed by Spratt et al [338] primarily to provide a system that exhibited dispersed plug flow that could be relatively easily modelled and to achieve substantial mass transfer of water and fatty acids out of the system. Each stage of the model comprised a fermenter with a membrane that separated the contents from an outer flow of aqueous polyethylene glycol solution to control removal of water and metabolites form the reactor (thus controlling pH).

4.6.6 Enteromix

The EnteroMix was in development by Danisco (acquired by DuPont in 2011) since the early 1990s and was first published by Mäkivuokko et al in 2005 [339]. This model is a 4-compartment system representing the ascending, transverse, descending and distal colon [339]. Each compartment is a glass vessel with small working volumes of 6 – 12 mL and a physiologically relevant pH of 5.5, 6.0, 6.5

and 7.0 respectively and purged with N_2 and NH_3 to maintain anaerobic conditions. Inoculum is incorporated into the first vessel initially. After three hours of mixing, 10 mL of the culture is pumped into the subsequent vessel and 10 mL fresh media is added to the first vessel. This continues for 48 hours, after which samples can be collected. The EnteroMix has been used to study the effects of probiotics and prebiotics using adult faecal sample donors [339-343] and more recently to model infant colonic fermentation [344].

4.6.7 VTT One compartment fermentation model

The VTT one compartment in vitro colon model was first described by Barry et al [345] in 1995 but described most recently by Aura et al [346], having undergone several studies in between and adaptations for pure phenolic compounds [346-349]. This is a simple closed anaerobic system stirred with a magnetic stirrer. The system is inoculated from a pooled faecal suspension prepared from samples of 3-6 donors to ensure biodiversity and reproducibility [350, 351]. The model employs a strong buffer with minerals as the main matrix of the medium [345] as opposed to a nutritive medium with additional carbon sources. Additional carbohydrates are provided by the faecal material. The one compartment model aims primarily to profile metabolites. For example, Aura et al [348] used the SIMGI model coupled with a bioinformatics tool to profile metabolites of plant foods.

4.6.8 The Artificial Colon (ARCOL)

ARCOL, developed by the University of Clermont Auvergne, France, is a one stage fermentation model of human [352-355] that was the first model to allow maintenance of anaerobiosis inside the fermenter solely through metabolic activity of the microbiota (as opposed to flushing with N_2 or CO_2. Water absorption is passive and a dialysis system using hollow fibre membranes maintains electrolyte and metabolite concentrations through passive absorption. The buffer system employed is phosphate, which is not representative of the in vivo situation. The main downfall is that the system represents average human colonic environment rather than having distinct sections that model the differences between the ascending, transverse and descending human colon.

4.6.9 Polyfermentor intestine model (PolyFermS)

The PolyfermS model traps faecal microbiota via microencapsulation technique. The system consists of five reactors each with an independent microbial inoculum which represents the stool microbiota of a healthy donor, preserving abundance and diversity of critical taxonomical groups throughout experiments (stable up to 38 days) [356]. The first reactor represents the human proximal colon which supplies downstream reactors arranged in parallel to explore the effects of different experimental treatments on the same microbiota produced in the AC vessel. The microbiota is immobilised in polysaccharide gel beads to create a sessile measure of bacteria that mimics the biofilm or mucus associated bacteria in addition to promoting the growth of planktonic bacteria culminating from the release of sessile bacteria into the bulk [357, 358]. The PolyFermS has been adapted to successfully cultivate colonic microbiota based on humans of varying ages [359, 360] and for swine, murine [361, 362] and chicken gut contents. A major advantage of this apparatus is the possibility to stably and reproducibly cultivate complex intestinal communities in multiple reactors allowing studying in parallel the impact of many different treatments (environmental parameters, dietary compounds, drugs, added microbes, etc.) compared to a control reactor.

4.6.10 TNO TIM-2

The TNO TIM-2 is a dynamic in vitro model of the colon [363]. The model consists of four interconnected glass compartments containing a flexible membrane representing the lumen [363]. The space between the glass and the flexible membrane is filled with water, the temperature of which can be controlled to maintain the desired temperature of the apparatus. Additionally, pressure can be applied to the water following a controlled sequence to cause the flexible membrane to contract, mimicking colonic peristalsis. A level sensor in the system maintains the volume at 120 mL through control of a pump to expel contents. This model boasts one of the most complex fermentation models of the colon simultaneous to applying physiologically relevant mixing conditions compared to many fermentation models which are simply stirred. The model is fed with inoculum of human faecal suspension. Accumulation of microbial metabolites is prevented by a bespoke dialysate system which

enables TIM-2 to maintain an active microbiota for up to 3 weeks. Gases produced by the microbiota can be sampled, in addition to material content sampled from the lumen or sample port. The system is maintained at pH 5.8 by secretion of NaOH, representing that of the human proximal colon. The effect of several food components that have been well-established in vivo have been confirmed in TIM-2; including the bifidogenic nature of inulin [364].

4.6.11 SIMGI

The SIMGI model includes five interconnected compartments, however only the colonic compartments are considered in this section [242], see section 2.5.12 for the gastric and section 3.6.10 for the intestinal aspects.. The stages of colonic transit are simulated in three stages, the AC, TC and DC, all of which are fermentative, double jacketed glass reactors that maintain the contents at 37 °C. The pH in the AC, TC and DC is maintained at 5.6 ± 0.2, – 6.3 ± 0.2 and 6.8 ± 0.2 respectively. Digested content of the small intestine compartment is transferred to the AC compartment, at which time sequential transit between colonic segments begins at equal flow rates. Colonic compartments are continuously flushed with N_2 and sample ports are available. Interestingly, the SIMGI has been used to investigate the relationship between viscosity and of media consisting of chia mucilage and the human intestinal microbiota [365]. SIMGI is a relatively new model as to date there is no literature that correlates data from this system to in vivo data.

4.6.12 M-SHIME

The Mucosal Simulator of Human Intestinal Microbial Ecosystem (M-SHIME) (ProDigest, Ghent) is an updated version of the SHIME that includes simulation of mucosal microbiota (which are primarily methanogenic Archaea, sulphate-reducing bacteria and acetogenic bacteria) [366]. This is achieved through incorporation of mucin type-II-agar-covered microcosms encapsulated in a polyethylene net. Different studies have investigated different setups of the M-SHIME system, for example, Giuliani et al (2016) [367] employed three pairs of reactors that mimicked proximal and distal colonic environment to investigate the effect of Vitis vinifera extract on intestinal microbiota. Truchado et al (2017) [368] utilised only a proximal colon vessel to study the effects of prebiotic long-chain arabinoxylans (LC-AX) on mucosal and luminal mucosa; it was found that supplementation of 6g / L LC-AX significantly increased relative abundance of Bifidobacterium in lumen and mucosa in addition to associated metabolic activity. These studies demonstrate the flexibility of the M-SHIME apparatus to be varied to focus on particular colonic segments of interest and may be useful for the development of ingestible devices that monitor media and gas compositions or microbial activity. Liu et al [369] employed the Twin Simulator of the Human Intestinal Microbial Ecosystem (TWINSHIME) which consists of two separate systems, the SHIME and M-SHIME to enable evaluation of the differences and similarities between mucosal and luminal microbial communities over six weeks. Mucosal colonisers included the Firmicutes phylum with species varying between the mimicked colonic sections. In contrast, Bacteroidacaeae were enriched in the gut lumen of all three regions of the colon.

4.6.13 Single batch fermentation system (SBFS)

Takagi et al (2016) [370] devised a single-batch fermentation system with the aim of using next-generation sequencing (NGS) to compare in vitro and in vivo colonic microbiota. The fermentation took place in 100 mL working volume vessels maintained at 37 °C, mixed with a magnetic stirrer. The system was inoculated with faecal samples from healthy human volunteers. Results from a study on high throughput evaluation of probiotics suggested that this fermentation system may be useful for in vitro, pre-clinical evaluation of the effects of prebiotics prior to testing in humans [315].

4.6.14 CoMiniGut

The Copenhagen MiniGut (CoMiniGut) was developed with the objective of conducting high-throughput, low volume investigations on the interactions of gut microbiota with pharmaceutics, pre- and probiotics with pH and temperature control [371]. The system consists of a box containing five single-vessel, anaerobic reactor units with a working capacity of only 5 mL in parallel. Throughput can be increased by increasing the number of parallel units in multiples of five. Each vessel has 10 mL capacity with 5 mL working volume. Since only 250 micrograms of faecal matter is required for inoculation, faecal cryostock libraries can be constructed, facilitating multiple repeat experiments of

test material that is difficult to obtain. Headspace gas sampling is facilitated via gas inlet / outlet ports which can be used to maintain anaerobiosis. Additionally, fermentate can be sampled at any time during fermentation using a programmable syringe pump system. Mixing is achieved using a magnetic stirrer. Simulation of passage through the colon is simply represented by pH increment over time. Wiese et al (2018) [371] used the CoMiniGut to demonstrate significant differences in microbiota composition and short-chain fatty acid (SCFA) profiles between using inulin or lactose as the fermentation substrate.

4.6.15 MicroMatrix

The microMatrix (Applikon Biotechnology, Heertjeslaan 2, 2629 JG Delft, Netherlands) is a mini-fermentation system (1 – 10 mL). This system utilises mini-batch fermentation of frozen standardised inoculum to obtain a highly reproducible microbiota that can easily be evaluated for changes due to variation in treatment conditions. The microMatrix system was first used by O'Donnell et al (2018) [316] to mimic the distal colon to differentiate the initial microbiota from one that has undergone fermentation of a prebiotic carbohydrate in a reproducible manner. However, in this initial study, metabolites were not evaluated. The buffer system used was potassium phosphate.

4.6.15.1 Mini-Bio in vitro *model*

The Mini-Bio in vitro model by Applikon Biotechnology (Deft, Netherlands) is a patented flexible in vitro system that can be operated in batch mode or dynamically. The software is able to remotely supervise fermentation reactions in up to 32 separate bioreactors. The online data logger identifies real-time changes in pH, temperature, dissolved oxygen or NaOH addition. The length of set-up time (including stabilization periods) for each fermentation system can range from hours to weeks to months; thus a simple parallel system to allow multiple simultaneous experiments is advantageous, particularly for screening projects as a precursor to animal studies[316].Various attachments can be employed depending on the task at hand, such as mechanical impellers that can rotate at up to 2000 rpm. In terms of flexibility, the volume of the system can be varied to the desired value, from a minimum of 50 mL.

4.6.16 Toddler-SHIME

Bondue et al (2020) [372] adapted the SHIME to reflect the colonic microbiota of healthy donors aged 1 – 2 years old, highlighting that the 'first 1000 days of life' determine the gut microbiota composition and can have long term influences on health. In addition to inoculation with faeces from healthy children, modifications were made to adapt the system in terms of volumes and pH with the ascending: 100 mL, pH 5.4 - 5.6; transverse: 160 mL, pH 6.0-6.3; descending colon: 120 mL, pH 6.3 – 6.5 in addition to age-appropriate changes to the nutritional medium.

4.6.17 Dynamic colon model (DCM)

The Dynamic Colon Model (DCM) is an anatomically representative in vitro model of the human ascending colon, designed based upon cine-MRI images that showed the anatomical architecture and wall motility patterns of the undisturbed colon [373]. The DCM is comprised of 10 haustral segmental with a total length of 200 mm (209 ± 47 mm is the length of the caecum-ascending colonic region in humans [374]) and volume of 290 mL (within the physical range of 76 – 390 mL. Each haustral segment is connected to a syringe controlled by a stepper motor which pushes and pulls the plunger of the syringe to pre-programmed displacement values, inflating and deflating the DCM wall to manipulate the degree of luminal occlusion. The pattern of contractile activity is synchronised between segments to reproduce the widely accepted law of the intestine [375]. Manometric studies showed that the DCM can reproduce the physical amplitudes within the human colon [376]. The current design of the DCM operates: (i) in a horizontal orientation in accordance with the normal supine position adopted by patients during scintigraphy and MRI procedures; (ii) in the fed state in which more frequent propagating sequences of pressure waves occur in the proximal colon [377]. The DCM is the only in vitro model to data (known by the authors) to replicate peristaltic motility in a lumen with the segmented architecture of the human colon. The DCM may be suitable for the development of ingestible devices that investigate intraluminal hydrodynamics and colonic motility, rather than the complex physicochemical characteristics of GI fluids. Although a vast range media can be used inside

the DCM across different levels of complexity, the system is not anaerobic and therefore cannot support relevant microbial activity and fermentation.

Model name and Reference	AC/TC/DC Volume (mL)	Media Used	pH Control	Microbiota present	Biorelevant luminal media score	Biorelevant Intraluminal architecture	Biorelevance of representative anatomy	Mixing mechanism	Pattern of agitation	Pressure	Biorelevance of motility	Intestinal transit	Biorelev transit time
Three-stage continuous culture system [330]	AC: 300 TC: 500 DC: 800	Level 3 faecal slurry	AC: 6.0 TC: 6.5 DC: 7.0	Y	6	Cylindrical beaker	0	Stirring	Continuous	Not reported	0	Mapped to in vivo data	1
Three-stage continuous culture [332]	AC: 80 TC: 100 DC: 120	Level 3 faecal slurry	AC: 5.5 TC: 6.2 DC: 6.8	Y	6	Cylindrical vessel	0	Magnetic stirrer	Continuous stirring	Not reported	0	27.1 h or 66.7 h	1
SHIME [333]	AC: 500 TC: 800 DC: 600	Level 3 faecal slurry	AC: 5.6-5.9 TC: 6.1-6.4 DC: 6.6-6.9	Y	5	Cylindrical vessel	0	Magnestic stirrer	Continuous	Not reported	0	72-76 h	0
BCFFM [337]	100	Level 3 faecal slurry	7.2	Y	6	Cylindrical vessel	0	Stirring	Continuous	Not reported	0	24h	1
EBFM [337]	100	Level 2 fluid	7.2	Y	5	Cylindrical vessel	0	Stirring	Continuous	Not reported	0	24h	1
3 stage tubular [338]	Flow through system	Level 3 faecal slurry	Y – removal of fatty acids. Feed maintained at pH 5.8	Y	5	Cylindrical fermenter	0	Not reported	Not reported	Not reported	0	40 h	1
Enteromix [339]	AC: 3 TC: 5 DC: 7	Level 3 faecal slurry	AC: 5.5 TC: 6.0 DC: 6.5-7.0	Y	5	Cylindrical vessel	0	Magnestic stirrer	Continuous	Not reported	0	48h	1

VTT One compartment fermentation model [345]	10	Level 3 faecal slurry	Controlled but value not reported	Y	5	Cylindrical vessel	0	Orbital mixing	Continuous	Not reported	0	24h	1
ARCOL [352, 354, 355]	2000 (capacity) 450 working	Level 3 faecal slurry	6	Y	6	Cylindrical vessel	0	Stirring	Continuous at 400 rpm	Not reported	0	72h	0
PolyFerm-S [356]	300	Level 3 faecal slurry	5.7	Y – microencapsulation technique	6	Cylindrical vessel	0	Overhead mixing	Continuous	Not reported	0	7.5 h	0
TNO TIM-2 [363]	Proximal colon only (200 mL capacity, 120 mL working volume)	Level 3 faecal slurry	Y – secretion of NaOH to neutralise acids as a product of metabolism, maintain pH 5.8. Can also have TC=6.4; DC=7.0	Y	6	Flexible cylindrical tube	0	External pressure to replicate peristalsis	Discontinuous	Not reported	2	Mapped to in vivo data	1
SIMGI [167, 242]	AC: 250 TC: 400 DC: 300	Level 3 faecal slurry	AC: 5.6 ± 0.2 TC: 6.3 ± 0.2 DC: 56.8 ± 0.2	Y	6	Cylindrical vessel	0	Stirring	Continuous	Not reported	0	76h	0

M-SHIME [367]	AC: 500 TC: 800 DC: 600	Level 3 faecal slurry	AC: 5.6-5.9 TC: 6.1-6.4 DC: 6.6-6.9	Y Mucosal and luminal	5	Cylindrical vessle	0	Magnetic stirrer	Continuous	Not reported	0	72-76 h	0
SBFS [315]	100	Level 3 faecal slurry	6.5	Y	6	Cylindrical vessel	1	Stirring	Continuous	Not reported	1	24h	1
CoMiniGut [371]	5	Level 3 faecal slurry	AC: 5.7-6.0 TC: 6.0-6.5 DC: 6.5-6.9	Y	5	Cylindrical vessel	0	Magnetic stirrer	Continuous	Not reported	0	AC: 0-8h TC: 8-16h DC: 16-24h	1
MicroMatrix [378]	6	Level 3 faecal slurry	6.8	Y	6	Cylindrical vessel	0	Orbital mixing	Continuous 250 rpm	Not reported	0	24h	1
Toddler SHIME [372]	AC: 100 TC: 160 DC: 120	Level 3 faecal slurry	AC: 5.4-5.6 TC: 6.0-6.3 DC: 6.3-6.5	Y	6	Cylindrical vessel	0	Magnestic stirrer	Continuous	Not reported	0	24h	1
Dynamic Colon Model (DCM) [373, 379]	290 mL (capacity); 100 mL working volume	Level 1 fluid	Not reported	N	6	Anatomically accurate model of the human colon	2	Externally applied forces	Mapped from in vivo data	Mapped from in vivo data	4	Mapped from in vivo data	1

Table 17. Summary of in vitro *models of the colon*

The data presented in Table 17 highlights the large number of in vitro models of the colon that are reported in the literature. The majority have focussed on reproducing the luminal environment in terms of the media composition, mainly as they have been used to probe digestion. However, there are some efforts to replicate the motility within the colon in some models.

4.7 Organoid models of the colon

In 2011, Sato et al [75] developed a protocol to grow epithelial organoids from mouse and human colon, in addition to human colorectal cancer cells. Since, colonoids have been grown from human [81, 251, 380-387], murine [202, 255], porcine [388] and even bat [261] primary tissue. Human colonic organoids have also been generated from hIPSCs [78, 380]. Human intestinal organoids expressing colonic markers and colon-specific cell populations [78] and resembling the proximal colon [380] have been generated from the differentiation of hIPSCs.

Colonoids have been used to study genetic diseases; colonoids make for a suitable model of cystic fibrosis (CF) due to their expression of cystic fibrosis transmembrane regulator [386, 389]. Colorectal cancer [81, 255], the CRISP-Cas9 genome-editing system has also been used to introduce mutations to normal colonoids [81]. Colonoids have been used to model infectious diseases such as *C. difficile* [380], human rotavirus [251, 381, 383], E. Coli [382, 384, 385], and SARS-CoV-2 [261]. Additionally, high-throughput biobank systems have been developed for drug screening applications, such as for colorectal cancers [79, 81, 255, 387], therapeutics and and CF [389] in rectal organoids.

Colonoids grown as 2D epithelial monolayers on permeable Transwell inserts are rapidly becoming the new gold standard. These models comprise goblet cells and an apical mucous layer, permitting studies of pathogen-mucus interaction [384]. In a study of infection of a colonoid monolayer with EHEC, a layer of MUC2-containing apical mucous was reported, however it was uncharacteristically thin, measuring approximately 25 microns thick [385]. In vivo, the human colon produces a mucous layer that is approximately 600 microns [390]. In order to recapitulate a physiologically relevant mucous environment, Wang et al (2019) [391] cultured human colonic epithelial cells on a Transwell plate under an air-liquid interface. This resulted in obtaining a mucous layer of 300 microns, although a significant improvement, this is still approximately 50% of the thickness of the human colonic mucous layer.

4.8 Organ-on-a-chip models of the colon

Table 18 presents microfluidic models of the colon. In a landmark study, the first of its kind Colon Chip was produced by Sontheimer-Phelps et al (2020) [392] using primary patient-derived fragmented colonoids.

The Colon Chip represented a breakthrough in the study of human colonic mucosa. The colonic mucous layer is the first line of defense against invading pathogens and heavily influences the solubility of molecular compounds in close proximity to cells; thereby presenting as a pivotal factor in drug permeability studies. The Colon Chip produced a mucous bilayer with total thickness of 500-600 microns, similar to the living human colon, which permitted non-invasive visual analysis of accumulation and physiology in real time [392]. This model therefore demonstrates a notable advantage; no other studies using human colonic epithelial cell cultures in Transwell plates, organoids or any other in vitro model resulted in the production of a thick mucous layer with a bilayer structure consistent with in vivo observations [64]. Furthermore, it is not currently possible to study intestinal mucous physiology within the living human colon and ex vivo tissue explants permit study over very short timescales (< 1 day). Mucous physiology can be studied in animal models but only currently with low resolution, highly invasive and technically challenging methods. In addition, mucous physiology differs between species, therefore animal models may not accurately reflect human colonic mucosa. Therefore, Sontheimer-Phelps et al (2020) [392] have made a significant breakthrough in in vitro modelling. This model may be of use to the development of any ingestible microdevices that interact with the colonic mucosa.

Gazzaniga et al (2021) [276] developed a murine colon chip following a similar approach to Sontheimer-Phelps et al (2020) [392]. This chip cocultured murine colonic epithelium with both complex species-specific microbiota and particular individual strains to investigate effects on epithelial and mucosal physiological function and protection against pathogens. Additionally, the use of animal colon chips enables direct comparison to the results of prior animal studies, whilst also enabling the study of physiologically relevant cells that can be difficult to obtain from human biopsies.

Ref	Cell type	Lumen dimensions	Luminal flow	Molecular transport	Wall shear stress	Mucous layer thickness	Peristalsis	Commensal microbiota	Disease / pathogen	Co-culture with other cells
Gazzaniga et al [276]	Murine colonoid	H: 1000 µm W: 1000 µm MT: 50 µm	n/a	N	n/a	n/a		Human and mouse microbiota	*S*. Typhimurium	N
Beaurivage et al [393] 2020	Colonoids	W: 400 µm OrganoPlate	n/a	N	n/a	n/a	N	N	IBD	Monocyte-derived macrophages (immune cells)
Sontheimer-Phelps [392] 2020	AC and sigmoid Colonoids	H: 1000 µm W: 1000 µm MT: 50 µm	1.6, 6 & 10 $mL*h^{-1}$	N	n/a	570 µm	N	N	Exposure to PGE2 (to model ulcerative colitis)	N
Shin et al [394]	Colonoid	H: 500 µm W: 1000 µm L: 10 mm MT: 50 µm	30+ $mL*h^{-1}$	N	N	N	N	N	N	N
Apostolou et al [395] 2020	Colonoids	H: 1000 µm W: 1000 µm V = 28.041 µL cell surface 28 mm^2	60 $mL*h^{-1}$	N	n/a	n/a	10% strain at 0.15 Hz	N	Interferon (IFN)-γ in inflammation and leaky-gut	N
Tovaglieri et al [396] 2019	Colonoids	H: 1000 µm W: 1000 µm MT: 50 µm	60 $mL*h^{-1}$	N	N	n/a	N	Hmm or Mmm	EHEC	N
Shin et al [397] 2019	Human Caco-2 & AC colonoid	W: 1 mm L: 10 mm H: 0.15 mm MT: 20 µm	30, 100 & 200 $mL*h^{-1}$	N	0.02 dyne $*cm^{-2}$ at 30 $µL*h^{-1}$	N	10% strain at 0.15 Hz	N	N	N

Table 18: Microfluidic models of the colon. VSL#3 is a therapeutic probiotic formulation containing *Lactobacillus acidophilus*, *Lactobacillus plantarum*, *Lactobacillus paracasei*, *Bifidobacterium breve*, *Bifidobacterium longum*, and *Bifidobacterium infantis; Hmm = human microbiome metabolites; Mmm = mouse microbiome metabolites*

5 Conclusions

Developing and evaluation of ingested devices is a complex field where the evaluation to be undertaken will be strongly linked to the functionality of the device under test. The multitude of in vitro methods available that mimic the human GI tract provides a wide selection of methods yet some of these are only available in particular laboratories and may not be accessible for all researchers.

This review has presented a wide range of in vitro models that have been reported to simulate the stomach, small intestine, colon or a combination of these sites. Each model has been developed to replicate a specific aspect of the GI environment from the composition of the luminal fluids to the morphology or motility pattern or transit time. The majority of models have originated from either pharmaceutical or nutrition research where there have been some attempts to link performance within the model to in vivo data. However, full validation of a model is complex, often due to the limited in vivo data that is available.

Several models are adaptations of standard apparatus, for example the modified pharmacopoeial dissolution apparatus, this means that the methodology can be replicated in a number of laboratories. Other models are commercial systems where access may not be possible or may only be possible for a fee. The selection of the best model to use for an ingestible device will depend upon the purpose of the ingested device; the mechanism of action of the device and the availability of the apparatus.

The information presented in Table 7, Table 12 and Table 17 highlight the strengths and limitations of the models reported in the literature. The scores for the level of biorelevance associated with the luminal media; anatomy; motility and transit reflect the strength of the models presented; these scores can be used as guidance when selecting the most appropriate model to use. However, it is also critical to consider the mechanisms of the device under test to ensure that the most suitable system is used.

Key factors to consider in any in vitro method include the relative dimensions compared to the size of the device and the critical functional parameters of the device; for example a device intended to measure pH within the GI tract needs to be evaluated in a system where pH changes can occur and the timing of these can be closely controlled; whereas a device intended to respond to the microbiome needs to be evaluated in a system where the microbiome can be controlled. The technical hurdles in generating appropriate in vitro models that are dynamic are high. The large number of models and fact that many are based in academic research centres means that the regulatory precedence of use is often low and few are validated against clinical data. There is clear area of active research in replicating both the macro and micro environment within the gastro-intestinal tract and future work should focus on the combination of macro and micro environments to better replicate the complexity within the human stomach; small intestine and colon. This links to the range of pre-clinical models available for evaluation of ingestible devices which is covered in a second paper in this special edition [8].

A future direction would be to consider the development of computational “in silico” models that integrate artificial intelligence and machine learning techniques. The use of digital twin systems has gained precedence within pharmaceutical processing and aspects of this may help to improve the design of invitro systems and provide a smarter as well as faster evaluation of ingestible devices.

In summary, there are impressive in vitro models that have been developed in recent years to replicate the gastrointestinal tract where all models may have value at some stage of the development of ingestible devices. However, it is crucial to highlight that presently there is no “one model fits all” choice. The selection of the model should always be selected based on the analysis criteria and the final aim of the study. In future, the focus on clinical validation of models will be a crucial step in advancing the translation of ingestible devices to the clinic.

Declaration of Competing Interest

The authors declare that they have no known competing financial interests or personal relationships that could have appeared to influence the work reported in this paper.

Acknowledgements

COF received funding from the EPSRC Centre for Doctoral Training in Formulation Engineering (EP/L015153/1) and AstraZeneca AB R&D, Gothenburg.

We thank Jonathan Goldfinch for his work in collating the information presented in Table 16.

6 Supplementary Material

Review synopsis	Date of review	Reference
Comparison of non-compendial dissolution models (ASD, biorelevant dissolution stress-test device, dynamic in vitro lipolysis model, DGM, TNO TIM1) to assess drug product performance under physiologically relevant conditions	2010	[12]
Eight dynamic digestion systems (DGM, HGS, ARCOL, DIDGI, TIM-1, tiny-TIM AGC, SHIME, ESIN and SIMGI) are presented as well as their validation towards in vivo data in order to determine what aspects of food digestion they are able to mimic.	2019	[13]
Comparison of in vitro digestion models in terms of suitability to predict in vivo performance of lipid-based drug delivery systems (DGM, TIM-1, HTP, pH-stat lipolysis model)	2019	[14]
In vitro digestion systems (COST INFOGEST static model, DGM, HGS, GDS, SHIME, TIM, IMGS, DRSD, DHSI) with regards to the human GI physiology, and their advantages versus limitations in the understanding of various food digestion processes. Specific details on the type of mixing are listed	2020	[15]
A comparison of physical stomach models (HGS, SHIME, v-form glass vessel, MIDA, DIVRS, DGM, DGSM, ESIN, SIMGI, TNO, TIMagc, BGR, RD-IV-HSM, DIVHS, AGDS, GSM, HGS, GDS, iHGS) specifically looking at shear stress and strain within the systems	2020	[16]
Comparison of gastric emptying parameters in dynamic digestion models (HGS (NZ), DGM; GDS; GSM; DGSM; IMGS; AGDS)	2020	[5]
Comparison of in vitro models to study food-induced gut microbiota shift (Batch fermentation model; Reading model; TIM-2; SHIME; M-SHIME; SIMGI; PolyFermS; MiniBio; TSI)	2020	[17]
Comparison of dynamic in vitro models and their relevance to the human digestive system were described (TIM, SHIME, ESIN, DIDGI, SIMGI, DGM, DGSM, c-GDS, AGDS, ARCOL)	2021	[398]

Supplementary Table 1. Relevant review papers that describe in vitro models of the gastro-intestinal tract

Reference	Population	Fluids characterised	Co-administration of water	pH	Osmolality mOsm*kg^{-1}	Surface tension	Buffer capacity (mmol/L*pH)	Bile salt concentration (mM)	Protein concentration (mg*mL^{-1})	Neutral Lipid concentration(mM)	Phospholipid concentration(mM)	Viscosity
[118]	24 adult healthy volunteers (19-37 years)	Fasted jejunal fluid	None	7.1 ± 0.6	271 ± 15			2.9 ± 2.9				
[124]	9 healthy volunteers (age not reported)	Fasted jejunal fluid	None	6.7 ± 0.9	278 ± 16	33.7 ± 2.8		1.52 ± 1.77				
[399]	12 healthy volunteers aged 24-40	Fasted jejunum	None	7.5		28 ± 1	Range 2.4-2.8	2.0 ± 0.2	1 ± 0.1	0.1 ± 0.01	0.2 ± 0.07	
[400]	6 adult volunteers (22-35 years)	Fasted duodenal fluid	None	7.0 ± 0.4	137 ± 54			2.6 ± 1.6				
[400]	6 adult volunteers (22-35 years)	Fasted jejunal fluid	None	6.8 ± 0.4	200 ± 68			3.5 ± 1.6				
[401]	4 adult volunteers	Duodenum	None	6.45 ± 0.5				3.47 ± 1.8			0.09 ± 0.05	
[402]	5 adult healthy volunteers	Fasted duodenal fluid	None	6.7 ± 0.6	214 ± 57	40.6 ± 4.7		2.65 ± 0.4		0.6 ± 0.7	0.68 ± 0.6	
[403]	5 healthy volunteers (24-39 years)	Fasted duodenal fluid	Sampling followed 15 minutes post ingestion of 250 mL water	6.24	205			3.64 ± 0.42			1.81 ± 0.16	
[404]	4 healthy volunteers (19-35 years)	Fasted duodenal fluid	Sampling followed ingestion of 200 mL water	7.5	224			8.125				0.65

[120]	20 healthy volunteers (20-32 years)	Fasted duodenal fluid	Samples followed ingestion of 250 mL of mineral water containing 10 mg*mL^{-1} PEG 4000 as a nonabsorbable marker	Median 6.2	178	32.3	5.6	2.6	3.1			
[123]	8 adult healthy volunteers (23-34 years)	Fasted duodenum	Sampling followed ingestion of 240 mL table water	Range 6.2-6.8	Range 92.5-217.4	32.7 ± 0.51	8.9-19.2	Range 1.1-7.7	Range 1.0-3.7	Range 0.28-0.95	Range 0.12-0.61	0.76 ± 0.01
[405]	11 adult healthy volunteers	Fasted duodenum	Sampling followed ingestion of 200 mL water					4.2				
[406]	20 adult healthy volunteers (18-31 years)	Fasted duodenal fluid	250 mL water administered prior to sampling	6.78				4.61			0.95	

Supplementary Table 2. Summary of cohort details from studies reported where fasted intestinal fluid was collected for characterisation. Data shown are mean (± standard deviation) unless otherwise stated.

Reference	Fed conditions	Parameters measured	Time points
[399]	NuTRIflex®; Braun, (Berlin, Germany) (nitrogen 0.8 g, amino acids 5.8 g, glucose 11.5 g, lipids 7.2 g, energy 576 kJ)	pH, total protein concentration, bile secretion components, surface tension, buffer capacity, and total nutritional lipid content	Single time point at 20–60 minutes post ingestion
[402]	400 mL Ensure Plus® (Abbott Laboratories B.V., Zwolle, the Netherlands) plus 250 mL water was used to simulate a standard meal. One portion of 200 mL has an energy content of 300 kcal of which lipids, carbohydrates and proteins constitute 29%, 54%, and 17%, respectively.	pH. Osmolality, surface tension, bile acid concentration, total phospholipid content, lipid content.	15, 30, 45, 60, 75, 90, 105, 120, 135, 150, 165, 180, 195, 210, 225, 240, 255, 270, 285, 300 minutes post ingestion
[402]	300 mL Scandishake Mix® (Nutricia, Liverpool, UK) plus 350 mL water was used to simulate a fat-enriched meal. One portion amounts to 300 mL with a total energy of 600 kcal, consisting of 46% lipids, 46% carbohydrates, and 8% proteins on energy basis.	Osmolality, surface tension, bile acid concentration, total phospholipid content, lipid content.	15, 30, 45, 60, 75, 90, 105, 120, 135, 150, 165, 180, 195, 210, 225, 240, 255, 270, 285, 300 minutes post ingestion
[404]	400 mL Ensure Plus® (Abbott Laboratories B.V., Zwolle, the Netherlands) plus 200 mL water was used to simulate a standard meal. One portion 200 mL (Ensure plus) has an energy content of 300 kcal of which lipids, carbohydrates and proteins constitute 29%, 54%, and 17%, respectively.	pH, osmolality, bile salt concentration, lecithin concentration, viscosity	15, 30, 45, 60, 75, 90, 105, 120 minutes post ingestion
[120]	500 mL Ensure Plus® (Abbott Laboratories B.V., Zwolle, the Netherlands). One portion 200 mL (Ensure plus) has an energy content of 300 kcal of which lipids, carbohydrates and proteins constitute 29%, 54%, and 17%, respectively.	pH, buffer capacity, protein content, bile salt concentration, osmolality, surface tension	30, 60, 90, 120, 150, 180, 210 minutes post ingestion
[405]	400 mL Ensure Plus® (Abbott Laboratories B.V., Zwolle, the Netherlands) plus 200 mL water was used to simulate a standard meal. One portion 200 mL (Ensure plus) has an energy content of 300 kcal of which lipids, carbohydrates and proteins constitute 29%, 54%, and 17%, respectively.	Bile salt concentration, lecithin concentration	15, 30, 45, 60, 75, 90, 105, 120 minutes post ingestion
[406]	400 mL Ensure Plus® (Abbott Laboratories B.V., Zwolle, the Netherlands) plus 250 mL water was used to simulate a standard meal. One portion	pH, phospholipid concentration; cholesterol concentration bile salt	10, 20, 30, 40, 50, 60, 70, 80, 90 minutes post ingestion

	200 mL (Ensure plus) has an energy content of 300 kcal of which lipids, carbohydrates and proteins constitute 29%, 54%, and 17%, respectively.	concentration; lipid content; pancreatic lipase activity; phospholipase A2 activity;	
[125]	Standard high-calorie, high-fat meal (example suggested by the regulatory authorities today consists of two eggs fried in butter, two strips of bacon, two slices of toast with butter, four ounces of hash brown potatoes and a glass of whole milk)	pH, buffer capacity, lipid content, bile acid content, and viscosity	45, 105, 165 and 225 minutes post ingestion
[122]	A liquid meal. Two cans of Pulmocare (total volume of 474 mL, containing 29.6 g of proteins, 44.2 g of fat, 25 g of carbohydrates, and a total amount of 710 calories)	pH, buffer capacity	0, 15, 30, 45, 60, 90, 120, 150, 180, 240, 300, 360, 420 minutes post ingestion

Supplementary Table 3. Studies on the composition of fed intestinal media

References

[1] E. Grignard, R. Taylor, M. McAllister, K. Box, N. Fotaki, Considerations for the development of in vitro dissolution tests to reduce or replace preclinical oral absorption studies, European Journal of Pharmaceutical Sciences, 99 (2017) 193-201.
[2] Z. Li, X. He, Physiologically based in vitro models to predict the oral dissolution and absorption of a solid drug delivery system, Current Drug Metabolism, 16 (2015) 777-806.
[3] J. Costa, A. Ahluwalia, Advances and Current Challenges in Intestinal in vitro Model Engineering: A Digest, Frontiers in Bioengineering and Biotechnology, 7 (2019).
[4] J. Campbell, J. Berry, Y. Liang, Anatomy and Physiology of the Small Intestine, in: C.J. Yeo (Ed.) Shackelford's Surgery of the Alimentary Tract, 2 Volume Set (Eighth Edition), Elsevier, Philadelphia, 2019, pp. 817-841.
[5] W. Liu, Y. Jin, P.J. Wilde, Y. Hou, Y. Wang, J. Han, Mechanisms, physiology, and recent research progress of gastric emptying, Critical Reviews in Food Science and Nutrition, (2020) 1-14.
[6] V. Mahadevan, Anatomy of the stomach, Surgery (Oxford), 38 (2020) 683-686.
[7] Z. Vinarov, M. Abdallah, J.A.G. Agundez, K. Allegaert, A.W. Basit, M. Braeckmans, J. Ceulemans, M. Corsetti, B.T. Griffin, M. Grimm, D. Keszthelyi, M. Koziolek, C.M. Madla, C. Matthys, L.E. McCoubrey, A. Mitra, C. Reppas, J. Stappaerts, N. Steenackers, N.L. Trevaskis, T. Vanuytsel, M. Vertzoni, W. Weitschies, C. Wilson, P. Augustijns, Impact of gastrointestinal tract variability on oral drug absorption and pharmacokinetics: An UNGAP review, European Journal of Pharmaceutical Sciences, 162 (2021) 105812.
[8] K. Stamatopolous, C. O'Farrell, M.J.H. Simmons, H.K. Batchelor, In vivo models to evaluate ingestible devices: present status and current trends, Advanced Drug Delivery Reviews, Submitted (2021).
[9] E. Caffarel-Salvador, A. Abramson, R. Langer, G. Traverso, Oral delivery of biologics using drug-device combinations, Curr Opin Pharmacol, 36 (2017) 8-13.
[10] N.K. Mandsberg, J.F. Christfort, K. Kamguyan, A. Boisen, S.K. Srivastava, Orally ingestible medical devices for gut engineering, Advanced Drug Delivery Reviews, 165-166 (2020) 142-154.
[11] K. Kalantar-zadeh, N. Ha, J.Z. Ou, K.J. Berean, Ingestible Sensors, ACS Sensors, 2 (2017) 468-483.
[12] M. McAllister, Dynamic Dissolution: A Step Closer to Predictive Dissolution Testing?, Molecular Pharmaceutics, 7 (2010) 1374-1387.
[13] D. Dupont, M. Alric, S. Blanquet-Diot, G. Bornhorst, C. Cueva, A. Deglaire, S. Denis, M. Ferrua, R. Havenaar, J. Lelieveld, A.R. Mackie, M. Marzorati, O. Menard, M. Minekus, B. Miralles, I. Recio, P. Van den Abbeele, Can dynamic in vitro digestion systems mimic the physiological reality?, Critical Reviews in Food Science and Nutrition, 59 (2019) 1546-1562.
[14] R. Berthelsen, M. Klitgaard, T. Rades, A. Müllertz, In vitro digestion models to evaluate lipid based drug delivery systems; present status and current trends, Advanced Drug Delivery Reviews, 142 (2019) 35-49.
[15] C. Li, W. Yu, P. Wu, X.D. Chen, Current in vitro digestion systems for understanding food digestion in human upper gastrointestinal tract, Trends in Food Science & Technology, 96 (2020) 114-126.
[16] C. Zhong, T. Langrish, A comparison of different physical stomach models and an analysis of shear stresses and strains in these system, Food Research International, 135 (2020) 109296.
[17] L. Nissen, F. Casciano, A. Gianotti, Intestinal fermentation in vitro models to study food-induced gut microbiota shift: an updated review, FEMS Microbiology Letters, 367 (2020).
[18] P. Swain, A. Toor, F. Volke, J. Keller, J. Gerber, E. Rabinovitz, R.I. Rothstein, Remote magnetic manipulation of a wireless capsule endoscope in the esophagus and stomach of humans (with), Gastrointestinal Endoscopy, 71 (2010) 1290-1293.
[19] S.N. Adler, Y.C. Metzger, PillCam COLON capsule endoscopy: recent advances and new insights, Therapeutic Advances in Gastroenterology, 4 (2011) 265-268.

[20] J. Rey, H. Ogata, N. Hosoe, K. Ohtsuka, N. Ogata, K. Ikeda, H. Aihara, I. Pangtay, T. Hibi, S. Kudo, H. Tajiri, Feasibility of stomach exploration with a guided capsule endoscope, Endoscopy, 42 (2010) 541-545.
[21] J.P. Holden, P. Dureja, P.R. Pfau, D.C. Schwartz, M. Reichelderfer, R.H. Judd, I. Danko, L.V. Iyer, D.V. Gopal, Endoscopic placement of the small-bowel video capsule by using a capsule endoscope delivery device, Gastrointestinal Endoscopy, 65 (2007) 842-847.
[22] A. Benken, Y. Gianchandani, Passive Wireless Pressure Sensing for Gastric Manometry, Micromachines, 10 (2019).
[23] T.O. Vilz, D. Pantelis, P. Lingohr, R. Fimmers, A. Esmann, T. Randau, J.C. Kalff, M. Coenen, S. Wehner, SmartPill®as an objective parameter for determination of severity and duration of postoperative ileus: study protocol of a prospective, two-arm, open-label trial (the PIDuSA study), BMJ Open, 6 (2016).
[24] H.O. Diaz Tartera, D.L. Webb, A.K. Al-Saffar, M.A. Halim, G. Lindberg, P. Sangfelt, P.M. Hellström, Validation of SmartPill®wireless motility capsule for gastrointestinal transit time: Intra-subject variability, software accuracy and comparison with video capsule endoscopy, Neurogastroenterology & Motility, 29 (2017).
[25] K. Kalantar-Zadeh, K.J. Berean, N. Ha, A.F. Chrimes, K. Xu, D. Grando, J.Z. Ou, N. Pillai, J.L. Campbell, R. Brkljača, K.M. Taylor, R.E. Burgell, C.K. Yao, S.A. Ward, C.S. McSweeney, J.G. Muir, P.R. Gibson, A human pilot trial of ingestible electronic capsules capable of sensing different gases in the gut, Nature Electronics, 1 (2018) 79-87.
[26] B. Abrahamsson, A. Pal, M. Sjöberg, M. Carlsson, E. Laurell, J.G. Brasseur, A Novel in Vitro and Numerical Analysis of Shear-Induced Drug Release from Extended-Release Tablets in the Fed Stomach, Pharmaceutical Research, 22 (2005) 1215-1226.
[27] C. Schiller, C.P. Frohlich, T. Giessmann, W. Siegmund, H. Monnikes, N. Hosten, W. Weitschies, Intestinal fluid volumes and transit of dosage forms as assessed by magnetic resonance imaging, Alimentary Pharmacology and Therapeutics, 22 (2005) 971-979.
[28] J.-R. Malagelada, G.F. Longstreth, W.H.J. Summerskill, V.L.W. Go, Measurement of Gastric Functions During Digestion of Ordinary Solid Meals in Man, Gastroenterology, 70 (1976) 203-210.
[29] S. Klein, J.B. Dressman, J. Butler, J.M. Hempenstall, C. Reppas, Media to simulate the postprandial stomach I. Matching the physicochemical characteristics of standard breakfasts, Journal of Pharmacy and Pharmacology, 56 (2004) 605-610.
[30] M. Koziolek, M. Grimm, F. Schneider, P. Jedamzik, M. Sager, J.P. Kuhn, W. Siegmund, W. Weitschies, Navigating the human gastrointestinal tract for oral drug delivery: Uncharted waters and new frontiers, Advanced Drug Delivery Reviews, 101 (2016) 75-88.
[31] A. Diakidou, M. Vertzoni, K. Goumas, E. Söderlind, B. Abrahamsson, J. Dressman, C. Reppas, Characterization of the Contents of Ascending Colon to Which Drugs are Exposed After Oral Administration to Healthy Adults, Pharmaceutical Research, 26 (2009) 2141-2151.
[32] E.S. Kostewicz, M. Wunderlich, U. Brauns, R. Becker, T. Bock, J.B. Dressman, Predicting the precipitation of poorly soluble weak bases upon entry in the small intestine, Journal of Pharmacy and Pharmacology, 56 (2004) 43-51.
[33] C.H. Gu, D. Rao, R.B. Gandhi, J.o.n. Hilden, K. Raghavan, Using a Novel Multicompartment Dissolution System to Predict the Effect of Gastric pH on the Oral Absorption of Weak Bases with Poor Intrinsic Solubility, Journal of Pharmaceutical Sciences, 94 (2005) 199-208.
[34] A. Kourentas, M. Vertzoni, N. Stavrinoudakis, A. Symillidis, J. Brouwers, P. Augustijns, C. Reppas, M. Symillides, An in vitro biorelevant gastrointestinal transfer (BioGIT) system for forecasting concentrations in the fasted upper small intestine: Design, implementation, and evaluation, European Journal of Pharmaceutical Sciences, 82 (2016) 106-114.
[35] D.P. McNamara, K.M. Whitney, S.L. Goss, Use of a physiologic bicarbonate buffer system for dissolution characterization of ionizable drugs, Pharmaceutical Research, 20 (2003) 1641-1646.

[36] H.M. Fadda, H.A. Merchant, B.T. Arafat, A.W. Basit, Physiological bicarbonate buffers: stabilisation and use as dissolution media for modified release systems, International Journal of Pharmaceutics, 382 (2009) 56-60.
[37] H.A. Merchant, A. Goyanes, N. Parashar, A.W. Basit, Predicting the gastrointestinal behaviour of modified-release products: utility of a novel dynamic dissolution test apparatus involving the use of bicarbonate buffers, International Journal of Pharmaceutics, 475 (2014) 585-591.
[38] G. Garbacz, B. Kołodziej, M. Koziolek, W. Weitschies, S. Klein, An Automated System for Monitoring and Regulating the pH of Bicarbonate Buffers, AAPS PharmSciTech, 14 (2013) 517-522.
[39] G. Garbacz, B. Kołodziej, M. Koziolek, W. Weitschies, S. Klein, A dynamic system for the simulation of fasting luminal pH-gradients using hydrogen carbonate buffers for dissolution testing of ionisable compounds, European Journal of Pharmaceutical Sciences, 51 (2014) 224-231.
[40] D. Zakowiecki, M. Szczepanska, T. Hess, K. Cal, B. Mikolaszek, J. Paszkowska, M. Wiater, D. Hoc, G. Garbacz, Preparation of delayed-release multiparticulate formulations of diclofenac sodium and evaluation of their dissolution characteristics using biorelevant dissolution methods, Journal of Drug Delivery Science and Technology, 60 (2020).
[41] X. Wei, M. Beltrán-Gastélum, E. Karshalev, B. Esteban-Fernández de Ávila, J. Zhou, D. Ran, P. Angsantikul, R.H. Fang, J. Wang, L. Zhang, Biomimetic Micromotor Enables Active Delivery of Antigens for Oral Vaccination, Nano Letters, 19 (2019) 1914-1921.
[42] B.E.-F. de Ávila, P. Angsantikul, J. Li, M. Angel Lopez-Ramirez, D.E. Ramírez-Herrera, S. Thamphiwatana, C. Chen, J. Delezuk, R. Samakapiruk, V. Ramez, M. Obonyo, L. Zhang, J. Wang, Micromotor-enabled active drug delivery for in vivo treatment of stomach infection, Nature Communications, 8 (2017).
[43] J. Li, P. Angsantikul, W. Liu, B. Esteban-Fernández de Ávila, S. Thamphiwatana, M. Xu, E. Sandraz, X. Wang, J. Delezuk, W. Gao, L. Zhang, J. Wang, Micromotors Spontaneously Neutralize Gastric Acid for pH-Responsive Payload Release, Angewandte Chemie International Edition, 56 (2017) 2156-2161.
[44] W. Gao, R. Dong, S. Thamphiwatana, J. Li, W. Gao, L. Zhang, J. Wang, Artificial Micromotors in the Mouse's Stomach: A Step toward in Vivo Use of Synthetic Motors, ACS Nano, 9 (2015) 117-123.
[45] S. Sundararajan, P.E. Lammert, A.W. Zudans, V.H. Crespi, A. Sen, Catalytic Motors for Transport of Colloidal Cargo, Nano Letters, 8 (2008) 1271-1276.
[46] Z. Wu, Y. Wu, W. He, X. Lin, J. Sun, Q. He, Self-Propelled Polymer-Based Multilayer Nanorockets for Transportation and Drug Release, Angewandte Chemie International Edition, 52 (2013) 7000-7003.
[47] W. Gao, J. Wang, Synthetic micro/nanomotors in drug delivery, Nanoscale, 6 (2014) 10486-10494.
[48] J. Li, P. Angsantikul, W. Liu, B. Esteban-Fernández de Ávila, S. Thamphiwatana, M. Xu, E. Sandraz, X. Wang, J. Delezuk, W. Gao, L. Zhang, J. Wang, Micromotors Spontaneously Neutralize Gastric Acid for pH-Responsive Payload Release, Angewandte Chemie, 129 (2017) 2188-2193.
[49] K.M. Ainslie, R.D. Lowe, T.T. Beaudette, L. Petty, E.M. Bachelder, T.A. Desai, Microfabricated Devices for Enhanced Bioadhesive Drug Delivery: Attachment to and Small-Molecule Release Through a Cell Monolayer Under Flow, Small, 5 (2009) 2857-2863.
[50] S.L. Tao, T.A. Desai, Micromachined devices: The impact of controlled geometry from cell-targeting to bioavailability, Journal of Controlled Release, 109 (2005) 127-138.
[51] S.L. Tao, T.A. Desai, Gastrointestinal patch systems for oral drug delivery, Drug Discovery Today, 10 (2005) 909-915.
[52] S.L. Tao, M.W. Lubeley, T.A. Desai, Bioadhesive poly(methyl methacrylate) microdevices for controlled drug delivery, Journal of Controlled Release, 88 (2003) 215-228.
[53] K.M. Ainslie, C.M. Kraning, T.A. Desai, Microfabrication of an asymmetric, multi-layered microdevice for controlled release of orally delivered therapeutics, Lab on a Chip, 8 (2008).
[54] J. Guan, H. He, L.J. Lee, D.J. Hansford, Fabrication of Particulate Reservoir-Containing, Capsulelike, and Self-Folding Polymer Microstructures for Drug Delivery, Small, 3 (2007) 412-418.

[55] P. Zhang, Y. Liu, J. Xia, Z. Wang, B. Kirkland, J. Guan, Top-Down Fabrication of Polyelectrolyte-Thermoplastic Hybrid Microparticles for Unidirectional Drug Delivery to Single Cells, Advanced Healthcare Materials, 2 (2013) 540-545.
[56] H.D. Chirra, L. Shao, N. Ciaccio, C.B. Fox, J.M. Wade, A. Ma, T.A. Desai, Planar Microdevices for Enhanced In Vivo Retention and Oral Bioavailability of Poorly Permeable Drugs, Advanced Healthcare Materials, 3 (2014) 1648-1654.
[57] C.B. Fox, C.L. Nemeth, R.W. Chevalier, J. Cantlon, D.B. Bogdanoff, J.C. Hsiao, T.A. Desai, Picoliter-volume inkjet printing into planar microdevice reservoirs for low-waste, high-capacity drug loading, Bioengineering & Translational Medicine, 2 (2017) 9-16.
[58] C.B. Fox, Y. Cao, C.L. Nemeth, H.D. Chirra, R.W. Chevalier, A.M. Xu, N.A. Melosh, T.A. Desai, Fabrication of Sealed Nanostraw Microdevices for Oral Drug Delivery, ACS Nano, 10 (2016) 5873-5881.
[59] A. Ahmed, C. Bonner, T.A. Desai, Bioadhesive microdevices with multiple reservoirs: a new platform for oral drug delivery, Journal of Controlled Release, 81 (2002) 291-306.
[60] L. Chen, L. Gruzinskyte, S.L. Jørgensen, A. Boisen, S.K. Srivastava, An Ingestible Self-Polymerizing System for Targeted Sampling of Gut Microbiota and Biomarkers, ACS Nano, 14 (2020) 12072-12081.
[61] M. Mimee, P. Nadeau, A. Hayward, S. Carim, S. Flanagan, L. Jerger, J. Collins, S. McDonnell, R. Swartwout, R.J. Citorik, V. Bulović, R. Langer, G. Traverso, A.P. Chandrakasan, T.K. Lu, An ingestible bacterial-electronic system to monitor gastrointestinal health, Science, 360 (2018) 915-918.
[62] C.A. Thompson, A. DeLaForest, M.A. Battle, Patterning the gastrointestinal epithelium to confer regional-specific functions, Developmental Biology, 435 (2018) 97-108.
[63] N. Barker, M. van de Wetering, H. Clevers, The intestinal stem cell, Genes & Development, 22 (2008) 1856-1864.
[64] J.Y. Lock, T.L. Carlson, R.L. Carrier, Mucus models to evaluate the diffusion of drugs and particles, Advanced Drug Delivery Reviews, 124 (2018) 34-49.
[65] F. Afonso-Pereira, L. Dou, S.J. Trenfield, C.M. Madla, S. Murdan, J. Sousa, F. Veiga, A.W. Basit, Sex differences in the gastrointestinal tract of rats and the implications for oral drug delivery, European Journal of Pharmaceutical Sciences, 115 (2018) 339-344.
[66] L. Dou, F.K.H. Gavins, Y. Mai, C.M. Madla, F. Taherali, M. Orlu, S. Murdan, A.W. Basit, Effect of Food and an Animal's Sex on P-Glycoprotein Expression and Luminal Fluids in the Gastrointestinal Tract of Wistar Rats, Pharmaceutics, 12 (2020) 296.
[67] C.M. Madla, F.K.H. Gavins, H. Merchant, M. Orlu, S. Murdan, A.W. Basit, Let's Talk About Sex: Differences in Drug Therapy in Males and Females, Advanced Drug Delivery Reviews, (2021).
[68] K. Shah, C.E. McCormack, N.A. Bradbury, Do you know the sex of your cells?, Am J Physiol Cell Physiol, 306 (2014) C3-C18.
[69] M. Poletti, K. Arnauts, M. Ferrante, T. Korcsmaros, Organoid-based Models to Study the Role of Host-microbiota Interactions in IBD, Journal of Crohn's and Colitis, (2020).
[70] H. Hisha, T. Tanaka, S. Kanno, Y. Tokuyama, Y. Komai, S. Ohe, H. Yanai, T. Omachi, H. Ueno, Establishment of a Novel Lingual Organoid Culture System: Generation of Organoids Having Mature Keratinized Epithelium from Adult Epithelial Stem Cells, Scientific Reports, 3 (2013).
[71] E. Aihara, M.M. Mahe, M.A. Schumacher, A.L. Matthis, R. Feng, W. Ren, T.K. Noah, T. Matsu-ura, S.R. Moore, C.I. Hong, Y. Zavros, S. Herness, N.F. Shroyer, K. Iwatsuki, P. Jiang, M.A. Helmrath, M.H. Montrose, Characterization of stem/progenitor cell cycle using murine circumvallate papilla taste bud organoid, Scientific Reports, 5 (2015).
[72] W. Ren, B.C. Lewandowski, J. Watson, E. Aihara, K. Iwatsuki, A.A. Bachmanov, R.F. Margolskee, P. Jiang, Single Lgr5- or Lgr6-expressing taste stem/progenitor cells generate taste bud cells ex vivo, Proceedings of the National Academy of Sciences, 111 (2014) 16401-16406.
[73] Lalitha S.Y. Nanduri, M. Baanstra, H. Faber, C. Rocchi, E. Zwart, G. de Haan, R. van Os, Robert P. Coppes, Purification and Ex Vivo Expansion of Fully Functional Salivary Gland Stem Cells, Stem Cell Reports, 3 (2014) 957-964.

[74] Aaron D. DeWard, J. Cramer, E. Lagasse, Cellular Heterogeneity in the Mouse Esophagus Implicates the Presence of a Nonquiescent Epithelial Stem Cell Population, Cell Reports, 9 (2014) 701-711.
[75] T. Sato, D.E. Stange, M. Ferrante, R.G.J. Vries, J.H. van Es, S. van den Brink, W.J. van Houdt, A. Pronk, J. van Gorp, P.D. Siersema, H. Clevers, Long-term Expansion of Epithelial Organoids From Human Colon, Adenoma, Adenocarcinoma, and Barrett's Epithelium, Gastroenterology, 141 (2011) 1762-1772.
[76] M. Stelzner, M. Helmrath, J.C.Y. Dunn, S.J. Henning, C.W. Houchen, C. Kuo, J. Lynch, L. Li, S.T. Magness, M.G. Martin, M.H. Wong, J. Yu, A nomenclature for intestinal in vitro cultures, American Journal of Physiology-Gastrointestinal and Liver Physiology, 302 (2012) G1359-G1363.
[77] S. Yui, T. Nakamura, T. Sato, Y. Nemoto, T. Mizutani, X. Zheng, S. Ichinose, T. Nagaishi, R. Okamoto, K. Tsuchiya, H. Clevers, M. Watanabe, Functional engraftment of colon epithelium expanded in vitro from a single adult Lgr5+ stem cell, Nature Medicine, 18 (2012) 618-623.
[78] J.O. Múnera, N. Sundaram, S.A. Rankin, D. Hill, C. Watson, M. Mahe, J.E. Vallance, N.F. Shroyer, K.L. Sinagoga, A. Zarzoso-Lacoste, J.R. Hudson, J.C. Howell, P. Chatuvedi, J.R. Spence, J.M. Shannon, A.M. Zorn, M.A. Helmrath, J.M. Wells, Differentiation of Human Pluripotent Stem Cells into Colonic Organoids via Transient Activation of BMP Signaling, Cell Stem Cell, 21 (2017) 51-64.e56.
[79] A. Fumagalli, J. Drost, S.J.E. Suijkerbuijk, R. van Boxtel, J. de Ligt, G.J. Offerhaus, H. Begthel, E. Beerling, E.H. Tan, O.J. Sansom, E. Cuppen, H. Clevers, J. van Rheenen, Genetic dissection of colorectal cancer progression by orthotopic transplantation of engineered cancer organoids, Proceedings of the National Academy of Sciences, 114 (2017) E2357-E2364.
[80] N.G. Steele, J. Chakrabarti, J. Wang, J. Biesiada, L. Holokai, J. Chang, L.M. Nowacki, J. Hawkins, M. Mahe, N. Sundaram, N. Shroyer, M. Medvedovic, M. Helmrath, S. Ahmad, Y. Zavros, An Organoid-Based Preclinical Model of Human Gastric Cancer, Cellular and Molecular Gastroenterology and Hepatology, 7 (2019) 161-184.
[81] M. Matano, S. Date, M. Shimokawa, A. Takano, M. Fujii, Y. Ohta, T. Watanabe, T. Kanai, T. Sato, Modeling colorectal cancer using CRISPR-Cas9–mediated engineering of human intestinal organoids, Nature Medicine, 21 (2015) 256-262.
[82] N.C. Zachos, O. Kovbasnjuk, J. Foulke-Abel, J. In, S.E. Blutt, H.R. de Jonge, M.K. Estes, M. Donowitz, Human Enteroids/Colonoids and Intestinal Organoids Functionally Recapitulate Normal Intestinal Physiology and Pathophysiology, Journal of Biological Chemistry, 291 (2016) 3759-3766.
[83] A. Fumagalli, S.J.E. Suijkerbuijk, H. Begthel, E. Beerling, K.C. Oost, H.J. Snippert, J. van Rheenen, J. Drost, A surgical orthotopic organoid transplantation approach in mice to visualize and study colorectal cancer progression, Nature Protocols, 13 (2018) 235-247.
[84] G.-S. Park, M.H. Park, W. Shin, C. Zhao, S. Sheikh, S.J. Oh, H.J. Kim, Emulating Host-Microbiome Ecosystem of Human Gastrointestinal Tract in Vitro, Stem Cell Reviews and Reports, 13 (2017) 321-334.
[85] N. Gupta, J.R. Liu, B. Patel, D.E. Solomon, B. Vaidya, V. Gupta, Microfluidics-based 3D cell culture models: Utility in novel drug discovery and delivery research, Bioengineering & Translational Medicine, 1 (2016) 63-81.
[86] A. Bein, W. Shin, S. Jalili-Firoozinezhad, M.H. Park, A. Sontheimer-Phelps, A. Tovaglieri, A. Chalkiadaki, H.J. Kim, D.E. Ingber, Microfluidic Organ-on-a-Chip Models of Human Intestine, Cellular and Molecular Gastroenterology and Hepatology, 5 (2018) 659-668.
[87] J.M. Donkers, H. Eslami Amirabadi, E. van de Steeg, Intestine-on-a-chip: Next level in vitro research model of the human intestine, Current Opinion in Toxicology, 25 (2021) 6-14.
[88] M. Kasendra, R. Luc, J. Yin, D.V. Manatakis, G. Kulkarni, C. Lucchesi, J. Sliz, A. Apostolou, L. Sunuwar, J. Obrigewitch, K.-J. Jang, G.A. Hamilton, M. Donowitz, K. Karalis, Duodenum Intestine-Chip for preclinical drug assessment in a human relevant model, eLife, 9 (2020).
[89] H.J. Kim, D.E. Ingber, Gut-on-a-Chip microenvironment induces human intestinal cells to undergo villus differentiation, Integrative Biology, 5 (2013).

[90] H.J. Kim, D. Huh, G. Hamilton, D.E. Ingber, Human gut-on-a-chip inhabited by microbial flora that experiences intestinal peristalsis-like motions and flow, Lab on a Chip, 12 (2012).
[91] M. Chi, B. Yi, S. Oh, D.-J. Park, J.H. Sung, S. Park, A microfluidic cell culture device (μFCCD) to culture epithelial cells with physiological and morphological properties that mimic those of the human intestine, Biomedical Microdevices, 17 (2015).
[92] C. Beaurivage, E. Naumovska, Y. Chang, E. Elstak, A. Nicolas, H. Wouters, G. van Moolenbroek, H. Lanz, S. Trietsch, J. Joore, P. Vulto, R. Janssen, K. Erdmann, J. Stallen, D. Kurek, Development of a Gut-on-a-Chip Model for High Throughput Disease Modeling and Drug Discovery, International Journal of Molecular Sciences, 20 (2019).
[93] A. Choe, S.K. Ha, I. Choi, N. Choi, J.H. Sung, Microfluidic Gut-liver chip for reproducing the first pass metabolism, Biomedical Microdevices, 19 (2017).
[94] A.P. Ramme, L. Koenig, T. Hasenberg, C. Schwenk, C. Magauer, D. Faust, A.K. Lorenz, A.-C. Krebs, C. Drewell, K. Schirrmann, A. Vladetic, G.-C. Lin, S. Pabinger, W. Neuhaus, F. Bois, R. Lauster, U. Marx, E.-M. Dehne, Autologous induced pluripotent stem cell-derived four-organ-chip, Future Science OA, 5 (2019).
[95] Y. Imai, et al., Antral recirculation in the stomach during gastric mixing, American Journal of Physiology-Gastrointestinal and Liver Physiology

304 (2012) G536–G542.
[96] J.F. Munk, R.M. Gannaway, M. Hoare, A.G. Johnson, Direct measurement of pyloric diameter and tone in man and their response to cholecystokinin, in: H.L. Duthie (Ed.) Gastrointestinal Motility in Health and Disease: Proceedings of the 6th International Symposium on Gastrointestinal Motility, held at the Royal College of Surgeons of Edinburgh, 12–16th September, 1977, Springer Netherlands, Dordrecht, 1978, pp. 349-359.
[97] N. Salessiotis, Measurement of the diameter of the pylorus in man: Part I. Experimental project for clinical application, The American Journal of Surgery, 124 (1972) 331-333.
[98] W.A. Ritschel, Targeting in the gastrointestinal tract: new approaches, Methods Find Exp Clin Pharmacol, 13 (1991) 313-336.
[99] A. Thomas, Gut motility, sphincters and reflex control, Anaesthesia & Intensive Care Medicine, 7 (2006) 57-58.
[100] D.I. Soybel, Anatomy and Physiology of the Stomach, Surgical Clinics of North America, 85 (2005) 875-894.
[101] J.L. Newton, N. Jordan, J. Pearson, G.V. Williams, A. Allen, O.F. James, The adherent gastric antral and duodenal mucus gel layer thins with advancing age in subjects infected with Helicobacter pylori, Gerontology, 46 (2000) 153-157.
[102] J. Newton, N. Jordan, L. Oliver, V. Strugala, J. Pearson, O. James, A. Allen, Helicobacter pylori in vivo causes structural changes in the adherent gastric mucus layer but barrier thickness is not compromised, Gut, 43 (1998) 470-475.
[103] M. Vertzoni, P. Augustijns, M. Grimm, M. Koziolek, G. Lemmens, N. Parrott, C. Pentafragka, C. Reppas, J. Rubbens, J. Van Den Alphabeele, T. Vanuytsel, W. Weitschies, C.G. Wilson, Impact of regional differences along the gastrointestinal tract of healthy adults on oral drug absorption: An UNGAP review, European Journal of Pharmaceutical Sciences, 134 (2019) 153-175.
[104] M.L. Schubert, Gastric secretion, Current Opinion in Gastroenterology, 30 (2014).
[105] W. Buayam, W. Punchuklang, S. Udompunthurak, P. Vichitvejpaisal, Volume and pH of gastric contents in patients undergoing gynecologic laparoscopic surgery during emergence from general anesthesia: A prospective observational study, Journal of the Medical Association of Thailand, 104 (2021) 38-43.
[106] C.A.T. da Rocha, L.M.K. Kamada, P.H. de Andrade Filho, I.A. Villaverde, J.Y.B. Shiro, J.M. Silva, Ultrasonographic evaluation of gastric content and volume: A systematic review, Revista da Associacao Medica Brasileira, 66 (2020) 1725-1730.
[107] C.H. Pham, Z.J. Collier, W.L. Garner, C.M. Kuza, T.J. Gillenwater, Measuring gastric residual volumes in critically ill burn patients — A systematic review, Burns, 45 (2019) 509-525.

[108] F. Matsumoto, I. Sakurai, M. Morita, T. Takahashi, N. Mori, T. Sugihara, A. Sakai, S. Yamaji, Y. Akaike, K. Yano, Effects of the quantity of water and milk ingested concomitantly with AS-924, a novel ester-type cephem antibiotic, on its pharmacokinetics, International Journal of Antimicrobial Agents, 18 (2001) 471-476.
[109] C. Schiller, C.-P. Frohlich, T. Giessmann, W. Siegmund, H. Monnikes, N. Hosten, W. Weitschies, Intestinal fluid volumes and transit of dosage forms as assessed by magnetic resonance imaging., Alimentary Pharmacology and Therapeutics, 22 (2005) 971-979.
[110] A. Steingoetter, M. Fox, R. Treier, D. Weishaupt, B. Marincek, P. Boesiger, M. Fried, W. Schwizer, Effects of posture on the physiology of gastric emptying: a magnetic resonance imaging study, Scandinavian journal of gastroenterology, 41 (2006) 1155-1164.
[111] H. Fruehauf, O. Goetze, A. Steingoetter, M. Kwiatek, P. Boesiger, M. Thumshirn, W. Schwizer, M. Fried, Intersubject and intrasubject variability of gastric volumes in response to isocaloric liquid meals in functional dyspepsia and health, Neurogastroenterology & Motility, 19 (2007) 553-561.
[112] D.M. Mudie, K. Murray, C.L. Hoad, S.E. Pritchard, M.C. Garnett, G.L. Amidon, P.A. Gowland, R.C. Spiller, G.E. Amidon, L. Marciani, Quantification of Gastrointestinal Liquid Volumes and Distribution Following a 240 mL Dose of Water in the Fasted State, Molecular Pharmaceutics, 11 (2014) 3039-3047.
[113] M. Koziolek, M. Grimm, G. Garbacz, J.-P. Kühn, W. Weitschies, Intragastric Volume Changes after Intake of a High-Caloric, High-Fat Standard Breakfast in Healthy Human Subjects Investigated by MRI, Molecular Pharmaceutics, 11 (2014) 1632-1639.
[114] M. Grimm, E. Scholz, M. Koziolek, J.P. Kühn, W. Weitschies, Gastric Water Emptying under Fed State Clinical Trial Conditions Is as Fast as under Fasted Conditions, Molecular Pharmaceutics, 14 (2017) 4262-4271.
[115] M. Grimm, M. Koziolek, M. Saleh, F. Schneider, G. Garbacz, J.P. Kühn, W. Weitschies, Gastric Emptying and Small Bowel Water Content after Administration of Grapefruit Juice Compared to Water and Isocaloric Solutions of Glucose and Fructose: A Four-Way Crossover MRI Pilot Study in Healthy Subjects, Molecular Pharmaceutics, 15 (2018) 548-559.
[116] M. Grimm, M. Koziolek, J.P. Kuhn, W. Weitschies, Interindividual and intraindividual variability of fasted state gastric fluid volume and gastric emptying of water, European Journal of Pharmaceutics and Biopharmaceutics, 127 (2018) 309-317.
[117] T. de Waal, J. Rubbens, M. Grimm, V. Vandecaveye, J. Tack, W. Weitschies, J. Brouwers, P. Augustijns, Exploring the Effect of Esomeprazole on Gastric and Duodenal Fluid Volumes and Absorption of Ritonavir, Pharmaceutics 12 (2020) 670.
[118] A. Lindahl, A.-L. Ungell, L. Knutson, H. Lennernäs, Characterization of Fluids from the Stomach and Proximal Jejunum in Men and Women, Pharmaceutical Research, 14 (1997) 497-502.
[119] M. Efentakis, J.B. Dressman, Gastric juice as a dissolution medium: Surface tension and pH, European Journal of Drug Metabolism and Pharmacokinetics, 23 (1998) 97-102.
[120] L. Kalantzi, K. Goumas, V. Kalioras, B. Abrahamsson, J.B. Dressman, C. Reppas, Characterization of the human upper gastrointestinal contents under conditions simulating bioavailability/bioequivalence studies, Pharmaceutical Research, 23 (2006) 165-176.
[121] P.B. Pedersen, P. Vilmann, D. Bar-Shalom, A. Müllertz, S. Baldursdottir, Characterization of fasted human gastric fluid for relevant rheological parameters and gastric lipase activities, European Journal of Pharmaceutics and Biopharmaceutics, 85 (2013) 958-965.
[122] B. Hens, Y. Tsume, M. Bermejo, P. Paixao, M.J. Koenigsknecht, J.R. Baker, W.L. Hasler, R. Lionberger, J. Fan, J. Dickens, K. Shedden, B. Wen, J. Wysocki, R. Loebenberg, A. Lee, A. Frances, G. Amidon, A. Yu, G. Benninghoff, N. Salehi, A. Talattof, D. Sun, G.L. Amidon, Low Buffer Capacity and Alternating Motility along the Human Gastrointestinal Tract: Implications for in Vivo Dissolution and Absorption of Ionizable Drugs, Molecular Pharmaceutics, 14 (2017) 4281-4294.
[123] C. Litou, M. Vertzoni, C. Goumas, V. Vasdekis, W. Xu, F. Kesisoglou, C. Reppas, Characteristics of the Human Upper Gastrointestinal Contents in the Fasted State Under Hypo- and A-chlorhydric

Gastric Conditions Under Conditions of Typical Drug - Drug Interaction Studies, Pharmaceutical Research, 33 (2016) 1399-1412.
[124] B.L. Pedersen, A. Müllertz, H. Brøndsted, H.G. Kristensen, A Comparison of the Solubility of Danazol in Human and Simulated Gastrointestinal Fluids, Pharmaceutical Research, 17 (2000) 891-894.
[125] C. Pentafragka, M. Vertzoni, J. Dressman, M. Symillides, K. Goumas, C. Reppas, Characteristics of contents in the upper gastrointestinal lumen after a standard high-calorie high-fat meal and implications for the in vitro drug product performance testing conditions, European Journal of Pharmaceutical Sciences, 155 (2020) 105535.
[126] A. Diakidou, M. Vertzoni, J. Dressman, C. Reppas, Estimation of intragastric drug solubility in the fed state: comparison of various media with data in aspirates, Biopharmaceutics and Drug Disposition, 30 (2009) 318-325.
[127] S. Amara, C. Bourlieu, L. Humbert, D. Rainteau, F. Carrière, Variations in gastrointestinal lipases, pH and bile acid levels with food intake, age and diseases: Possible impact on oral lipid-based drug delivery systems, Advanced Drug Delivery Reviews, 142 (2019) 3-15.
[128] M. Vertzoni, J. Dressman, J. Butler, J. Hempenstall, C. Reppas, Simulation of fasting gastric conditions and its importance for the in vivo dissolution of lipophilic compounds, European Journal of Pharmaceutics and Biopharmaceutics, 60 (2005) 413-417.
[129] M. Vertzoni, E. Pastelli, D. Psachoulias, L. Kalantzi, C. Reppas, Estimation of intragastric solubility of drugs: in what medium?, Pharmaceutical Research, 24 (2007) 909-917.
[130] M.R.C. Marques, R. Loebenberg, M. Almukainzi, Simulated Biological Fluids with Possible Application in Dissolution Testing, Dissolution Technologies, August 2011 (2011).
[131] P. Macheras, M. Koupparis, E. Apostolelli, Dissolution of 4 controlled-release theophylline formulations in milk, International Journal of Pharmaceutics, 36 (1987) 73-79.
[132] N. Janssen, E. Jantratid, J. Dressman, Bio relevant media to simulate postprandial conditions in the proximal gut, AAPS PharmSciTech, 4 (2007) 45-54.
[133] L. Egger, O. Ménard, C. Delgado-Andrade, P. Alvito, R. Assunção, S. Balance, R. Barberá, A. Brodkorb, T. Cattenoz, A. Clemente, I. Comi, D. Dupont, G. Garcia-Llatas, M.J. Lagarda, S. Le Feunteun, L. JanssenDuijghuijsen, S. Karakaya, U. Lesmes, A.R. Mackie, C. Martins, A. Meynier, B. Miralles, B.S. Murray, A. Pihlanto, G. Picariello, C.N. Santos, S. Simsek, I. Recio, N. Rigby, L.-E. Rioux, H. Stoffers, A. Tavares, L. Tavares, S. Turgeon, E.K. Ulleberg, G.E. Vegarud, G. Vergères, R. Portmann, The harmonized INFOGEST in vitro digestion method: From knowledge to action, Food Research International, 88 (2016) 217-225.
[134] A. Brodkorb, L. Egger, M. Alminger, P. Alvito, R. Assunção, S. Ballance, T. Bohn, C. Bourlieu-Lacanal, R. Boutrou, F. Carrière, A. Clemente, M. Corredig, D. Dupont, C. Dufour, C. Edwards, M. Golding, S. Karakaya, B. Kirkhus, S. Le Feunteun, U. Lesmes, A. Macierzanka, A.R. Mackie, C. Martins, S. Marze, D.J. McClements, O. Ménard, M. Minekus, R. Portmann, C.N. Santos, I. Souchon, R.P. Singh, G.E. Vegarud, M.S.J. Wickham, W. Weitschies, I. Recio, INFOGEST static in vitro simulation of gastrointestinal food digestion, Nature Protocols, 14 (2019) 991-1014.
[135] A. Pal, J.G. Brasseur, B. Abrahamsson, A stomach road or “Magenstrasse” for gastric emptying, Journal of Biomechanics, 40 (2007) 1202-1210.
[136] A.Y. Abuhelwa, D.J.R. Foster, R.N. Upton, A Quantitative Review and Meta-models of the Variability and Factors Affecting Oral Drug Absorption-Part II: Gastrointestinal Transit Time, The AAPS journal, 18 (2016) 1322-1333.
[137] H.I. Jacoby, Gastric Emptying, Reference Module in Biomedical Sciences, Elsevier2017.
[138] M. Martinez, S. Bhoopathy, S. Carlert, M. Cirit, T. Flanagan, B. Forbes, M. Jamei, M. Khan, V. Lukacova, J. Mochel, X. Pepin, D. Pade, C. Reppas, P. Sinko, D. Sperry, K. Tsinman, M. Vertzoni, Workshop Report: USP Workshop on Exploring the Science of Drug Absorption, Dissolution Technologies, 26 (2019) 38-66.

[139] C. Markopoulos, C.J. Andreas, M. Vertzoni, J. Dressman, C. Reppas, In-vitro simulation of luminal conditions for evaluation of performance of oral drug products: Choosing the appropriate test media, European Journal of Pharmaceutics and Biopharmaceutics, 93 (2015) 173-182.
[140] S. Fernandez, S. Chevrier, N. Ritter, B. Mahler, F. Demarne, F. Carrière, V. Jannin, In vitro gastrointestinal lipolysis of four formulations of piroxicam and cinnarizine with the self emulsifying excipients Labrasol and Gelucire 44/14, Pharmaceutical Research, 26 (2009) 1901-1910.
[141] K. Molly, M.V. Woestyne, I.D. Smet, W. Verstraete, Validation of the Simulator of the Human Intestinal Microbial Ecosystem (SHIME) Reactor Using Microorganism-associated Activities, Microbial Ecology in Health and Disease, 7 (1994) 191-200.
[142] P. De Boever, B. Deplancke, W. Verstraete, Fermentation by Gut Microbiota Cultured in a Simulator of the Human Intestinal Microbial Ecosystem Is Improved by Supplementing a Soygerm Powder, The Journal of nutrition, 130 (2000) 2599-2606.
[143] T. Van de Wiele, P. Van den Abbeele, W. Ossieur, S. Possemiers, M. Marzorati, The Simulator of the Human Intestinal Microbial Ecosystem (SHIME®), in: K. Verhoeckx (Ed.) The Impact of Food Bioactives on Health, Springer, Cham2015.
[144] M. Voropaiev, D. Nock, Onset of acid-neutralizing action of a calcium/magnesium carbonate-based antacid using an artificial stomach model: an in vitro evaluation, BMC Gastroenterology, 21 (2021) 112.
[145] S. Blanquet, E. Zeijdner, E. Beyssac, J.-P. Meunier, S. Denis, R. Havenaar, M. Alric, A Dynamic Artificial Gastrointestinal System for Studying the Behavior of Orally Administered Drug Dosage Forms Under Various Physiological Conditions, Pharmaceutical Research, 21 (2004) 585-591.
[146] K. Venema, J. Verhoeven, C. Beckman, D. Keller, Survival of a probiotic-containing product using capsule-within-capsule technology in an in vitro model of the stomach and small intestine (TIM-1), Beneficial Microbes, 11 (2020) 403-409.
[147] K. Venema, J. Verhoeven, S. Verbruggen, L. Espinosa, S. Courau, Probiotic survival during a multi-layered tablet development as tested in a dynamic, computer-controlled in vitro model of the stomach and small intestine (TIM-1), Letters in Applied Microbiology, 69 (2019) 325-332.
[148] S.R. Carino, D.C. Sperry, M. Hawley, Relative bioavailability estimation of carbamazepine crystal forms using an artificial stomach-duodenum model, Journal of Pharmaceutical Sciences, 95 (2006) 116-125.
[149] C.S. Polster, F. Atassi, S.J. Wu, D.C. Sperry, Use of artificial stomach-duodenum model for investigation of dosing fluid effect on clinical trial variability, Molecular Pharmaceutics, 7 (2010) 1533-1538.
[150] G. Garbacz, R.-S. Wedemeyer, S. Nagel, T. Giessmann, H. Mönnikes, C.G. Wilson, W. Siegmund, W. Weitschies, Irregular absorption profiles observed from diclofenac extended release tablets can be predicted using a dissolution test apparatus that mimics in vivo physical stresses, European Journal of Pharmaceutics and Biopharmaceutics, 70 (2008) 421-428.
[151] G. Garbacz, G.-M. Rappen, M. Koziolek, W. Weitschies, Dissolution of mesalazine modified release tablets under standard and bio-relevant test conditions, Journal of Pharmacy and Pharmacology, 67 (2015) 199-208.
[152] Q. Guo, A. Ye, M. Lad, D. Dalgleish, H. Singh, Effect of gel structure on the gastric digestion of whey protein emulsion gels, Soft Matter, 10 (2014) 1214-1223.
[153] F. Kong, R.P. Singh, A Human Gastric Simulator (HGS) to Study Food Digestion in Human Stomach, Journal of Food Science, 75 (2010) E627-E635.
[154] A. Selen, W.J. Rodriguez, W.H. Doub, L.F. Buhse, E.G. Chikhale, S.K. De, Z. Gao, A.S. Gehris, L. Hughes, R. Lu, H. Mahayni, P.K. Maturu, T.D. Mehta, AAPS 2011 Poster Presentation: Application of FloVitro™ Technology to Evaluate Dissolution of Furosemide and Danazol in Simulated Media at Fed and Fasted Conditions, https://pqri.org/wp-content/uploads/2015/10/03-PQRI-Dissolution-Buhse-2015.pdf, Accessed March 2021 (2011).
[155] J. Chen, V. Gaikwad, M. Holmes, B. Murray, M. Povey, Y. Wang, Y. Zhang, Development of a simple model device for in vitro gastric digestion investigation, Food & function, 2 (2011) 174-182.

[156] E.C. Thuenemann, G. Mandalari, G.T. Rich, R.M. Faulks, Dynamic Gastric Model (DGM), in: K. Verhoeckx, P. Cotter, I. López-Expósito, C. Kleiveland, T. Lea, A. Mackie, T. Requena, D. Swiatecka, H. Wichers (Eds.) The Impact of Food Bioactives on Health: in vitro and ex vivo models, Springer International Publishing, Cham, 2015, pp. 47-59.
[157] J.C. Mann, S.R. Pygall, A formulation case study comparing the dynamic gastric model with conventional dissolution methods, Dissolution Technologies, 19 (2012) 14-19.
[158] A. Mercuri, R. Faulks, D. Craig, S. Barker, M. Wickham, Assessing drug release and dissolution in the stomach by means of Dynamic Gastric Model: a biorelevant approach, Journal of Pharmacy and Pharmacology, 61 (2009).
[159] M. Vardakou, A. Mercuri, T. Naylor, D. Rizzo, J. Butler, P. Connolly, M. Wickham, R. Faulks, Predicting the human in vivo performance of different oral capsule shell types using a novel in vitro dynamic gastric model, International Journal of Pharmaceutics, 419 (2011) 192-199.
[160] I. Pitino, C.L. Randazzo, K.L. Cross, M.L. Parker, C. Bisignano, M.S. Wickham, G. Mandalari, C. Caggia, Survival of Lactobacillus rhamnosus strains inoculated in cheese matrix during simulated human digestion, Journal of Food Microbiology, 31 (2012) 57-63.
[161] L. Chen, A. Jayemanne, X.D. Chen, Venturing into In Vitro Physiological Upper GI System Focusing on the Motility Effect Provided by a Mechanised Rat Stomach Model, Food Digestion, 4 (2013) 36-48.
[162] K. Takeuchi, H. Niida, J. Matsumoto, K. Ueshima, S. Okabe, Gastric motility changes in capsaicin-induced cytoprotection in the rat stomach, The Japanese Journal of Pharmacology, 55 (1991) 147-155.
[163] P. Wu, Z. Liao, T. Luo, L. Chen, X.D. Chen, Enhancement of Digestibility of Casein Powder and Raw Rice Particles in an Improved Dynamic Rat Stomach Model Through an Additional Rolling Mechanism, Journal of Food Science, 82 (2017) 1387-1394.
[164] X. Zhang, Z. Liao, P. Wu, L. Chen, X.D. Chen, Effects of the gastric juice injection pattern and contraction frequency on the digestibility of casein powder suspensions in an in vitro dynamic rat stomach made with a 3D printed model, Food Research International, 106 (2018) 495-502.
[165] O. Ménard, T. Cattenoz, H. Guillemin, I. Souchon, A. Deglaire, D. Dupont, D. Picque, Validation of a new in vitro dynamic system to simulate infant digestion, Food Chemistry, 145 (2014) 1039-1045.
[166] Y. Reynaud, A. Couvent, A. Manach, D. Forest, M. Lopez, D. Picque, I. Souchon, D. Rémond, D. Dupont, Food-dependent set-up of the DiDGI® dynamic in vitro system: Correlation with the porcine model for protein digestion of soya-based food, Food Chemistry, 341 (2021) 128276.
[167] E. Barroso, C. Cueva, C. Peláez, M.C. Martínez-Cuesta, T. Requena, Development of human colonic microbiota in the computer-controlled dynamic SIMulator of the GastroIntestinal tract SIMGI, LWT - Food Science and Technology, 61 (2015) 283-289.
[168] L. Chen, Y. Xu, T. Fan, Z. Liao, P. Wu, X. Wu, X.D. Chen, Gastric emptying and morphology of a 'near real' in vitro human stomach model (RD-IV-HSM), Journal of Food Engineering, 183 (2016) 1-8.
[169] A. Guerra, S. Denis, O. le Goff, V. Sicardi, O. François, A.F. Yao, G. Garrait, A.P. Manzi, E. Beyssac, M. Alric, S. Blanquet-Diot, Development and validation of a new dynamic computer-controlled model of the human stomach and small intestine, Biotechnology and Bioengineering, 113 (2016) 1325-1335.
[170] D.H. Tran Do, F. Kong, C. Penet, D. Winetzky, K. Gregory, Using a dynamic stomach model to study efficacy of supplemental enzymes during simulated digestion, LWT - Food Science and Technology, 65 (2016) 580-588.
[171] L. Barros, C. Retamal, H. Torres, R.N. Zúñiga, E. Troncoso, Development of an in vitro mechanical gastric system (IMGS) with realistic peristalsis to assess lipid digestibility, Food Research International, 90 (2016) 216-225.
[172] S. Bellmann, J. Lelieveld, T. Gorissen, M. Minekus, R. Havenaar, Development of an advanced in vitro model of the stomach and its evaluation versus human gastric physiology, Food Research International, 88 (2016) 191-198.

[173] M. Hopgood, G. Reynolds, R. Barker, Using Computational Fluid Dynamics to Compare Shear Rate and Turbulence in the TIM-Automated Gastric Compartment With USP Apparatus II, Journal of Pharmaceutical Sciences, 107 (2018) 1911-1919.
[174] A.-I. Mulet-Cabero, N.M. Rigby, A. Brodkorb, A.R. Mackie, Dairy food structures influence the rates of nutrient digestion through different in vitro gastric behaviour, Food Hydrocolloids, 67 (2017) 63-73.
[175] M. Minekus, M. Alminger, P. Alvito, S. Ballance, T. Bohn, C. Bourlieu, F. Carriere, R. Boutrou, M. Corredig, D. Dupont, A standardised static in vitro digestion method suitable for food–an international consensus, Food & function, 5 (2014) 1113-1124.
[176] F. Passannanti, F. Nigro, M. Gallo, F. Tornatore, A. Frasso, G. Saccone, A. Budelli, M.V. Barone, R. Nigro, In vitro dynamic model simulating the digestive tract of 6-month-old infants, PLoS ONE, 12 (2017) e0189807.
[177] H. Kozu, I. Kobayashi, M. Nakajima, M.A. Neves, K. Uemura, H. Isoda, S. Ichikawa, Mixing characterization of liquid contents in human gastric digestion simulator equipped with gastric secretion and emptying, Biochemical Engineering Journal, 122 (2017) 85-90.
[178] M. Neumann, F. Schneider, M. Koziolek, G. Garbacz, W. Weitschies, A novel mechanical antrum model for the prediction of the gastroretentive potential of dosage forms, International Journal of Pharmaceutics, 530 (2017) 63-70.
[179] P. Schick, M. Sager, F. Wegner, M. Wiedmann, E. Schapperer, W. Weitschies, M. Koziolek, Application of the GastroDuo as an in Vitro Dissolution Tool To Simulate the Gastric Emptying of the Postprandial Stomach, Molecular Pharmaceutics, 16 (2019) 4651-4660.
[180] P. Schick, M. Sager, M. Voelker, W. Weitschies, M. Koziolek, Application of the GastroDuo to study the interplay of drug release and gastric emptying in case of immediate release Aspirin formulations, European Journal of Pharmaceutics and Biopharmaceutics, 151 (2020) 9-17.
[181] M. Sager, P. Schick, M. Mischek, C. Schulze, M. Hasan, M.-L. Kromrey, H. Benameur, M. Wendler, M.V. Tzvetkov, W. Weitschies, M. Koziolek, Comparison of In Vitro and In Vivo Results Using the GastroDuo and the Salivary Tracer Technique: Immediate Release Dosage Forms under Fasting Conditions, Pharmaceutics, 11 (2019).
[182] W. Liu, D. Fu, X. Zhang, J. Chai, S. Tian, J. Han, Development and validation of a new artificial gastric digestive system, Food Research International, 122 (2019) 183-190.
[183] Y. Li, L. Fortner, F. Kong, Development of a Gastric Simulation Model (GSM) incorporating gastric geometry and peristalsis for food digestion study, Food Research International, 125 (2019).
[184] J. Wang, P. Wu, M. Liu, Z. Liao, Y. Wang, Z. Dong, X.D. Chen, An advanced near real dynamic: In vitro human stomach system to study gastric digestion and emptying of beef stew and cooked rice, Food and Function, 10 (2019) 2914-2925.
[185] J. Wang, P. Wu, M. Liu, Z. Liao, Y. Wang, Z. Dong, X.D. Chen, An advanced near real dynamic in vitro human stomach system to study gastric digestion and emptying of beef stew and cooked rice, Food & function, 10 (2019) 2914-2925.
[186] Z.-t. Li, L. Zhu, W.-l. Zhang, X.-b. Zhan, M.-j. Gao, New dynamic digestion model reactor that mimics gastrointestinal function, Biochemical Engineering Journal, 154 (2020) 107431.
[187] S. Keppler, S. O'Meara, S. Bakalis, P.J. Fryer, G.M. Bornhorst, Characterization of individual particle movement during in vitro gastric digestion in the Human Gastric Simulator (HGS), Journal of Food Engineering, 264 (2020).
[188] S. Ranganathan, E.M. Vasikaran, A. Elumalai, J.A. Moses, C. Anandharamakrishnan, Gastric emptying pattern and disintegration kinetics of cooked rice in a 3D printed in vitro dynamic digestion model ARK® International Journal of Food Engineering, 17 (2021) 385-393.
[189] M. Wickham, R. Faulks, J. Mann, G. Mandalari, The Design, Operation, and Application of a Dynamic Gastric Model, Dissolution Technologies, 19 (2012) 15-22.
[190] Julie Y. Huang, Emily G. Sweeney, M. Sigal, H.C. Zhang, S.J. Remington, Michael A. Cantrell, Calvin J. Kuo, K. Guillemin, Manuel R. Amieva, Chemodetection and Destruction of Host Urea Allows Helicobacter pylori to Locate the Epithelium, Cell Host & Microbe, 18 (2015) 147-156.

[191] P. Schlaermann, B. Toelle, H. Berger, S.C. Schmidt, M. Glanemann, J. Ordemann, S. Bartfeld, H.J. Mollenkopf, T.F. Meyer, A novel human gastric primary cell culture system for modellingHelicobacter pyloriinfection in vitro, Gut, 65 (2016) 202-213.
[192] S.R. Blanke, N. Bertaux-Skeirik, R. Feng, M.A. Schumacher, J. Li, M.M. Mahe, A.C. Engevik, J.E. Javier, R.M. Peek Jr, K. Ottemann, V. Orian-Rousseau, G.P. Boivin, M.A. Helmrath, Y. Zavros, CD44 Plays a Functional Role in Helicobacter pylori-induced Epithelial Cell Proliferation, PLOS Pathogens, 11 (2015).
[193] H.H.N. Yan, H.C. Siu, S. Law, S.L. Ho, S.S.K. Yue, W.Y. Tsui, D. Chan, A.S. Chan, S. Ma, K.O. Lam, S. Bartfeld, A.H.Y. Man, B.C.H. Lee, A.S.Y. Chan, J.W.H. Wong, P.S.W. Cheng, A.K.W. Chan, J. Zhang, J. Shi, X. Fan, D.L.W. Kwong, T.W. Mak, S.T. Yuen, H. Clevers, S.Y. Leung, A Comprehensive Human Gastric Cancer Organoid Biobank Captures Tumor Subtype Heterogeneity and Enables Therapeutic Screening, Cell Stem Cell, 23 (2018) 882-897.e811.
[194] S. Bartfeld, T. Bayram, M. van de Wetering, M. Huch, H. Begthel, P. Kujala, R. Vries, P.J. Peters, H. Clevers, In Vitro Expansion of Human Gastric Epithelial Stem Cells and Their Responses to Bacterial Infection, Gastroenterology, 148 (2015) 126-136.e126.
[195] J. Chakrabarti, Y. Zavros, Generation and use of gastric organoids for the study of Helicobacter pylori pathogenesis, Human Pluripotent Stem Cell Derived Organoid Models2020, pp. 23-46.
[196] T. Seidlitz, S.R. Merker, A. Rothe, F. Zakrzewski, C. von Neubeck, K. Grützmann, U. Sommer, C. Schweitzer, S. Schölch, H. Uhlemann, A.-M. Gaebler, K. Werner, M. Krause, G.B. Baretton, T. Welsch, B.-K. Koo, D.E. Aust, B. Klink, J. Weitz, D.E. Stange, Human gastric cancer modelling using organoids, Gut, 68 (2019) 207-217.
[197] L.E. Wroblewski, M.B. Piazuelo, R. Chaturvedi, M. Schumacher, E. Aihara, R. Feng, J.M. Noto, A. Delgado, D.A. Israel, Y. Zavros, M.H. Montrose, N. Shroyer, P. Correa, K.T. Wilson, R.M. Peek, Helicobacter pyloritargets cancer-associated apical-junctional constituents in gastroids and gastric epithelial cells, Gut, 64 (2015) 720-730.
[198] K.W. McCracken, E.M. Catá, C.M. Crawford, K.L. Sinagoga, M. Schumacher, B.E. Rockich, Y.-H. Tsai, C.N. Mayhew, J.R. Spence, Y. Zavros, J.M. Wells, Modelling human development and disease in pluripotent stem-cell-derived gastric organoids, Nature, 516 (2014) 400-404.
[199] L.D. Nadauld, S. Garcia, G. Natsoulis, J.M. Bell, L. Miotke, E.S. Hopmans, H. Xu, R.K. Pai, C. Palm, J.F. Regan, H. Chen, P. Flaherty, A. Ootani, N.R. Zhang, J.M. Ford, C.J. Kuo, H.P. Ji, Metastatic tumor evolution and organoid modeling implicate TGFBR2as a cancer driver in diffuse gastric cancer, Genome Biology, 15 (2014).
[200] J. Chakrabarti, L. Holokai, L. Syu, N. Steele, J. Chang, A. Dlugosz, Y. Zavros, Mouse-Derived Gastric Organoid and Immune Cell Co-culture for the Study of the Tumor Microenvironment, Epithelial Cell Culture2018, pp. 157-168.
[201] M.A. Schumacher, E. Aihara, R. Feng, A. Engevik, N.F. Shroyer, K.M. Ottemann, R.T. Worrell, M.H. Montrose, R.A. Shivdasani, Y. Zavros, The use of murine-derived fundic organoids in studies of gastric physiology, The Journal of Physiology, 593 (2015) 1809-1827.
[202] X. Yin, H.F. Farin, J.H. van Es, H. Clevers, R. Langer, J.M. Karp, Niche-independent high-purity cultures of Lgr5+ intestinal stem cells and their progeny, Nature Methods, 11 (2013) 106-112.
[203] T.-a.K. Noguchi, N. Ninomiya, M. Sekine, S. Komazaki, P.-C. Wang, M. Asashima, A. Kurisaki, Generation of stomach tissue from mouse embryonic stem cells, Nature Cell Biology, 17 (2015) 984-993.
[204] H. Xu, Y. Jiao, S. Qin, W. Zhao, Q. Chu, K. Wu, Organoid technology in disease modelling, drug development, personalized treatment and regeneration medicine, Exp Hematol Oncol, 7 (2018) 30-30.
[205] K.K. Lee, H.A. McCauley, T.R. Broda, M.J. Kofron, J.M. Wells, C.I. Hong, Human stomach-on-a-chip with luminal flow and peristaltic-like motility, Lab on a Chip, 18 (2018) 3079-3085.
[206] J.M. Sauer, H.A. Merchant, Physiology of the Gastrointestinal System☆, in: C.A. McQueen (Ed.) Comprehensive Toxicology (Third Edition), Elsevier, Oxford, 2018, pp. 16-44.
[207] J.L. Boyer, Bile formation and secretion, Compr Physiol, 3 (2013) 1035-1078.

[208] H.F. Helander, L. Fändriks, Surface area of the digestive tract - revisited, Scandinavian journal of gastroenterology, 49 (2014) 681-689.
[209] L. Marciani, E.F. Cox, C.L. Hoad, S. Pritchard, J.J. Totman, S. Foley, A. Mistry, S. Evans, P.A. Gowland, R.C. Spiller, Postprandial changes in small bowel water content in healthy subjects and patients with irritable bowel syndrome, Gastroenterology, 138 (2010) 469-477. e461.
[210] L.O. Wilken, M.M. Kochhar, D.P. Bennett, F.P. Cosgrove, Cellulose Acetate Succinate as an Enteric Coating for Some Compressed Tablets, Journal of Pharmaceutical Sciences, 51 (1962) 484-490.
[211] V. Gray, J. Dressman, Change of pH requirements for simulated intestinal fluid TS, Pharmacopeial Forum, US PHARMACOPEIAL CONVENTION 12601 TWINBROOK PKWY, ROCKVILLE, MD 20852, 1996, pp. 1943-1945.
[212] A.Y. Abuhelwa, D.J.R. Foster, R.N. Upton, A Quantitative Review and Meta-Models of the Variability and Factors Affecting Oral Drug Absorption-Part I: Gastrointestinal pH, The AAPS journal, 18 (2016) 1309-1321.
[213] E. Stippler, S. Kopp, J.B. Dressman, Comparison of US Pharmacopeia Simulated Intestinal Fluid TS (without pancreatin) and Phosphate Standard Buffer pH 6.8, TS of the International Pharmacopoeia with Respect to Their Use in In Vitro Dissolution Testing, Dissolution Technologies, http://dissolutiontech.com/DTresour/200405Articles/DT200405_A01.pdf (2004).
[214] B.J. Krieg, S.M. Taghavi, G.L. Amidon, G.E. Amidon, In Vivo Predictive Dissolution: Comparing the Effect of Bicarbonate and Phosphate Buffer on the Dissolution of Weak Acids and Weak Bases, Journal of Pharmaceutical Sciences, 104 (2015) 2894-2904.
[215] A. Kambayashi, T. Yasuji, J.B. Dressman, Prediction of the precipitation profiles of weak base drugs in the small intestine using a simplified transfer ("dumping") model coupled with in silico modeling and simulation approach, European Journal of Pharmaceutics and Biopharmaceutics, 103 (2016) 95-103.
[216] E. Galia, E. Nicolaides, D. Hörter, R. Löbenberg, C. Reppas, J.B. Dressman, Evaluation of various dissolution media for predicting in vivo performance of class I and II drugs, Pharmaceutical Research, 15 (1998) 698-705.
[217] J.B. Dressman, G.L. Amidon, C. Reppas, V.P. Shah, Dissolution testing as a prognostic tool for oral drug absorption: immediate release dosage forms, Pharmaceutical Research, 15 (1998) 11-22.
[218] E. Jantratid, N. Janssen, C. Reppas, J.B. Dressman, Dissolution media simulating conditions in the proximal human gastrointestinal tract: an update, Pharmaceutical Research, 25 (2008) 1663.
[219] A. Fuchs, M. Leigh, B. Kloefer, J.B. Dressman, Advances in the design of fasted state simulating intestinal fluids: FaSSIF-V3, European Journal of Pharmaceutics and Biopharmaceutics, 94 (2015) 229-240.
[220] S. Klein, The use of biorelevant dissolution media to forecast the in vivo performance of a drug, The AAPS journal, 12 (2010) 397-406.
[221] L. Klumpp, M. Leigh, J. Dressman, Dissolution behavior of various drugs in different FaSSIF versions, European Journal of Pharmaceutical Sciences, 142 (2020) 105138.
[222] N. Bou-Chacra, K.J.C. Melo, I.A.C. Morales, E.S. Stippler, F. Kesisoglou, M. Yazdanian, R. Löbenberg, Evolution of Choice of Solubility and Dissolution Media After Two Decades of Biopharmaceutical Classification System, The AAPS journal, 19 (2017) 989-1001.
[223] A.R. Mackie, N. Rigby, InfoGest Consensus Method, in: Verhoeckx K, Cotter P, L.-E. I (Eds.) The Impact of Food Bioactives on Health: in vitro and ex vivo models, Springer, [Internet]. Cham (CH), 2015.
[224] A.I. Mulet-Cabero, L. Egger, R. Portmann, O. Ménard, S. Marze, M. Minekus, S. Le Feunteun, A. Sarkar, M.M. Grundy, F. Carrière, M. Golding, D. Dupont, I. Recio, A. Brodkorb, A. Mackie, A standardised semi-dynamic in vitro digestion method suitable for food - an international consensus, Food & function, 11 (2020) 1702-1720.
[225] D.N. Villageliú, S. Rasmussen, M. Lyte, A microbial endocrinology-based simulated small intestinal medium for the evaluation of neurochemical production by gut microbiota, FEMS Microbiology Ecology, 94 (2018).

[226] J. Zhang, J. Zhang, R. Wang, Gut microbiota modulates drug pharmacokinetics, Drug Metabolism Reviews, 50 (2018) 357-368.
[227] E.F. Enright, C.G.M. Gahan, S.A. Joyce, B.T. Griffin, The Impact of the Gut Microbiota on Drug Metabolism and Clinical Outcome, Yale J Biol Med, 89 (2016) 375-382.
[228] Y. Xie, F. Hu, D. Xiang, H. Lu, W. Li, A. Zhao, L. Huang, R. Wang, The metabolic effect of gut microbiota on drugs, Drug Metabolism Reviews, 52 (2020) 139-156.
[229] J.E. Kellow, T.J. Borody, S.F. Phillips, R.L. Tucker, A.C. Haddad, Human interdigestive motility: Variations in patterns from esophagus to colon, Gastroenterology, 91 (1986) 386-395.
[230] C. Liu, K.S. Saw, P.G. Dinning, G. O'Grady, I. Bissett, Manometry of the Human Ileum and Ileocaecal Junction in Health, Disease and Surgery: A Systematic Review, Frontiers in Surgery, 7 (2020).
[231] C. Stillhart, K. Vučićević, P. Augustijns, A.W. Basit, H. Batchelor, T.R. Flanagan, I. Gesquiere, R. Greupink, D. Keszthelyi, M. Koskinen, C.M. Madla, C. Matthys, G. Miljuš, M.G. Mooij, N. Parrott, A.-L. Ungell, S.N. de Wildt, M. Orlu, S. Klein, A. Müllertz, Impact of gastrointestinal physiology on drug absorption in special populations—An UNGAP review, European Journal of Pharmaceutical Sciences, 147 (2020) 105280.
[232] S. Ceuppens, M. Uyttendaele, K. Drieskens, M. Heyndrickx, A. Rajkovic, N. Boon, T.V.d. Wiele, Survival and Germination of Bacillus cereus Spores without Outgrowth or Enterotoxin Production during In Vitro Simulation of Gastrointestinal Transit, Applied and Environmental Microbiology, 78 (2012) 7698-7705.
[233] P.A. Dickinson, R. Abu Rmaileh, L. Ashworth, R.A. Barker, W.M. Burke, C.M. Patterson, N. Stainforth, M. Yasin, An investigation into the utility of a multi-compartmental, dynamic, system of the upper gastrointestinal tract to support formulation development and establish bioequivalence of poorly soluble drugs, The AAPS journal, 14 (2012) 196-205.
[234] J. Van Den Abeele, C. Kostantini, R. Barker, A. Kourentas, J.C. Mann, M. Vertzoni, S. Beato, C. Reppas, J. Tack, P. Augustijns, The effect of reduced gastric acid secretion on the gastrointestinal disposition of a ritonavir amorphous solid dispersion in fasted healthy volunteers: an in vivo - in vitro investigation, European Journal of Pharmaceutical Sciences, 151 (2020) 105377.
[235] A. Dahan, A. Hoffman, Use of a dynamic in vitro lipolysis model to rationalize oral formulation development for poor water soluble drugs: correlation with in vivo data and the relationship to intra-enterocyte processes in rats, Pharmaceutical Research, 23 (2006) 2165-2174.
[236] A. Tharakan, I.T. Norton, P.J. Fryer, S. Bakalis, Mass Transfer and Nutrient Absorption in a Simulated Model of Small Intestine, Journal of Food Science, 75 (2010) E339-E346.
[237] G. Mandalari, R.M. Faulks, C. Bisignano, K.W. Waldron, A. Narbad, M.S.J. Wickham, In vitro evaluation of the prebiotic properties of almond skins (Amygdalus communis L.), FEMS Microbiology Letters, 304 (2010) 116-122.
[238] M. Verwei, M. Minekus, E. Zeijdner, R. Schilderink, R. Havenaar, Evaluation of two dynamic in vitro models simulating fasted and fed state conditions in the upper gastrointestinal tract (TIM-1 and tiny-TIM) for investigating the bioaccessibility of pharmaceutical compounds from oral dosage forms, International Journal of Pharmaceutics, 498 (2016) 178-186.
[239] R. Havenaar, Physiologically relevant in vitro methodology to determine true digestibility of carbohydrates and to predict the glycaemic response, http://www.agfdt.de/loads/st06/havenabb.pdf, 2006.
[240] T. Cieplak, M. Wiese, S. Nielsen, T. Van de Wiele, F. van den Berg, D.S. Nielsen, The Smallest Intestine (TSI)—a low volume in vitro model of the small intestine with increased throughput, FEMS Microbiology Letters, 365 (2018).
[241] O. Ramírez-Fernández, L. Cacopardo, B. Leon-Mancilla, J. Costa, Design and development of a dual-flow bioreactor mimicking intestinal peristalsis and permeability in epithelial tissue barriers for drug transport assessment, Biocell, 43 (2019) 29--36.

[242] E. Barroso, C. Cueva, C. Peláez, M.C. Martínez-Cuesta, T. Requena, The Computer-Controlled Multicompartmental Dynamic Model of the Gastrointestinal System SIMGI, The Impact of Food Bioactives on Health2015, pp. 319-327.
[243] M. Minekus, The TNO Gastro-Intestinal Model (TIM), in: K. Verhoeckx, P. Cotter, I. López-Expósito, C. Kleiveland, T. Lea, A. Mackie, T. Requena, D. Swiatecka, H. Wichers (Eds.) The Impact of Food Bioactives on Health: in vitro and ex vivo models, Springer International Publishing, Cham, 2015, pp. 37-46.
[244] K. Ettayebi, S.E. Crawford, K. Murakami, J.R. Broughman, U. Karandikar, V.R. Tenge, F.H. Neill, S.E. Blutt, X.L. Zeng, L. Qu, B. Kou, A.R. Opekun, D. Burrin, D.Y. Graham, S. Ramani, R.L. Atmar, M.K. Estes, Replication of human noroviruses in stem cell-derived human enteroids, Science, 353 (2016) 1387-1393.
[245] K. Saxena, S.E. Blutt, K. Ettayebi, X.-L. Zeng, J.R. Broughman, S.E. Crawford, U.C. Karandikar, N.P. Sastri, M.E. Conner, A.R. Opekun, D.Y. Graham, W. Qureshi, V. Sherman, J. Foulke-Abel, J. In, O. Kovbasnjuk, N.C. Zachos, M. Donowitz, M.K. Estes, R.M. Sandri-Goldin, Human Intestinal Enteroids: a New Model To Study Human Rotavirus Infection, Host Restriction, and Pathophysiology, Journal of Virology, 90 (2016) 43-56.
[246] I. Heo, D. Dutta, D.A. Schaefer, N. Iakobachvili, B. Artegiani, N. Sachs, K.E. Boonekamp, G. Bowden, A.P.A. Hendrickx, R.J.L. Willems, P.J. Peters, M.W. Riggs, R. O'Connor, H. Clevers, Modelling Cryptosporidium infection in human small intestinal and lung organoids, Nature Microbiology, 3 (2018) 814-823.
[247] V. Costantini, E.K. Morantz, H. Browne, K. Ettayebi, X.-L. Zeng, R.L. Atmar, M.K. Estes, J. Vinjé, Human Norovirus Replication in Human Intestinal Enteroids as Model to Evaluate Virus Inactivation, Emerging Infectious Diseases, 24 (2018) 1453-1464.
[248] M.K. Holly, J.G. Smith, J.K. Pfeiffer, Adenovirus Infection of Human Enteroids Reveals Interferon Sensitivity and Preferential Infection of Goblet Cells, Journal of Virology, 92 (2018).
[249] W.Y. Zou, S.E. Blutt, S.E. Crawford, K. Ettayebi, X.-L. Zeng, K. Saxena, S. Ramani, U.C. Karandikar, N.C. Zachos, M.K. Estes, Human Intestinal Enteroids: New Models to Study Gastrointestinal Virus Infections, Organoids2017, pp. 229-247.
[250] S. Boulant, A.O. Kolawole, C. Mirabelli, D.R. Hill, S.A. Svoboda, A.B. Janowski, K.D. Passalacqua, B.N. Rodriguez, M.K. Dame, P. Freiden, R.P. Berger, D.-l. Vu, M. Hosmillo, M.X.D. O'Riordan, S. Schultz-Cherry, S. Guix, J.R. Spence, D. Wang, C.E. Wobus, Astrovirus replication in human intestinal enteroids reveals multi-cellular tropism and an intricate host innate immune landscape, PLOS Pathogens, 15 (2019).
[251] Y. Yin, M. Bijvelds, W. Dang, L. Xu, A.A. van der Eijk, K. Knipping, N. Tuysuz, J.F. Dekkers, Y. Wang, J. de Jonge, D. Sprengers, L.J.W. van der Laan, J.M. Beekman, D. ten Berge, H.J. Metselaar, H. de Jonge, M.P.G. Koopmans, M.P. Peppelenbosch, Q. Pan, Modeling rotavirus infection and antiviral therapy using primary intestinal organoids, Antiviral Research, 123 (2015) 120-131.
[252] Y.-G. Zhang, S. Wu, Y. Xia, J. Sun, Salmonella

-infected crypt-derived intestinal organoid culture system for host-bacterial interactions, Physiol Rep, 2 (2014).
[253] L. Huang, Q. Hou, L. Ye, Q. Yang, Q. Yu, Crosstalk between H9N2 avian influenza virus and crypt-derived intestinal organoids, Veterinary Research, 48 (2017).
[254] T.P. Resende, R.L. Medida, Y. Guo, F.A. Vannucci, M. Saqui-Salces, C. Gebhart, Evaluation of mouse enteroids as a model for Lawsonia intracellularis infection, Veterinary Research, 50 (2019).
[255] A. Boilève, L. Senovilla, I. Vitale, D. Lissa, I. Martins, D. Métivier, S. van den Brink, H. Clevers, L. Galluzzi, M. Castedo, G. Kroemer, Immunosurveillance against tetraploidization-induced colon tumorigenesis, Cell Cycle, 12 (2014) 473-479.
[256] S.R. Finkbeiner, X.-L. Zeng, B. Utama, R.L. Atmar, N.F. Shroyer, M.K. Estes, T.S. Dermody, Stem Cell-Derived Human Intestinal Organoids as an Infection Model for Rotaviruses, mBio, 3 (2012).
[257] J.L. Forbester, D. Goulding, L. Vallier, N. Hannan, C. Hale, D. Pickard, S. Mukhopadhyay, G. Dougan, B.A. McCormick, Interaction of Salmonella enterica Serovar Typhimurium with Intestinal

Organoids Derived from Human Induced Pluripotent Stem Cells, Infection and Immunity, 83 (2015) 2926-2934.
[258] D.R. Hill, S. Huang, M.S. Nagy, V.K. Yadagiri, C. Fields, D. Mukherjee, B. Bons, P.H. Dedhia, A.M. Chin, Y.-H. Tsai, S. Thodla, T.M. Schmidt, S. Walk, V.B. Young, J.R. Spence, Bacterial colonization stimulates a complex physiological response in the immature human intestinal epithelium, eLife, 6 (2017).
[259] S. Sato, K. Hisaie, S. Kurokawa, A. Suzuki, N. Sakon, Y. Uchida, Y. Yuki, H. Kiyono, Human Norovirus Propagation in Human Induced Pluripotent Stem Cell–Derived Intestinal Epithelial Cells, Cellular and Molecular Gastroenterology and Hepatology, 7 (2019) 686-688.e685.
[260] C.G. Drummond, A.M. Bolock, C. Ma, C.J. Luke, M. Good, C.B. Coyne, Enteroviruses infect human enteroids and induce antiviral signaling in a cell lineage-specific manner, Proceedings of the National Academy of Sciences, 114 (2017) 1672-1677.
[261] J. Zhou, C. Li, X. Liu, M.C. Chiu, X. Zhao, D. Wang, Y. Wei, A. Lee, A.J. Zhang, H. Chu, J.-P. Cai, C.C.-Y. Yip, I.H.-Y. Chan, K.K.-Y. Wong, O.T.-Y. Tsang, K.-H. Chan, J.F.-W. Chan, K.K.-W. To, H. Chen, K.Y. Yuen, Infection of bat and human intestinal organoids by SARS-CoV-2, Nature Medicine, 26 (2020) 1077-1083.
[262] R. Villenave, S.Q. Wales, T. Hamkins-Indik, E. Papafragkou, J.C. Weaver, T.C. Ferrante, A. Bahinski, C.A. Elkins, M. Kulka, D.E. Ingber, Human Gut-On-A-Chip Supports Polarized Infection of Coxsackie B1 Virus In Vitro, PLoS ONE, 12 (2017).
[263] H.J. Kim, H. Li, J.J. Collins, D.E. Ingber, Contributions of microbiome and mechanical deformation to intestinal bacterial overgrowth and inflammation in a human gut-on-a-chip, Proceedings of the National Academy of Sciences, 113 (2016) E7-E15.
[264] K.-Y. Shim, D. Lee, J. Han, N.-T. Nguyen, S. Park, J.H. Sung, Microfluidic gut-on-a-chip with three-dimensional villi structure, Biomedical Microdevices, 19 (2017).
[265] K. Kulthong, L. Duivenvoorde, H. Sun, S. Confederat, J. Wu, B. Spenkelink, L. de Haan, V. Marin, M. van der Zande, H. Bouwmeester, Microfluidic chip for culturing intestinal epithelial cell layers: Characterization and comparison of drug transport between dynamic and static models, Toxicology in Vitro, 65 (2020).
[266] J.H. Sung, J. Yu, D. Luo, M.L. Shuler, J.C. March, Microscale 3-D hydrogel scaffold for biomimetic gastrointestinal (GI) tract model, Lab Chip, 11 (2011) 389-392.
[267] J. Yu, S. Peng, D. Luo, J.C. March, In vitro 3D human small intestinal villous model for drug permeability determination, Biotechnology and Bioengineering, 109 (2012) 2173-2178.
[268] M.B. Esch, J.H. Sung, J. Yang, C. Yu, J. Yu, J.C. March, M.L. Shuler, On chip porous polymer membranes for integration of gastrointestinal tract epithelium with microfluidic 'body-on-a-chip' devices, Biomedical Microdevices, 14 (2012) 895-906.
[269] C.M. Costello, J. Hongpeng, S. Shaffiey, J. Yu, N.K. Jain, D. Hackam, J.C. March, Synthetic small intestinal scaffolds for improved studies of intestinal differentiation, Biotechnology and Bioengineering, 111 (2014) 1222-1232.
[270] S.H. Kim, M. Chi, B. Yi, S.H. Kim, S. Oh, Y. Kim, S. Park, J.H. Sung, Three-dimensional intestinal villi epithelium enhances protection of human intestinal cells from bacterial infection by inducing mucin expression, Integrative Biology, 6 (2014) 1122-1131.
[271] C.M. Costello, R.M. Sorna, Y.-L. Goh, I. Cengic, N.K. Jain, J.C. March, 3-D Intestinal Scaffolds for Evaluating the Therapeutic Potential of Probiotics, Molecular Pharmaceutics, 11 (2014) 2030-2039.
[272] C.M. Costello, M.B. Phillipsen, L.M. Hartmanis, M.A. Kwasnica, V. Chen, D. Hackam, M.W. Chang, W.E. Bentley, J.C. March, Microscale Bioreactors for in situ characterization of GI epithelial cell physiology, Scientific Reports, 7 (2017).
[273] Q. Ramadan, L. Jing, Characterization of tight junction disruption and immune response modulation in a miniaturized Caco-2/U937 coculture-based in vitro model of the human intestinal barrier, Biomedical Microdevices, 18 (2016).

[274] M. Kasendra, A. Tovaglieri, A. Sontheimer-Phelps, S. Jalili-Firoozinezhad, A. Bein, A. Chalkiadaki, W. Scholl, C. Zhang, H. Rickner, C.A. Richmond, H. Li, D.T. Breault, D.E. Ingber, Development of a primary human Small Intestine-on-a-Chip using biopsy-derived organoids, Scientific Reports, 8 (2018).
[275] J. Yin, L. Sunuwar, M. Kasendra, H. Yu, C.-M. Tse, C. Talbot, T.N. Boronina, R.N. Cole, K. Karalis, M. Donowitz, Fluid Shear Stress Enhances Differentiation of Jejunal Human Enteroids in Intestine-Chip, American Journal of Physiology-Gastrointestinal and Liver Physiology, (2020).
[276] F.S. Gazzaniga, D.M. Camacho, M. Wu, M.F. Silva Palazzo, A.L.M. Dinis, F.N. Grafton, M.J. Cartwright, M. Super, D.L. Kasper, D.E. Ingber, Harnessing Colon Chip Technology to Identify Commensal Bacteria That Promote Host Tolerance to Infection, Frontiers in Cellular and Infection Microbiology, 11 (2021).
[277] E. Naumovska, G. Aalderink, C. Wong Valencia, K. Kosim, A. Nicolas, S. Brown, P. Vulto, K.S. Erdmann, D. Kurek, Direct On-Chip Differentiation of Intestinal Tubules from Induced Pluripotent Stem Cells, International Journal of Molecular Sciences, 21 (2020).
[278] P. de Haan, M.J.C. Santbergen, M. van der Zande, H. Bouwmeester, M.W.F. Nielen, E. Verpoorte, A versatile, compartmentalised gut-on-a-chip system for pharmacological and toxicological analyses, Scientific Reports, 11 (2021).
[279] S. Ahadian, R. Civitarese, D. Bannerman, M.H. Mohammadi, R. Lu, E. Wang, L. Davenport-Huyer, B. Lai, B. Zhang, Y. Zhao, S. Mandla, A. Korolj, M. Radisic, Organ-On-A-Chip Platforms: A Convergence of Advanced Materials, Cells, and Microscale Technologies, Advanced Healthcare Materials, 7 (2018).
[280] D. Marrero, F. Pujol-Vila, D. Vera, G. Gabriel, X. Illa, A. Elizalde-Torrent, M. Alvarez, R. Villa, Gut-on-a-chip: Mimicking and monitoring the human intestine, Biosensors and Bioelectronics, 181 (2021) 113156.
[281] M.J.C. Santbergen, M. van der Zande, H. Bouwmeester, M.W.F. Nielen, Online and in situ analysis of organs-on-a-chip, TrAC Trends in Analytical Chemistry, 115 (2019) 138-146.
[282] S. Jalili-Firoozinezhad, F.S. Gazzaniga, E.L. Calamari, D.M. Camacho, C.W. Fadel, A. Bein, B. Swenor, B. Nestor, M.J. Cronce, A. Tovaglieri, O. Levy, K.E. Gregory, D.T. Breault, J.M.S. Cabral, D.L. Kasper, R. Novak, D.E. Ingber, A complex human gut microbiome cultured in an anaerobic intestine-on-a-chip, Nature Biomedical Engineering, 3 (2019) 520-531.
[283] S. Jalili-Firoozinezhad, R. Prantil-Baun, A. Jiang, R. Potla, T. Mammoto, J.C. Weaver, T.C. Ferrante, H.J. Kim, J.M.S. Cabral, O. Levy, D.E. Ingber, Modeling radiation injury-induced cell death and countermeasure drug responses in a human Gut-on-a-Chip, Cell Death & Disease, 9 (2018).
[284] W. Shin, H.J. Kim, Intestinal barrier dysfunction orchestrates the onset of inflammatory host–microbiome cross-talk in a human gut inflammation-on-a-chip, Proceedings of the National Academy of Sciences, 115 (2018) E10539-E10547.
[285] M.J. Workman, J.P. Gleeson, E.J. Troisi, H.Q. Estrada, S.J. Kerns, C.D. Hinojosa, G.A. Hamilton, S.R. Targan, C.N. Svendsen, R.J. Barrett, Enhanced Utilization of Induced Pluripotent Stem Cell–Derived Human Intestinal Organoids Using Microengineered Chips, Cellular and Molecular Gastroenterology and Hepatology, 5 (2018) 669-677.e662.
[286] K. Pocock, L. Delon, V. Bala, S. Rao, C. Priest, C. Prestidge, B. Thierry, Intestine-on-a-Chip Microfluidic Model for Efficient in Vitro Screening of Oral Chemotherapeutic Uptake, ACS Biomaterials Science & Engineering, 3 (2017) 951-959.
[287] P. Shah, J.V. Fritz, E. Glaab, M.S. Desai, K. Greenhalgh, A. Frachet, M. Niegowska, M. Estes, C. Jäger, C. Seguin-Devaux, F. Zenhausern, P. Wilmes, A microfluidics-based in vitro model of the gastrointestinal human–microbe interface, Nature Communications, 7 (2016).
[288] Y. Chen, Y. Lin, K.M. Davis, Q. Wang, J. Rnjak-Kovacina, C. Li, R.R. Isberg, C.A. Kumamoto, J. Mecsas, D.L. Kaplan, Robust bioengineered 3D functional human intestinal epithelium, Scientific Reports, 5 (2015).
[289] D. Gao, H. Liu, J.-M. Lin, Y. Wang, Y. Jiang, Characterization of drug permeability in Caco-2 monolayers by mass spectrometry on a membrane-based microfluidic device, Lab on a Chip, 13 (2013).

[290] Y. Imura, Y. Asano, K. Sato, E. Yoshimura, A Microfluidic System to Evaluate Intestinal Absorption, Analytical Sciences, 25 (2009) 1403-1407.
[291] V. Mahadevan, Anatomy of the caecum, appendix and colon, Surgery - Oxford International Edition, 38 (2020) 1-6.
[292] A. Erdogan, Y.Y. Lee, Colon and pelvic floor anatomy and physiology, in: S.S.C. Rao, Y.Y. Lee, U.C. Ghoshal (Eds.) Clinical and Basic Neurogastroenterology and Motility, Academic Press2020, pp. 113-126.
[293] K. Murray, C.L. Hoad, D.M. Mudie, J. Wright, K. Heissam, N. Abrehart, S.E. Pritchard, S. Al Atwah, P.A. Gowland, M.C. Garnett, G.E. Amidon, R.C. Spiller, G.L. Amidon, L. Marciani, Magnetic Resonance Imaging Quantification of Fasted State Colonic Liquid Pockets in Healthy Humans, Molecular Pharmaceutics, 14 (2017) 2629-2638.
[294] E. Placidi, L. Marciani, C.L. Hoad, A. Napolitano, K.C. Garsed, S.E. Pritchard, E.F. Cox, C. Costigan, R.C. Spiller, P.A. Gowland, The effects of loperamide, or loperamide plus simethicone, on the distribution of gut water as assessed by MRI in a mannitol model of secretory diarrhoea, Alimentary Pharmacology and Therapeutics, 36 (2012) 64-73.
[295] S.E. Pritchard, L. Marciani, K.C. Garsed, C.L. Hoad, W. Thongborisute, E. Roberts, P.A. Gowland, R.C. Spiller, Fasting and postprandial volumes of the undisturbed colon: normal values and changes in diarrhea-predominant irritable bowel syndrome measured using serial MRI, Neurogastroenterol Motil, 26 (2014) 124-130.
[296] M. Nilsson, T.H. Sandberg, J.L. Poulsen, M. Gram, J.B. Frøkjaer, L.R. Østergaard, K. Krogh, C. Brock, A.M. Drewes, Quantification and variability in colonic volume with a novel magnetic resonance imaging method, Neurogastroenterology & Motility, 27 (2015) 1755-1763.
[297] T.H. Sandberg, M. Nilsson, J.L. Poulsen, M. Gram, J.B. Frøkjær, L.R. Østergaard, A.M. Drewes, A novel semi-automatic segmentation method for volumetric assessment of the colon based on magnetic resonance imaging, Abdominal Imaging, 40 (2015) 2232-2241.
[298] M. Coletta, F.K. Gates, L. Marciani, H. Shiwani, G. Major, C.L. Hoad, G. Chaddock, P.A. Gowland, R.C. Spiller, Effect of bread gluten content on gastrointestinal function: a crossover MRI study on healthy humans, British Journal of Nutrition, 115 (2015) 55-61.
[299] C. Lam, G. Chaddock, L. Marciani, C. Costigan, J. Paul, E. Cox, C. Hoad, A. Menys, S. Pritchard, K. Garsed, S. Taylor, D. Atkinson, P. Gowland, R. Spiller, Colonic response to laxative ingestion as assessed by MRI differs in constipated irritable bowel syndrome compared to functional constipation, Neurogastroenterol Motil, 28 (2016) 861-870.
[300] K.A. Murray, C. Lam, S. Rehman, L. Marciani, C. Costigan, C.L. Hoad, M.R. Lingaya, R. Banwait, S.J. Bawden, P.A. Gowland, R.C. Spiller, Corticotropin-releasing factor increases ascending colon volume after a fructose test meal in healthy humans: a randomized controlled trial, The American Journal of Clinical Nutrition, 103 (2016) 1318-1326.
[301] M. Nilsson, J.L. Poulsen, C. Brock, T.H. Sandberg, M. Gram, J.B. Frøkjær, K. Krogh, A.M. Drewes, Opioid-induced bowel dysfunction in healthy volunteers assessed with questionnaires and MRI, European Journal of Gastroenterology & Hepatology, 28 (2016) 514-524.
[302] R.A. Bendezú, M. Mego, E. Monclus, X. Merino, A. Accarino, J.R. Malagelada, I. Navazo, F. Azpiroz, Colonic content: effect of diet, meals, and defecation, Neurogastroenterology & Motility, 29 (2017).
[303] S.E. Pritchard, J. Paul, G. Major, L. Marciani, P.A. Gowland, R.C. Spiller, C.L. Hoad, Assessment of motion of colonic contents in the human colon using MRI tagging, Neurogastroenterol Motil, 29 (2017).
[304] G. Major, K. Murray, G. Singh, A. Nowak, C.L. Hoad, L. Marciani, A. Silos-Santiago, C.B. Kurtz, J.M. Johnston, P. Gowland, R. Spiller, Demonstration of differences in colonic volumes, transit, chyme consistency, and response to psyllium between healthy and constipated subjects using magnetic resonance imaging, Neurogastroenterology & Motility, 30 (2018).

[305] J.L. Poulsen, E.B. Mark, C. Brock, J.B. Frøkjær, K. Krogh, A.M. Drewes, Colorectal Transit and Volume During Treatment With Prolonged-release Oxycodone/Naloxone Versus Oxycodone Plus Macrogol 3350, Journal of Neurogastroenterology and Motility, 24 (2018) 119-127.
[306] B.R. Southwell, M.C.C. Clarke, J. Sutcliffe, J.M. Hutson, Colonic transit studies: normal values for adults and children with comparison of radiological and scintigraphic methods, Pediatric Surgery International, 25 (2009) 559-572.
[307] S.S.C. Rao, R. Kavelock, J. Beaty, K. Ackerson, P. Stumbo, Effects of fat and carbohydrate meals on colonic motor response, Gut, 46 (2000) 205-211.
[308] Q. Tang, G. Jin, G. Wang, T. Liu, X. Liu, B. Wang, H. Cao, Current Sampling Methods for Gut Microbiota: A Call for More Precise Devices, Frontiers in Cellular and Infection Microbiology, 10 (2020).
[309] M. Vertzoni, A. Diakidou, M. Chatzilias, E. Söderlind, B. Abrahamsson, J.B. Dressman, C. Reppas, Biorelevant Media to Simulate Fluids in the Ascending Colon of Humans and Their Usefulness in Predicting Intracolonic Drug Solubility, Pharmaceutical Research, 27 (2010) 2187-2196.
[310] J.H. Cummings, Short chain fatty acids in the human colon, Gut, 22 (1981) 763-779.
[311] F. Liu, H.A. Merchant, R.P. Kulkarni, M. Alkademi, A.W. Basit, Evolution of a physiological pH6.8 bicarbonate buffer system: Application to the dissolution testing of enteric coated products, European Journal of Pharmaceutics and Biopharmaceutics, 78 (2011) 151-157.
[312] L. Yang, Biorelevant dissolution testing of colon-specific delivery systems activated by colonic microflora, Journal of Controlled Release, 125 (2008) 77-86.
[313] M. Wahlgren, M. Axenstrand, Å. Håkansson, A. Marefati, B. Lomstein Pedersen, In Vitro Methods to Study Colon Release: State of the Art and An Outlook on New Strategies for Better In-Vitro Biorelevant Release Media, Pharmaceutics, 11 (2019) 95.
[314] M. Vertzoni, A. Diakidou, M. Chatzilias, E. Söderlind, B. Abrahamsson, J.B. Dressman, C. Reppas, Biorelevant media to simulate fluids in the ascending colon of humans and their usefulness in predicting intracolonic drug solubility, Pharmaceutical Research, 27 (2010) 2187-2196.
[315] R. Takagi, K. Sasaki, D. Sasaki, I. Fukuda, K. Tanaka, K.-i. Yoshida, A. Kondo, R. Osawa, A Single-Batch Fermentation System to Simulate Human Colonic Microbiota for High-Throughput Evaluation of Prebiotics, PLOS ONE, 11 (2016) e0160533.
[316] M.M. O'Donnell, M.C. Rea, F. Shanahan, R.P. Ross, The Use of a Mini-Bioreactor Fermentation System as a Reproducible, High-Throughput ex vivo Batch Model of the Distal Colon, Frontiers in Microbiology, 9 (2018).
[317] F. Karkossa, S. Klein, Assessing the influence of media composition and ionic strength on drug release from commercial immediate-release and enteric-coated aspirin tablets, Journal of Pharmacy and Pharmacology, 69 (2017) 1327-1340.
[318] A. Mercuri, S. Wu, S. Stranzinger, S. Mohr, S. Salar-Behzadi, M. Bresciani, E. Fröhlich, In vitro and in silico characterisation of Tacrolimus released under biorelevant conditions, International Journal of Pharmaceutics, 515 (2016) 271-280.
[319] F. Franek, A. Jarlfors, F. Larsen, P. Holm, B. Steffansen, In vitro solubility, dissolution and permeability studies combined with semi-mechanistic modeling to investigate the intestinal absorption of desvenlafaxine from an immediate- and extended release formulation, European Journal of Pharmaceutical Sciences, 77 (2015) 303-313.
[320] R.C.A. Schellekens, F.E. Stuurman, F.H.J. van der Weert, J.G.W. Kosterink, H.W. Frijlink, A novel dissolution method relevant to intestinal release behaviour and its application in the evaluation of modified release mesalazine products, European Journal of Pharmaceutical Sciences, 30 (2007) 15-20.
[321] F. Karkossa, S. Klein, Individualized in vitro and in silico methods for predicting in vivo performance of enteric-coated tablets containing a narrow therapeutic index drug, European Journal of Pharmaceutics and Biopharmaceutics, 135 (2019) 13-24.
[322] N. Fine-Shamir, A. Dahan, Methacrylate-Copolymer Eudragit EPO as a Solubility-Enabling Excipient for Anionic Drugs: Investigation of Drug Solubility, Intestinal Permeability, and Their Interplay, Molecular Pharmaceutics, 16 (2019) 2884-2891.

[323] D. Georgaka, J. Butler, F. Kesisoglou, C. Reppas, M. Vertzoni, Evaluation of Dissolution in the Lower Intestine and Its Impact on the Absorption Process of High Dose Low Solubility Drugs, Molecular Pharmaceutics, 14 (2017) 4181-4191.
[324] M. Gulati, A. Yadav, M. Sadora, S. Singh, P. Maharshi, A. Sharma, B. Kumar, H. Rathee, D. Ghai, A. Malik, V. Garg, K. Gowthamrajan, Novel biorelevant dissolution medium as a prognostic tool for polysaccharide-based colon-targeted drug delivery system, Journal of Advanced Pharmaceutical Technology & Research, 8 (2017).
[325] C.J. Andreas, X. Pepin, C. Markopoulos, M. Vertzoni, C. Reppas, J.B. Dressman, Mechanistic investigation of the negative food effect of modified release zolpidem, European Journal of Pharmaceutical Sciences, 102 (2017) 284-298.
[326] C.J. Andreas, I. Tomaszewska, U. Muenster, D. van der Mey, W. Mueck, J.B. Dressman, Can dosage form-dependent food effects be predicted using biorelevant dissolution tests? Case example extended release nifedipine, European Journal of Pharmaceutics and Biopharmaceutics, 105 (2016) 193-202.
[327] C.J. Andreas, Y.-C. Chen, C. Markopoulos, C. Reppas, J. Dressman, In vitro biorelevant models for evaluating modified release mesalamine products to forecast the effect of formulation and meal intake on drug release, European Journal of Pharmaceutics and Biopharmaceutics, 97 (2015) 39-50.
[328] S.K. Singh, A.K. Yadav, G. Prudhviraj, M. Gulati, P. Kaur, Y. Vaidya, A novel dissolution method for evaluation of polysaccharide based colon specific delivery systems: A suitable alternative to animal sacrifice, European Journal of Pharmaceutical Sciences, 73 (2015) 72-80.
[329] F.J.O. Varum, G.B. Hatton, A.C. Freire, A.W. Basit, A novel coating concept for ileo-colonic drug targeting: Proof of concept in humans using scintigraphy, European Journal of Pharmaceutics and Biopharmaceutics, 84 (2013) 573-577.
[330] G.R. Gibson, J.H. Cummings, G.T. Macfarlane, Use of a three-stage continuous culture system to study the effect of mucin on dissimilatory sulfate reduction and methanogenesis by mixed populations of human gut bacteria, Applied and Environmental Microbiology, 54 (1988) 2750-2755.
[331] K. Venema, P. van den Abbeele, Experimental models of the gut microbiome, Best Practice & Research Clinical Gastroenterology, 27 (2013) 115-126.
[332] G.T. Macfarlane, S. Macfarlane, G.R. Gibson, Validation of a Three-Stage Compound Continuous Culture System for Investigating the Effect of Retention Time on the Ecology and Metabolism of Bacteria in the Human Colon, Microbial Ecology, 35 (1998) 180-187.
[333] S. Possemiers, K. Verthe, S. Uyttendaele, W. Verstraete, PCR-DGGE-based quantification of stability of the microbial community in a simulator of the human intestinal microbial ecosystem, FEMS Microbiology Ecology, 49 (2004) 495-507.
[334] G.T. Macfarlane, J.H. Cummings, S. Macfarlane, G.R. Gibson, Influence of retention time on degradation of pancreatic enzymes by human colonic bacteria grown in a 3-stage continuous culture system, Journal of Applied Bacteriology, 67 (1989) 521-527.
[335] M. Marzorati, B. Vanhoecke, T. De Ryck, M. Sadaghian Sadabad, I. Pinheiro, S. Possemiers, P. Van den Abbeele, L. Derycke, M. Bracke, J. Pieters, T. Hennebel, H.J. Harmsen, W. Verstraete, T. Van de Wiele, The HMI™ module: a new tool to study the Host-Microbiota Interaction in the human gastrointestinal tract in vitro, BMC Microbiology, 14 (2014).
[336] P. Guo, A.M. Weinstein, S. Weinbaum, A hydrodynamic mechanosensory hypothesis for brush border microvilli, American Journal of Physiology-Renal Physiology, 279 (2000) F698-F712.
[337] L.F. Siew, S.-M. Man, J.M. Newton, A.W. Basit, Amylose formulations for drug delivery to the colon: a comparison of two fermentation models to assess colonic targeting performance in vitro, International Journal of Pharmaceutics, 273 (2004) 129-134.
[338] P. Spratt, C. Nicolella, D.L. Pyle, An Engineering Model of the Human Colon, Food and Bioproducts Processing, 83 (2005) 147-157.
[339] H. Makivuokko, J. Nurmi, P. Nurminen, J. Stowell, N. Rautonen, In Vitro Effects on Polydextrose by Colonic Bacteria and Caco-2 Cell Cyclooxygenase Gene Expression, Nutrition and Cancer, 52 (2005) 94-104.

[340] H.S. Mäkeläinen, H.A. Mäkivuokko, S.J. Salminen, N.E. Rautonen, A.C. Ouwehand, The Effects of Polydextrose and Xylitol on Microbial Community and Activity in a 4-Stage Colon Simulator, Journal of Food Science, 72 (2007) M153-M159.
[341] H. Mäkeläinen, N. Ottman, S. Forssten, M.T. Saarinen, N.E. Rautonen, A.C. Ouwehand, Synbiotic effects of galacto-oligosaccharide, polydextrose and Bifidobacterium lactis Bi-07 in vitro, International Journal of Probiotics & Prebiotics, 5 (2010) 203-210.
[342] H.A. Mäkivuokko, M.T. Saarinen, A.C. Ouwehand, N.E. Rautonen, Effects of Lactose on Colon Microbial Community Structure and Function in a Four-Stage Semi-Continuous Culture System, Bioscience, Biotechnology, and Biochemistry, 70 (2014) 2056-2063.
[343] H. Mäkivuokko, H. Kettunen, M. Saarinen, T. Kamiwaki, Y. Yokoyama, J. Stowell, N. Rautonen, The Effect of Cocoa and Polydextrose on Bacterial Fermentation in Gastrointestinal Tract Simulations, Bioscience, Biotechnology, and Biochemistry, 71 (2014) 1834-1843.
[344] K. Salli, H. Anglenius, J. Hirvonen, A.A. Hibberd, I. Ahonen, M.T. Saarinen, K. Tiihonen, J. Maukonen, A.C. Ouwehand, The effect of 2′-fucosyllactose on simulated infant gut microbiome and metabolites; a pilot study in comparison to GOS and lactose, Scientific Reports, 9 (2019).
[345] J.L. Barry, C. Hoebler, G.T. MacFarlane, S. MacFarlane, J.C. Mathers, K.A. Reed, P.B. Mortensen, I. Nordgaard, I.R. Rowland, C.J. Rumney, Estimation of the fermentability of dietary fibrein vitro: a European interlaboratory study, British Journal of Nutrition, 74 (2007) 303-322.
[346] A.-M. Aura, J. Maukonen, One Compartment Fermentation Model, The Impact of Food Bioactives on Health2015, pp. 281-292.
[347] E. Nordlund, A.-M. Aura, I. Mattila, T. Kössö, X. Rouau, K. Poutanen, Formation of Phenolic Microbial Metabolites and Short-Chain Fatty Acids from Rye, Wheat, and Oat Bran and Their Fractions in the Metabolical in Vitro Colon Model, Journal of Agricultural and Food Chemistry, 60 (2012) 8134-8145.
[348] A.-M. Aura, I. Mattila, T. Hyötyläinen, P. Gopalacharyulu, V. Cheynier, J.-M. Souquet, M. Bes, C. Le Bourvellec, S. Guyot, M. Orešič, Characterization of microbial metabolism of Syrah grape products in an in vitro colon model using targeted and non-targeted analytical approaches, European Journal of Nutrition, 52 (2012) 833-846.
[349] S. Bazzocco, I. Mattila, S. Guyot, C.M.G.C. Renard, A.-M. Aura, Factors affecting the conversion of apple polyphenols to phenolic acids and fruit matrix to short-chain fatty acids by human faecal microbiota in vitro, European Journal of Nutrition, 47 (2008) 442-452.
[350] M.I. McBurney, L.U. Thompson, Effect of Human Faecal Donor on in Vitro Fermentation Variables, Scandinavian journal of gastroenterology, 24 (2009) 359-367.
[351] P.B. Mortensen, H. Hove, M.R. Clausen, K. Holtug, Fermentation to Short-Chain Fatty Acids and Lactate in Human Faecal Batch Cultures Intra- and Inter-Individual Variations versus Variations Caused by Changes in Fermented Saccharides, Scandinavian journal of gastroenterology, 26 (2009) 1285-1294.
[352] S. Blanquet-Diot, S. Denis, S. Chalancon, F. Chaira, J.-M. Cardot, M. Alric, Use of Artificial Digestive Systems to Investigate the Biopharmaceutical Factors Influencing the Survival of Probiotic Yeast During Gastrointestinal Transit in Humans, Pharmaceutical Research, 29 (2011) 1444-1453.
[353] C. Cordonnier, J. Thévenot, L. Etienne-Mesmin, S. Denis, M. Alric, V. Livrelli, S. Blanquet-Diot, Dynamic In Vitro Models of the Human Gastrointestinal Tract as Relevant Tools to Assess the Survival of Probiotic Strains and Their Interactions with Gut Microbiota, Microorganisms, 3 (2015) 725-745.
[354] J. Thévenot, C. Cordonnier, A. Rougeron, O. Le Goff, H.T.T. Nguyen, S. Denis, M. Alric, V. Livrelli, S. Blanquet-Diot, Enterohemorrhagic Escherichia coli infection has donor-dependent effect on human gut microbiota and may be antagonized by probiotic yeast during interaction with Peyer's patches, Applied Microbiology and Biotechnology, 99 (2015) 9097-9110.
[355] J. Thévenot, L. Etienne-Mesmin, S. Denis, S. Chalancon, M. Alric, V. Livrelli, S. Blanquet-Diot, Enterohemorrhagic Escherichia coli O157:H7 Survival in anIn VitroModel of the Human Large Intestine and Interactions with Probiotic Yeasts and Resident Microbiota, Applied and Environmental Microbiology, 79 (2013) 1058-1064.

[356] Y. Sanz, A. Zihler Berner, S. Fuentes, A. Dostal, A.N. Payne, P. Vazquez Gutierrez, C. Chassard, F. Grattepanche, W.M. de Vos, C. Lacroix, Novel Polyfermentor Intestinal Model (PolyFermS) for Controlled Ecological Studies: Validation and Effect of pH, PLoS ONE, 8 (2013).
[357] R. De Weirdt, T. Van de Wiele, Micromanagement in the gut: microenvironmental factors govern colon mucosal biofilm structure and functionality, npj Biofilms and Microbiomes, 1 (2015).
[358] L. Bircher, C. Schwab, A. Geirnaert, A. Greppi, C. Lacroix, P. Wilmes, Planktonic and Sessile Artificial Colonic Microbiota Harbor Distinct Composition and Reestablish Differently upon Frozen and Freeze-Dried Long-Term Storage, mSystems, 5 (2020).
[359] T.L. Weir, S. Fehlbaum, C. Chassard, M.C. Haug, C. Fourmestraux, M. Derrien, C. Lacroix, Design and Investigation of PolyFermS In Vitro Continuous Fermentation Models Inoculated with Immobilized Fecal Microbiota Mimicking the Elderly Colon, PLoS ONE, 10 (2015).
[360] E.-H. Doo, C. Chassard, C. Schwab, C. Lacroix, Effect of dietary nucleosides and yeast extracts on composition and metabolic activity of infant gut microbiota in PolyFermS colonic fermentation models, FEMS Microbiology Ecology, 93 (2017).
[361] M.M. Heimesaat, S.A. Tanner, A. Zihler Berner, E. Rigozzi, F. Grattepanche, C. Chassard, C. Lacroix, In Vitro Continuous Fermentation Model (PolyFermS) of the Swine Proximal Colon for Simultaneous Testing on the Same Gut Microbiota, PLoS ONE, 9 (2014).
[362] S.A. Poeker, C. Lacroix, T. de Wouters, M.R. Spalinger, M. Scharl, A. Geirnaert, Stepwise Development of an in vitro Continuous Fermentation Model for the Murine Caecal Microbiota, Frontiers in Microbiology, 10 (2019).
[363] K. Venema, The TNO In Vitro Model of the Colon (TIM-2), in: K. Verhoeckx, P. Cotter, I. Lopez-Exposito, C. Kleiveland, T. Lea, A. Mackie, T. Requena, D. Swiatecka, H. Wichers (Eds.) The Impact of Food Bioactives on Health: in vitro and ex vivo models, Cham (CH), 2015, pp. 293-304.
[364] M.H.M.C. van Nuenen, P. Diederick Meyer, K. Venema, The Effect of Various Inulins and Clostridium difficile on the Metabolic Activity of the Human Colonic Microbiota in vitro, Microbial Ecology in Health and Disease, 15 (2003) 137-144.
[365] A. Tamargo, C. Cueva, L. Laguna, M.V. Moreno-Arribas, L.A. Muñoz, Understanding the impact of chia seed mucilage on human gut microbiota by using the dynamic gastrointestinal model simgi®, Journal of Functional Foods, 50 (2018) 104-111.
[366] P. Van den Abbeele, S. Roos, V. Eeckhaut, D.A. MacKenzie, M. Derde, W. Verstraete, M. Marzorati, S. Possemiers, B. Vanhoecke, F. Van Immerseel, T. Van de Wiele, Incorporating a mucosal environment in a dynamic gut model results in a more representative colonization by lactobacilli, Microb Biotechnol, 5 (2012) 106-115.
[367] C. Giuliani, M. Marzorati, M. Innocenti, R. Vilchez-Vargas, M. Vital, D.H. Pieper, T. Van de Wiele, N. Mulinacci, Dietary supplement based on stilbenes: a focus on gut microbial metabolism by the in vitro simulator M-SHIME®, Food & function, 7 (2016) 4564-4575.
[368] P. Truchado, E. Hernandez-Sanabria, B.N. Salden, P. Van den Abbeele, R. Vilchez-Vargas, R. Jauregui, D.H. Pieper, S. Possemiers, T. Van de Wiele, Long chain arabinoxylans shift the mucosa-associated microbiota in the proximal colon of the simulator of the human intestinal microbial ecosystem (M-SHIME), Journal of Functional Foods, 32 (2017) 226-237.
[369] L. Liu, J. Firrman, C. Tanes, K. Bittinger, A. Thomas-Gahring, G.D. Wu, P. Van den Abbeele, P.M. Tomasula, Establishing a mucosal gut microbial community in vitro using an artificial simulator, PLoS ONE, 13 (2018).
[370] R. Takagi, K. Sasaki, D. Sasaki, I. Fukuda, K. Tanaka, K.-i. Yoshida, A. Kondo, R. Osawa, A Single-Batch Fermentation System to Simulate Human Colonic Microbiota for High-Throughput Evaluation of Prebiotics, Plos One, 11 (2016).
[371] M. Wiese, B. Khakimov, S. Nielsen, H. Sørensen, F. van den Berg, D.S. Nielsen, CoMiniGut—a small volumein vitrocolon model for the screening of gut microbial fermentation processes, PeerJ, 6 (2018).

[372] P. Bondue, S. Lebrun, B. Taminiau, N. Everaert, G. LaPointe, S. Crevecoeur, G. Daube, V. Delcenserie, A toddler SHIME® model to study microbiota of young children, FEMS Microbiology Letters, 367 (2020).
[373] K. Stamatopoulos, S. Karandikar, M. Goldstein, C. O'Farrell, L. Marciani, S. Sulaiman, C.L. Hoad, M.J.H. Simmons, H.K. Batchelor, Dynamic Colon Model (DCM): A Cine-MRI Informed Biorelevant In Vitro Model of the Human Proximal Large Intestine Characterized by Positron Imaging Techniques, Pharmaceutics, 12 (2020).
[374] L. Marciani, K.C. Garsed, C.L. Hoad, A. Fields, I. Fordham, S.E. Pritchard, E. Placidi, K. Murray, G. Chaddock, C. Costigan, C. Lam, J. Jalanka-Tuovinen, W.M. De Vos, P.A. Gowland, R.C. Spiller, Stimulation of colonic motility by oral PEG electrolyte bowel preparation assessed by MRI: comparison of split vs single dose, Neurogastroenterol Motil, 26 (2014) 1426-1436.
[375] W.M. Bayliss, E.H. Starling, The movements and innervation of the small intestine, The Journal of Physiology, 24 (1899) 99-143.
[376] K. Stamatopoulos, H.K. Batchelor, M.J.H. Simmons, Dissolution profile of theophylline modified release tablets, using a biorelevant Dynamic Colon Model (DCM), Eur J Pharm Biopharm, 108 (2016) 9-17.
[377] P.G. Dinning, L. Wiklendt, L. Maslen, I. Gibbins, V. Patton, J.W. Arkwright, D.Z. Lubowski, G. O'Grady, P.A. Bampton, S.J. Brookes, M. Costa, Quantification ofin vivocolonic motor patterns in healthy humans before and after a meal revealed by high-resolution fiber-optic manometry, Neurogastroenterology & Motility, 26 (2014) 1443-1457.
[378] M.M. O'Donnell, M.C. Rea, F. Shanahan, R.P. Ross, The Use of a Mini-Bioreactor Fermentation System as a Reproducible, High-Throughput ex vivo Batch Model of the Distal Colon, Frontiers in Microbiology, 9 (2018) 1844-1844.
[379] K. Stamatopoulos, H.K. Batchelor, M.J.H. Simmons, Dissolution profile of theophylline modified release tablets, using a biorelevant Dynamic Colon Model (DCM), European Journal of Pharmaceutics and Biopharmaceutics, 108 (2016) 9-17.
[380] M.A. Engevik, K.A. Engevik, M.B. Yacyshyn, J. Wang, D.J. Hassett, B. Darien, B.R. Yacyshyn, R.T. Worrell, HumanClostridium difficileinfection: inhibition of NHE3 and microbiota profile, American Journal of Physiology-Gastrointestinal and Liver Physiology, 308 (2015) G497-G509.
[381] Y. Yin, Y. Wang, W. Dang, L. Xu, J. Su, X. Zhou, W. Wang, K. Felczak, L.J.W. van der Laan, K.W. Pankiewicz, A.A. van der Eijk, M. Bijvelds, D. Sprengers, H. de Jonge, M.P.G. Koopmans, H.J. Metselaar, M.P. Peppelenbosch, Q. Pan, Mycophenolic acid potently inhibits rotavirus infection with a high barrier to resistance development, Antiviral Research, 133 (2016) 41-49.
[382] N. Fischer, E. Sechet, R. Friedman, A. Amiot, I. Sobhani, G. Nigro, P.J. Sansonetti, B. Sperandio, Histone deacetylase inhibition enhances antimicrobial peptide but not inflammatory cytokine expression upon bacterial challenge, Proceedings of the National Academy of Sciences, 113 (2016) E2993-E3001.
[383] Y. Yin, W. Dang, X. Zhou, L. Xu, W. Wang, W. Cao, S. Chen, J. Su, X. Cai, S. Xiao, M.P. Peppelenbosch, Q. Pan, PI3K-Akt-mTOR axis sustains rotavirus infection via the 4E-BP1 mediated autophagy pathway and represents an antiviral target, Virulence, 9 (2017) 83-98.
[384] L. Liu, W. Saitz-Rojas, R. Smith, L. Gonyar, J.G. In, O. Kovbasnjuk, N.C. Zachos, M. Donowitz, J.P. Nataro, F. Ruiz-Perez, Mucus layer modeling of human colonoids during infection with enteroaggragative E. coli, Scientific Reports, 10 (2020).
[385] J. In, J. Foulke-Abel, N.C. Zachos, A.-M. Hansen, J.B. Kaper, H.D. Bernstein, M. Halushka, S. Blutt, M.K. Estes, M. Donowitz, O. Kovbasnjuk, Enterohemorrhagic Escherichia coli Reduces Mucus and Intermicrovillar Bridges in Human Stem Cell-Derived Colonoids, Cellular and Molecular Gastroenterology and Hepatology, 2 (2016) 48-62.e43.
[386] G. Schwank, B.-K. Koo, V. Sasselli, Johanna F. Dekkers, I. Heo, T. Demircan, N. Sasaki, S. Boymans, E. Cuppen, Cornelis K. van der Ent, Edward E.S. Nieuwenhuis, Jeffrey M. Beekman, H. Clevers, Functional Repair of CFTR by CRISPR/Cas9 in Intestinal Stem Cell Organoids of Cystic Fibrosis Patients, Cell Stem Cell, 13 (2013) 653-658.

[387] M. van de Wetering, Hayley E. Francies, Joshua M. Francis, G. Bounova, F. Iorio, A. Pronk, W. van Houdt, J. van Gorp, A. Taylor-Weiner, L. Kester, A. McLaren-Douglas, J. Blokker, S. Jaksani, S. Bartfeld, R. Volckman, P. van Sluis, Vivian S.W. Li, S. Seepo, C. Sekhar Pedamallu, K. Cibulskis, Scott L. Carter, A. McKenna, Michael S. Lawrence, L. Lichtenstein, C. Stewart, J. Koster, R. Versteeg, A. van Oudenaarden, J. Saez-Rodriguez, Robert G.J. Vries, G. Getz, L. Wessels, Michael R. Stratton, U. McDermott, M. Meyerson, Mathew J. Garnett, H. Clevers, Prospective Derivation of a Living Organoid Biobank of Colorectal Cancer Patients, Cell, 161 (2015) 933-945.
[388] A.M. Barnett, J.A. Mullaney, C. Hendriks, L. Le Borgne, W.C. McNabb, N.C. Roy, Porcine colonoids and enteroids keep the memory of their origin during regeneration, American Journal of Physiology-Cell Physiology, 320 (2021) C794-C805.
[389] J.F. Dekkers, G. Berkers, E. Kruisselbrink, A. Vonk, H.R. de Jonge, H.M. Janssens, I. Bronsveld, E.A. van de Graaf, E.E.S. Nieuwenhuis, R.H.J. Houwen, F.P. Vleggaar, J.C. Escher, Y.B. de Rijke, C.J. Majoor, H.G.M. Heijerman, K.M. de Winter–de Groot, H. Clevers, C.K. van der Ent, J.M. Beekman, Characterizing responses to CFTR-modulating drugs using rectal organoids derived from subjects with cystic fibrosis, Science Translational Medicine, 8 (2016) 344ra384-344ra384.
[390] M.E.V. Johansson, J.K. Gustafsson, J. Holmén-Larsson, K.S. Jabbar, L. Xia, H. Xu, F.K. Ghishan, F.A. Carvalho, A.T. Gewirtz, H. Sjövall, G.C. Hansson, Bacteria penetrate the normally impenetrable inner colon mucus layer in both murine colitis models and patients with ulcerative colitis, Gut, 63 (2014) 281-291.
[391] Y. Wang, R. Kim, C.E. Sims, N.L. Allbritton, Building a Thick Mucus Hydrogel Layer to Improve the Physiological Relevance of In Vitro Primary Colonic Epithelial Models, Cellular and Molecular Gastroenterology and Hepatology, 8 (2019) 653-655.e655.
[392] A. Sontheimer-Phelps, D.B. Chou, A. Tovaglieri, T.C. Ferrante, T. Duckworth, C. Fadel, V. Frismantas, A.D. Sutherland, S. Jalili-Firoozinezhad, M. Kasendra, E. Stas, J.C. Weaver, C.A. Richmond, O. Levy, R. Prantil-Baun, D.T. Breault, D.E. Ingber, Human Colon-on-a-Chip Enables Continuous In Vitro Analysis of Colon Mucus Layer Accumulation and Physiology, Cellular and Molecular Gastroenterology and Hepatology, 9 (2020) 507-526.
[393] C. Beaurivage, A. Kanapeckaite, C. Loomans, K.S. Erdmann, J. Stallen, R.A.J. Janssen, Development of a human primary gut-on-a-chip to model inflammatory processes, Scientific Reports, 10 (2020).
[394] W. Shin, Y.M. Ambrosini, Y.C. Shin, A. Wu, S. Min, D. Koh, S. Park, S. Kim, H. Koh, H.J. Kim, Robust Formation of an Epithelial Layer of Human Intestinal Organoids in a Polydimethylsiloxane-Based Gut-on-a-Chip Microdevice, Frontiers in Medical Technology, 2 (2020).
[395] A. Apostolou, R.A. Panchakshari, A. Banerjee, D.V. Manatakis, M.D. Paraskevopoulou, R. Luc, G. AbuAli, A. Dimitriou, C. Lucchesi, G. Kulkarni, T.I. Maulana, B. Bleck, E.S. Manolakos, G.A. Hamilton, C. Giallourakis, K. Karalis, A Micro-engineered Human Colon Intestine-Chip Platform to Study Leaky Barrier, BioRxiv, Preprint (2020).
[396] A. Tovaglieri, A. Sontheimer-Phelps, A. Geirnaert, R. Prantil-Baun, D.M. Camacho, D.B. Chou, S. Jalili-Firoozinezhad, T. de Wouters, M. Kasendra, M. Super, M.J. Cartwright, C.A. Richmond, D.T. Breault, C. Lacroix, D.E. Ingber, Species-specific enhancement of enterohemorrhagic E. coli pathogenesis mediated by microbiome metabolites, Microbiome, 7 (2019).
[397] W. Shin, C.D. Hinojosa, D.E. Ingber, H.J. Kim, Human Intestinal Morphogenesis Controlled by Transepithelial Morphogen Gradient and Flow-Dependent Physical Cues in a Microengineered Gut-on-a-Chip, iScience, 15 (2019) 391-406.
[398] I. Sensoy, A review on the food digestion in the digestive tract and the used in vitro models, Current Research in Food Science, 4 (2021) 308-319.
[399] E.M. Persson, A.S. Gustafsson, A.S. Carlsson, R.G. Nilsson, L. Knutson, P. Forsell, G. Hanisch, H. Lennernäs, B. Abrahamsson, The effects of food on the dissolution of poorly soluble drugs in human and in model small intestinal fluids, Pharmaceutical Research, 22 (2005) 2141-2151.

[400] M. Perez de la Cruz Moreno, M. Oth, S. Deferme, F. Lammert, J. Tack, J. Dressman, P. Augustijns, Characterization of fasted-state human intestinal fluids collected from duodenum and jejunum, Journal of Pharmacy and Pharmacology, 58 (2006) 1079-1089.
[401] J. Brouwers, J. Tack, F. Lammert, P. Augustijns, Intraluminal drug and formulation behavior and integration in in vitro permeability estimation: A case study with amprenavir, Journal of Pharmaceutical Sciences, 95 (2006) 372-383.
[402] S. Clarysse, J. Tack, F. Lammert, G. Duchateau, C. Reppas, P. Augustijns, Postprandial Evolution in Composition and Characteristics of Human Duodenal Fluids in Different Nutritional States, Journal of Pharmaceutical Sciences, 98 (2009) 1177-1192.
[403] T. Heikkilä, M. Karjalainen, K. Ojala, K. Partola, F. Lammert, P. Augustijns, A. Urtti, M. Yliperttula, L. Peltonen, J. Hirvonen, Equilibrium drug solubility measurements in 96-well plates reveal similar drug solubilities in phosphate buffer pH 6.8 and human intestinal fluid, International Journal of Pharmaceutics, 405 (2011) 132-136.
[404] N. Holmstock, T. De Bruyn, J. Bevernage, P. Annaert, R. Mols, J. Tack, P. Augustijns, Exploring food effects on indinavir absorption with human intestinal fluids in the mouse intestine, European Journal of Pharmaceutical Sciences, 49 (2013) 27-32.
[405] J. Stappaerts, B. Wuyts, J. Tack, P. Annaert, P. Augustijns, Human and simulated intestinal fluids as solvent systems to explore food effects on intestinal solubility and permeability, European Journal of Pharmaceutical Sciences, 63 (2014) 178-186.
[406] D. Riethorst, R. Mols, G. Duchateau, J. Tack, J. Brouwers, P. Augustijns, Characterization of Human Duodenal Fluids in Fasted and Fed State Conditions, Journal of Pharmaceutical Sciences, 105 (2016) 673-681.